STRUCTURE ACTIVITY AND STRUCTURE PROPERTY RELATIONSHIPS OF ANTIMALARIAL IMIDAZOPYRIDAZINES

By

Luyanda Centani

Supervisor: Prof **Kelly Chibale,** Department of Chemistry

DECEMBER 10, 2018

Department of Chemistry, University of Cape Town

Declaration

I declare that this is my own work and plagiarism is wrong. All work presented in this dissertation is my original work except where I have cited or quoted articles, books, websites or journals. The work covered in this dissertation about synthesis, structure-activity relationship, and structure property relationship of imidazopyridazine has not been submitted to any university to obtain any degree.

Acknowledgements

I appreciate the support, opportunities, guidance and patience from my supervisor Professor Kelly Chibale. I thank Professor Kelly Chibale for sharing his skills and knowledge. Thank you for expanding my knowledge in chemistry especially in medicinal chemistry research.

I thank Peter Mubanga Cheuka for demonstrating how to carry out research and mentoring me throughout honours and masters. I also appreciate the support from Dr. Preshendren Govender and Dr. Malkeet Kumar. Thanks for coaching me, proof-reading my work and helping me to express scientific discoveries accurately and concise.

Wholeheartedly, I thank KC research group for their contribution directly or indirectly into this work. I am proud for all things I have learned in the group.

Special thanks to chemistry department at UCT in particular Peter Roberts for running NMR.

I want to thank Elaine Rutherfoord-Jones for sending latest group's publication, making sure everything is communicated efficiently amonst group members and also Deidre Van Rooyen for processing chemical orders and organising biological results.

Enkosi kakhulu maNkwali Nontuthuzelo Ndwandwa kunye naba ntakwethu ngexaso enithe na ndinikayo.

Conference

International conference on Biology of Host Parasite Interaction 2018

Poster Presenter at the Gordon Research Conference on Biology of Host-Parasite Interactions held June 10, 2018 - June 15, 2018 at Salve Regina University in Newport, RI, United States. Poster title: STRUCTURE ACTIVITY AND STRUCTURE PROPERTY RELATIONSHIPS OF ANTIMALARIAL IMIDAZOPYRIDAZINES.

Abstract

Malaria is one of the most pressing human health issues. Despite being an ancient disease, it is estimated to have an annual death rate of 445 000 with out of 216 million malaria related cases in 2016. Malaria is most widespread in developing regions of the world. Forty percent of the world's population is exposed to varying degrees of malaria. Malaria is caused by different species of the *Plasmodium* genus and the disease is vector-borne. The disease may be cured if diagnosed early. Most drugs that were once effective in the treatment of malaria have become ineffective due to the emergence of resistance, which has become the main driving force behind efforts to discover and develop new drugs able to circumvent the resistance.

Imidazopyridazines have been shown to have potent antiplasmodium activity. The lead compound **MMV652103** has been shown to display potent activity against the multidrug resistant K1 strain and the drug sensitive NF54 strain of the human malaria parasite *Plasmodium falciparum*.

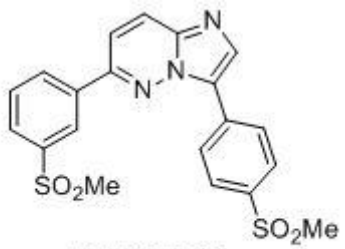

MMV652103
IC_{50}(nM)<10, K1 and NF54

However, the majority of the antimalarial imidazopyridazine compounds evaluated to date have solubility and off-target human *ether-a-go-go*-related gene (hERG) potassium ion channel liabilities.

Towards improving solubility and de-risking the hERG liability, a series of analogues was designed and synthesised. Structure-Activity Relationship (SAR) and Structure-Property Relationship (SPR) studies aimed at retaining the good antiplasmodium activity while improving solubility and reducing hERG channel inhibition, were conducted. Previous studies conducted on this series of imidazopyridazines have shown that incorporation of

hydrogen bond donors or acceptors resulted in improving solubility and hERG channel inhibition.

While the lead compound **MMV652103** at pH 6.5 has a sub-optimal solubility of 5 µM, all target compounds showed an improvement in solubility. Five analogues **59**, **78**, **84**, **85,** and **86** exhibiting impressive *in vitro* asexual blood stage antiplasmodium potency (IC_{50} < 100 nM) and aqueous solubility (> 200 µM) were identified from the study. The identified compounds also displayed good activity against the sexual late-stage gametocytes, the transmissible forms of the parasite.

List of abbreviations

MMV	Medicines for Malaria Venture
°C	Degrees Celsius
ADME	Absorption, Distribution, Metabolism and Excretion
AUC	Area under curve
Cl	Clearance
ClogP	Calculated Log P
COSY	Correlation spectroscopy
DCM	Dichloromethane
DFT	Density functional theory
DIPEA	*N*, *N*-Diisopropylethylamine
PD	Pharmacodynamics
T3P	Propylphosphonic anhydride solution ≥50 wt. % in ethyl acetate
DMPK	Drug metabolism and pharmacokinetics
DMSO-d_6	Deuterated dimethyl sulfoxide
DMSO	Dimethyl sulfoxide
FDA	Food and Drug Administration
Rf	Retardation factor
t_r	Retention time

HPLC	High Performance Liquid Chromatography
HSQC	Heteronuclear single quantum correlation
ESI	Electron Spray Ionization
IC_{50}	Half-maximal inhibitory concentration
LCMS	Liquid chromatography mass spectrometry
m/z	Mass-to-charge ratio
MeOH	Methanol
MDOD-$_{d4}$	Deuterated methanol
MHz	Megahertz
MLM	Mouse liver microsomes
mp	Melting point
MS	Mass spectrometry
Mol. wt	Molecular weight
ND	Not determined
NMR	Nuclear Magnetic Resonance
PBS	Phosphate buffered saline
$PdCl_2(PPh_3)_2$	Bis(triphenylphosphine)palladium(II) dichloride
PK	Pharmacokinetics
tPSA	Total Polar Surface Area
hERG	The human *ether-a-go-go*-related gene

SAR	Structure-activity relationship
TLC	Thin layer chromatography
WHO	World Health Organization
δ	Delta (NMR chemical shift)
μM	Micromolar
nM	Nanomolar
DMF	*N*, *N*-Dimethylformamide
mTOR	mammalian target of rapamycin
ATP	Attached Proton Test

LIST OF FIGURES

Figure 48: Solubility of reserpine.

List of tables

List of schemes

Contents

Chapter one

1.1 Malaria: History and introduction

Malaria symptoms were first described by the Chinese in the book *Nei Ching* in 2700 BC.[1] In the 4th century, malaria affected the Greeks with its depopulating effects in rural and urban areas. In *The compendium of Suśruta,* it is documented that after getting bitten by certain insects, patients showed malarial symptoms.[1] Before the discovery of the disease causing parasites by Antoni van Leeuwenhoe in 1676, Greeks were well aware of characteristic poor health, fever, and enlarged spleens for people who lived in marshy places.[2] Indeed, malaria has ravaged humans spreading and claiming lives over many years.

1.2 Epidemiology of malaria

Today, malaria is most prevalent in developing countries and its transmission can vary from region to region depending on rainfall patterns, social and environmental factors, availability of health services, and malaria control activities.[3] The intensity of malaria is mainly dependent on climatic conditions with some climates favouring transmission, reproduction and survival of mosquitoes (**Figure 1**). Malaria slows down economic growth in Africa costing more than 12 billion dollars every year.[4] There is a strong relationship between malaria and poor developing countries, where malaria is rampant and the society prospers the least.[4,5] The cost of malaria hinders development in many ways including diverting funds to medical costs, reduced population growth, absenteeism from work, saving and investments, and reduced worker productivity, as well as premature mortality.[5] Countries that have managed to eradicate malaria have gained economic growth.[4]

According to the World Health Organization (WHO) world malaria report, 216 million malaria cases and 445000 malaria-related deaths were reported in 2016.[6] The WHO reports that African region accounted for 90 and 91 % of the cases and deaths, respectively. A huge

portion of over two thirds (70 %) of these deaths were reported in children under the age of 5 years.[6]

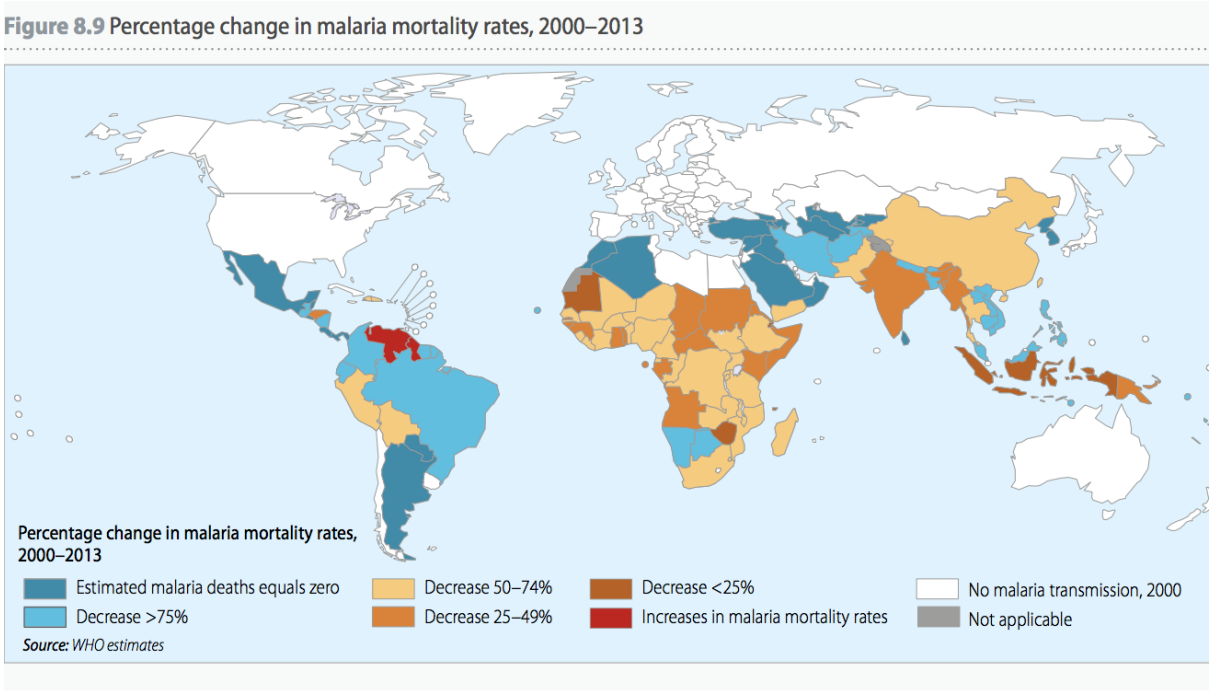

Figure 1: Geographic distribution of malaria (Source: https://www.undispatch.com/un-content/uploads/2014/12/Screen-Shot-2014-12-09-at-10.05.48-AM.png).

1.3 Aetiology of malaria

1.3.1 Parasites responsible for causing malaria

Malaria is a vector-borne disease, and in humans, it is caused by five species of *Plasmodium*, namely *P. falciparum*, *P. ovale*, *P. malariae*, *P. vivax*, and *P. knowlesi*.[7] The symptoms associated with malaria include fever, chills, muscle aches, fatigue, vomiting and abdominal discomfort.[3] When malaria has progressed to severe disease and the person remains untreated, death may result. Malaria deaths which are not caused by *P. falciparum* are rare.[3]

1.3.2 Malaria parasite life cycle

Malaria is transmitted by the bites of an infected female anopheles mosquito.[3,7] The transmission of the parasite can also occur when infected blood is passed to a recipient through blood transfusion, sharing of needles, and congenital infection.[3]

When an infected anopheles mosquito takes in a blood meal, it injects sporozoites into the human host, which are carried by the blood stream to the liver (**Figure 2**). At the liver stage, the sporozoites invade hepatocytes, where they mature into exoerythrocytic forms.[8] There are two different developmental pathways for exoerythrocytic parasites: Its either the parasites develop into schizonts or dormant forms called hypnozoites.[9] The hypnozoites are particularly known to develop in *P. vivax* and *P. ovale* infections.[9] These dormant forms can reactivate and develop at any time after the initial infection.[10] Fully matured schizonts develop into merozoites, which are released from the liver and enter the blood stream.[8] The merozoites in the blood begin to invade red blood cells and transform into trophozoites, which reproduce quickly through asexual reproduction into schizonts. This erythrocytic infection cycle is repeated.[11] The symptoms of malaria become visible during the breaking down of red blood cells by merozoites. As merozoites in the blood grow, they develop into male and female gametes, which are taken up by the mosquito when it takes in blood meal from an infected person.[7] The male and female gametes intermix and form zygotes inside the mosquito stomach. The zygotes are elongated (ookinetes) and mobile. The ookinetes move into the midgut wall of the mosquito where they grow into oocysts. These oocysts then grow and rupture releasing sporozoites, which in turn move to the salivary glands and are released with saliva when a female anopheles mosquito takes in a blood meal from a human host.

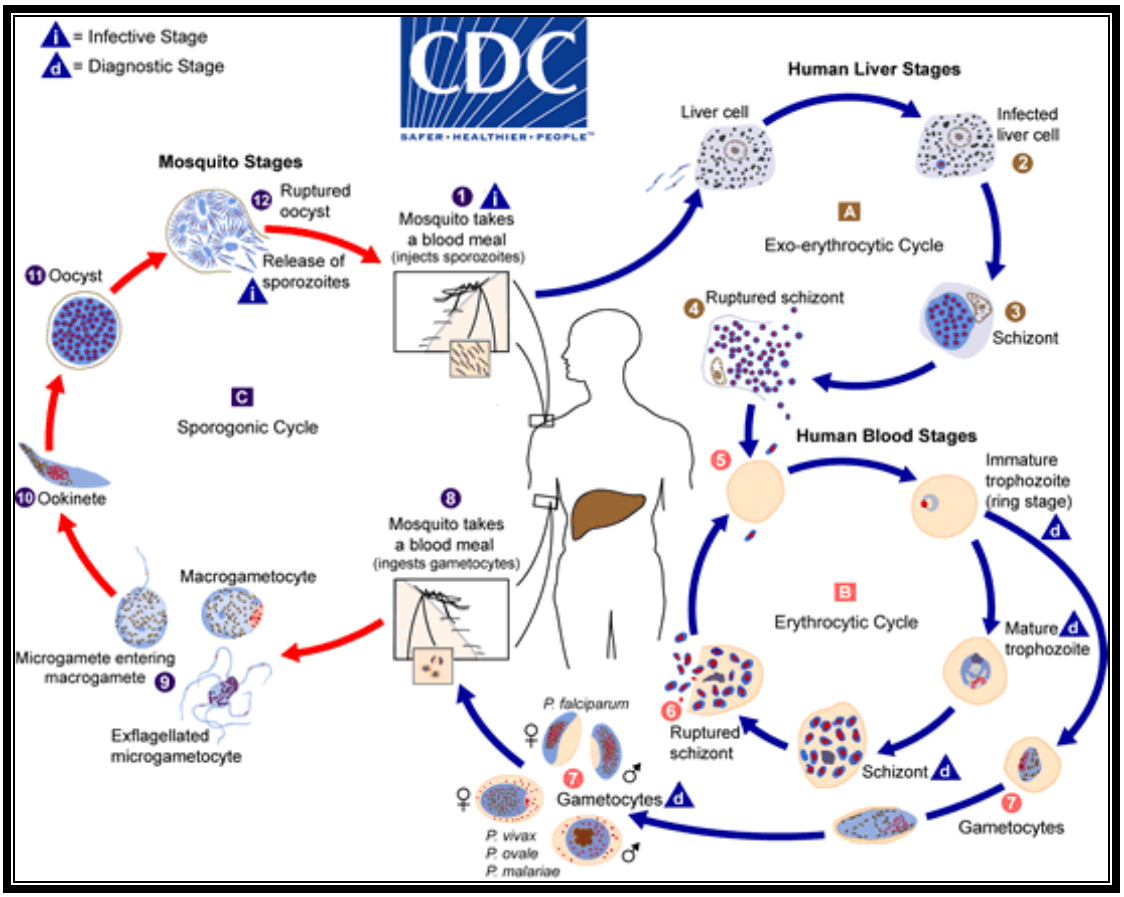

Figure 2: Malaria life cycle (Source:https://www.cdc.gov/malaria/about/disease.html).

1.4 Malaria control, prevention and treatment

1.4.1 Vector control

Global interventions to decrease the spread of malaria and its impact have involved many strategies such as vector control, use of chemoprophylaxis, chemotherapy, bed nets, genetically modified sporozoites and use of insecticides.[3,7] Strategies to control anopheles mosquitoes have limitations, for example, a limitation to the use of insecticides is that, the mosquito population that was exposed to the insecticide dies out and, once the insecticide is withdrawn, the mosquito population quickly grows back. Other methods such as sleeping under insecticide-treated nets (ITNs) and indoor residual spraying (IRS) have yielded good results. In this regard, using ITN and IRS has decreased child (under the age of 5 years) mortality rate by 55 %.[12,13] The economic burden imposed by malaria has caused poor

countries to discontinue the use of IRS and ITN because of limited funds. On the other hand, South Africa in particular continued to use IRS and ITN and has consequently achieved over 80 % malaria eradication.[14] It is difficult to kill a moving mosquito, but when their habitants are exposed to insecticide and larvicide, which will prevent egg nourishment leading to population decline as fewer mosquitoes are able to mature.[15] Recent research conducted by Mueller *et al*, has resulted in the identification of a gene, UIS3, expressed in the pre-erythrocytic stage of the malaria parasite life cycle and upregulated by infective sporozoites. It was demonstrated *in vivo* that sporozoites which lacked the UIS3 gene provide complete protection in a rodent malaria model.[16] In the studies, it was concluded that it is possible to have safe and effective genetically modified malaria parasites.

1.4.2 Chemoprophylaxis

Malaria is devastating during pregnancy as it increases the chances of transmission from the mother to the unborn child. In pregnant women, malaria infection can result in low birth weight for new born infants, stillborn babies, maternal anaemia and increased prenatal mortality.[17] People traveling to places where malaria is prevalent are advised to take medicines for chemoprophylaxis prior to departure. Chemoprophylaxis is the use of antimalarial medicines to prevent the development of malaria. It is noteworthy that there is no antimalarial drug that provides 100 % protection, but when supplemented with personal protective measures chemoprophylatic antimalarials can be effective.

Treatment taken depends on which area the person is travelling to, what type of species and which drug resistant strain is prevalent.[18] Primaquine (**1**) and proguanil (**2**) are recommended as causal prophylactic drugs (**Figure 3**). Casual prophylactics stop the development of disease in the liver by inhibiting pre-erythrocytic schizogony. Casual prophylatics are not recommended for daily use. On the other hand, suppressive prophylactics are used to treat malaria caused by asexual blood stage parasites, which results in the presentation of clinical

symptoms.[18] Doxycycline (**3**) is taken by travellers to an area which has ongoing transmission and is taken 1–2 days before arriving to the malaria endemic region. Mefloquine (**4**) is used for long trips and offers the advantage of being taken less frequently, once a week, which makes it convenient for users to complete the course. Relapsed malaria from hypnozoites is treated with primaquine over two weeks. Sulfadoxine (**5**) and pyrimethamine (**6**) are associated with reduced antenatal parasitaemia, low birthweight outcomes, and reduced severe or moderate anaemia.[19,20] For these reasons, the WHO recommended the use of sulfadoxine-pyrimethamine as intermittent preventive treatment for malaria in pregnancy (IPTp) and seasonal malaria chemoprevention (SMC). Primaquine belongs to a class of the 8-aminoquinolines and has been the only drug used to treat malaria relapse.[21] The challenge with primaquine is that it requires 14 days of treatment and patients do not adhere to take treatment consistently and finish the course. Furthermore, primaquine induces haemolytic effects and is not recommended for patients with glucose-6-phosphate dehydrogenase (G6PD) deficiency.[21] Recently, the United States Food and Drug Administration (FDA) has approved the use of tafenoquine (**7**) to cure *P. vivax* infections, which presents an improved alternative to primaquine.[22] Tafenoquine offers an advantage over primaquine in that it is a single dose treatment.[23] Although Tafenoquine has been approved by the FDA, it still retains haemolytic effects like primaquine and is not recommended for patients with G6PD defiency.[24]

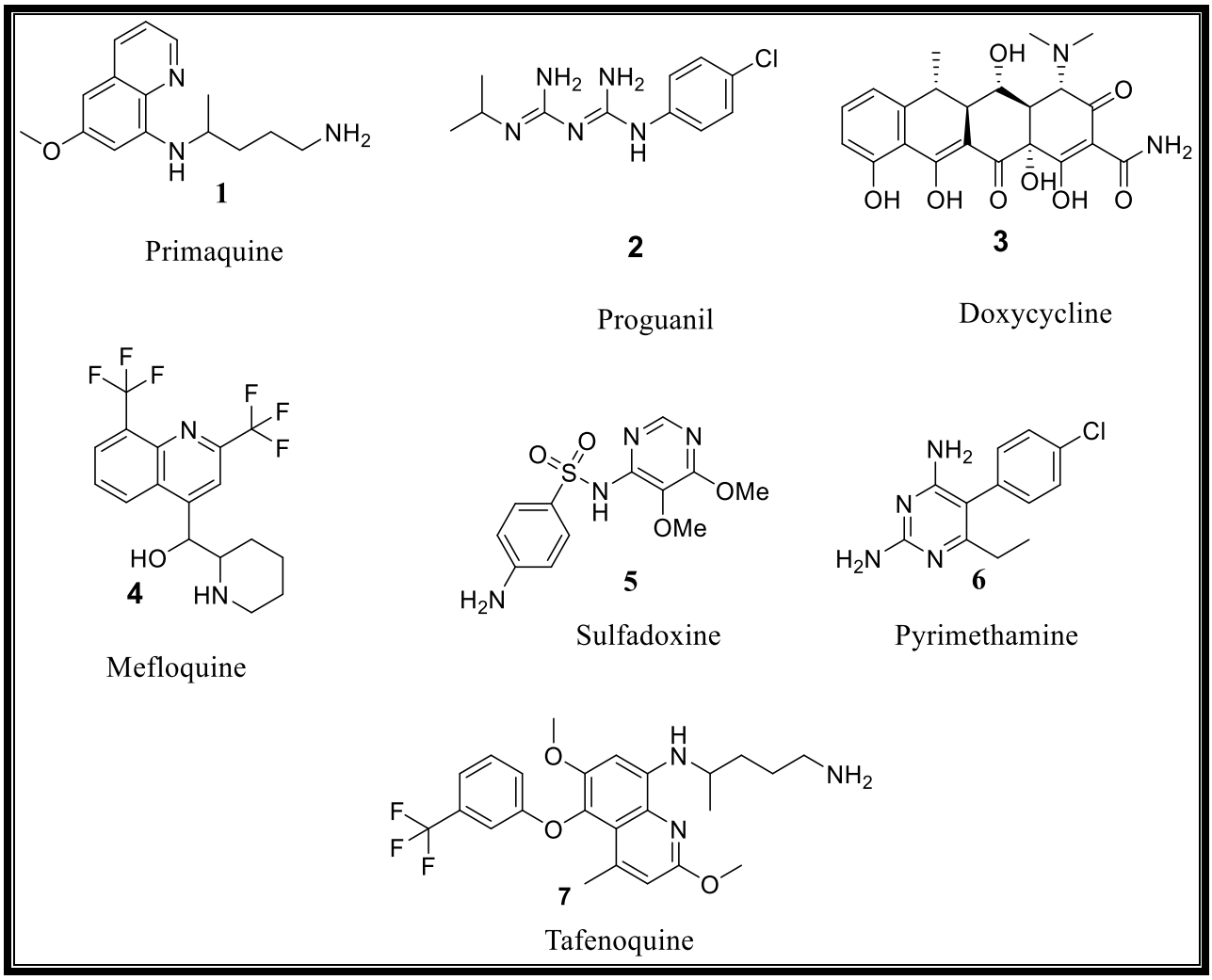

Figure 3: Chemical Structures of drugs use for Chemoprophylaxis.

1.4.3 Malaria vaccine

Currently there is no commercially available vaccine approved for protection against malaria. However, there are more than 20 vaccines in development, others are being evaluated in clinical trials while others are in advanced preclinical development.[25] The most advanced malaria vaccine is the RTS,S/AS01(RTS,S), which offers partial protection against *P. falciparum* in children.[26] The RTS,S/AS01(RTS,S) vaccine is also known as Mosquirix and its route of administration is through injection. The vaccine is being evaluated in sub-Saharan Africa, and the WHO announced in April 2017 a partnership with Ghana, Kenya and Malawi to make RTS,S/AS01(RTS,S) available in selected areas of the three countries.[27]

1.4.4 Current treatment regimens and parasite resistance to antimalarial drugs

Efforts to control malaria using currently available antimalarial drugs are becoming less effective because the malaria-causing parasite has developed varying degrees of resistance to drugs that are recommended as frontline treatments for malaria.[28] Drugs such as chloroquine (**12**) in **Figure 4** and sulfadoxine-pyrimethamine (**Figure 3**), which were once effective, are no longer in use because of widespread parasite resistance. Chloroquine offered one advantage as an antimalarial: it was cheaper and widely available.[3] In the 1970s the Chinese discovered the antimalarial properties of artemisinin (**8**) with its other semi-synthetic derivatives artemether (**10**), artesunate (**11**), and dihydroartemisinin (**9**) (**Figure 4**).[29] The WHO recommended in 2001 that short acting artemisinins should be used in combination with other long acting drugs (Artesunate (**11**)-Mefloquine (**4**), Artemether (**10)**-Lumefantrine (**15**), Artesunate (**11**)-Amodiaquine (**13**), Artesunate (**11**)-Sulfadoxine (**5**)-Pyrimethamine (**6**), and Dihydroartemisinin (**9**)-Piperaquine (**14**) in countries where *P. falciparum* had developed resistance to conventional antimalarial drugs.[29] Since then, the mainstay of antimalarial chemotherapy are the so called artemisinin-based combination therapies (ACTs) (**Figure 4**).[30] Regrettably, in Western Cambodia, it has been reported that the efficacy of ACTs has diminished, a phenomenon attributed to the emergence of resistance against these important antimalarials.[31,32]

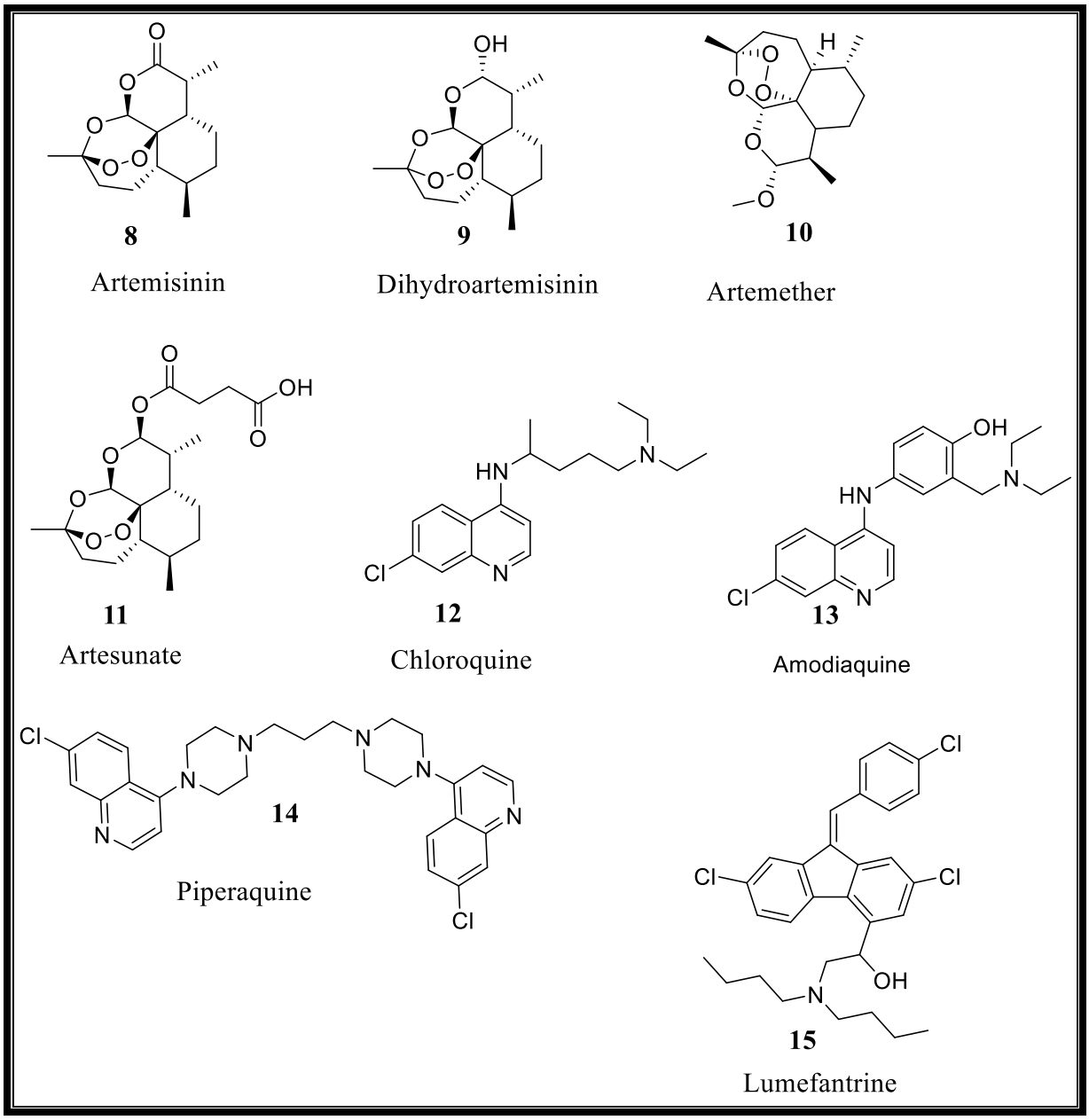

Figure 4: Structures of antimalarial drugs in clinical use.

1.4.5 Categories of antimalarial drugs based on parasite life cycle targeted

Understanding where the drug exerts its effect in the life cycle of the malaria parasite is important because it will require less effort to determine which drugs to use as partners in an attempt to delay the emergence of drug resistance.[33] Antimalarials are divided into different classes, each class differs from other by chemical structure, their mechanism of action or both (**Table 1**).[33]

Table 1: Example of antimalarials from different classes.

Class	Molecule
Endoperoxides	Artemether (**10)**
4-Aminoquinolines	Amodiaquine (**13)**
8-Aminoquinolines	Primaquine (**14)**
Antifolates	Pyrimethamine (**6)**
Sulfonamides	Sulfadoxine (**5)**
Antibiotics	Azithromycin
Amino alcohols	Lumefantrine (**15**)

Cycloguanil, pyrimethamine, and atovaquone drugs have shown to be highly potent in transmission blocking from the mosquito to human host by killing schizont in the liver.[33] In the same studies conducted by Delves *et al*, the endoperoxide OZ439 showed strong inhibition of gamete formation and gametocyte maturation.[33]

1.5 Antimalarial drug pipeline

Figure 5 shows selected drug candidates in clinical development. The advantage of the current antimalarial drug pipeline is that it is rich with molecules which have shown activity at different stages of the malaria parasite's life cycle. In the current pipeline, combinations and single molecular entities (Tafenoquine**,** Artefenomel (OZ439)/ferroquine, KAF156/lumefantrine, Cipargamin, DSM265, MMV048, SJ733, P218**,** M5717, and AN13762) are able to block transmission from mosquito to the human host and others are providing chemoprotection.[34] Within the compounds that are in development, two partner drugs (artefenomel (**16**) / ferroquine (**17**) and KAF156(**18**) / lumefantrine (**15**) have progressed to phase IIb clinical development.[34] **MMV048** (**19**) is a compound discovered by

an international team led by the University of Cape Town (UCT) Drug Discovery and Development centre, H3D.[35] **MMV048** (**19**) has potential to be used as a partner drug and could treat uncomplicated malaria in a single dose.[36]

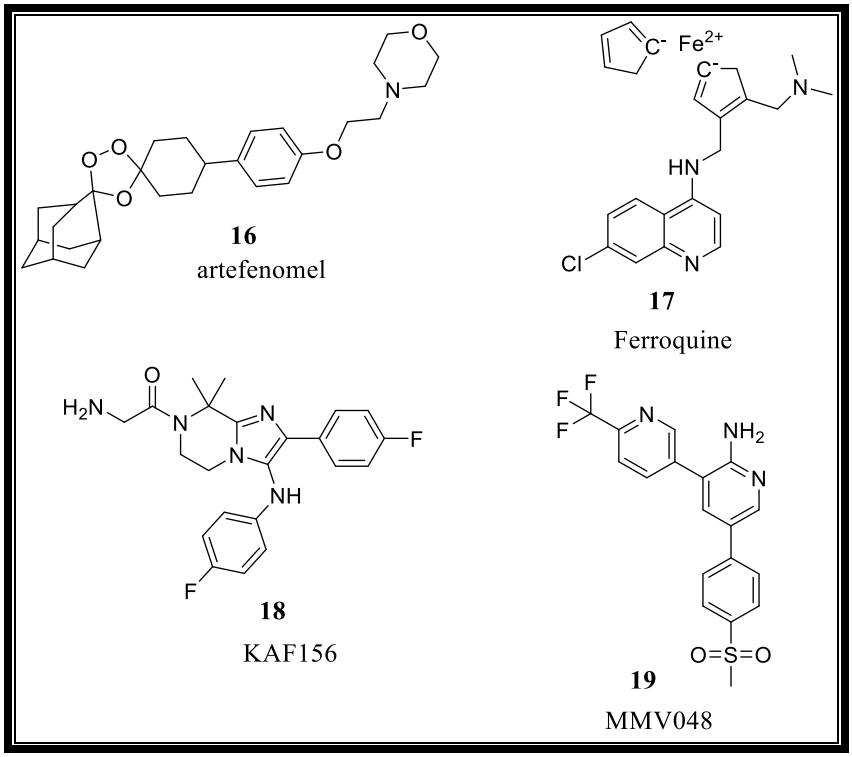

Figure 5: Selected compounds from the antimalarial drug candidate pipeline.

1.6 Solubility in drug design and development

1.6.1 Importance of solubility

Solubility is a property of a substance (solute) that is able to dissolve in a solvent (liquid and gaseous) resulting in a homogenous system. The solubility of the same solute under different conditions can vary because of the effect of the surrounding environment such as temperature, pressure and pH of the solution.[37] Saturation concentration is the concentration which cannot allow further dissolution of solute under specific conditions. Once the solution reaches saturation point, the solute will begin to precipitate out from the solution. For drugs, solubility is important because it influences how the drug must be administered to the patient, and influences absorption, distribution, metabolism and excretion (ADME).[38]

Drugs with poor aqueous solubility and low dissolution rates are associated with slow absorption, low bioavailability and gastrointestinal mucosal toxicity.[39] For drugs that are orally administered, solubility is important since it is a limiting parameter for the concentration required for the desired pharmacological effect.[39] Once administered, poorly soluble drugs may crystallize and cause acute toxicity.[40] Moreover, low solubility has caused many failures in drug development. In a classic case of poor solubility, ritonavir used to treat HIV-1 infection, was introduced in 1996 but withdrawn from market in 1998 because of a lower energy, more stable polymorph (II) appeared, causing a slowed dissolution rate of the marketed dosage form and reducing the bioavailability of the drug.[41] The equation that relates the solubility (M) of a compound with its melting point and lipophilicity (P) is as follows:

$$\text{Log[solubility (M)]} = 0.5 - (\log P) - 0.01\{[\text{melting point (°C)}] - 25\}.$$

The solubility of a solute is described by the equation as a function of two variables. For a solid solute, solubility depends on its ability to interact with water and also on its crystallinity.[42] Crystal packing and crystal lattice energy influences melting point. Disruption of crystal packing and crystal lattice energy will change the melting point and solubility.[43] LogP is the measure of interaction of the solute with water.

1.6.2 Methods to measure solubility

1.6.2.1 Kinetic and thermodynamic

There are two methods (kinetic and thermodynamic) used to measure the solubility of a compound and both have their own advantages and drawbacks. Kinetic solubility is relatively easy to perform compared to thermodynamic solubility. Kinetic solubility answers the question: “to what extent does the compound precipitate” while thermodynamic solubility answers the question: “to what extent does the compound dissolve”.[44] In kinetic solubility, the compound is dissolved in a solvent in which it is freely soluble, for instance DMSO.

Aliquots of the DMSO solutions are then added to aqueous buffer to precipitate the compound.[44] In thermodynamic solubility, the solid material is directly mixed in aqueous medium.[44] The concentration of the compound in the supernatant is taken to be its solubility. Kinetic solubility has the following advantages.

- Solubility results could be obtained within few hours.
- Easy to handle samples (oily or solid) and since they are dissolved in DMSO, this cancels the effect of solid form differences.
- Scientists are informed early to identify potential issues pertaining to poor absorption and bioassay result reliability.[45]
- Enables medicinal chemists to deduce structure-solubility relationships.[45]

Thermodynamic solubility has the following advantages.

- Allows scientists to be able to determine the required formulation for development.
- Allows scientists to plan a development strategy.
- Important for file regulatory submission.

Kinetic solubility values are relatively higher than thermodynamic ones, and with the ease associated with performing kinetic solubility, it is often used to give guidance on structure-solubility relationships.[45] Thermodynamic solubility is more accurate and its results are affected by the nature of the solid form. Chirality affects thermodynamic solubility because of the compound crystal form, e.g. *S*-ketoprofen (**20**) (**Figure 6**) and racemic *RS*-ketoprofen have different solubility values, 2.4 mg/L and 1.4 mg/L, respectively.[45] Both solubility results are a measure of the concentration of the saturated aqueous phase, which could be either determined by HPLC- or UV-methods. A drawback of using the UV-method is that it is unable to detect impurities, compound degradation, starting material or by products from

synthesis.[44] The HPLC-based method is time consuming, but offers the advantage of knowing the purity of the compound.

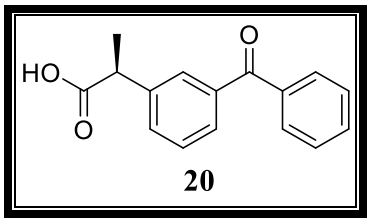

20

Figure 6: *S*-Ketoprofen structure.

1.6.2.2 Strategies to improve solubility

Chemical approaches: In these approaches, a molecule is modified by incorporating molecular features, which have the potential to improve solubility. These modifications also have the potential to either compromise or improve activity. Examples of chemical modifications strategies include introduction of hydrogen bonding, ionisable groups, disruption of molecular planarity, reducing lipophilicity, and decreasing aromaticity.

Figure 7 shows changes from parent compound to a derivative which incorporates amide and alcohol functional groups capable of forming H-bonds with water molecules.[46] Functional groups in a molecule that can participate in hydrogen bonding interactions will contribute to the overall aqueous solubility and increase the hydrophilicity of a molecule.[38] While adding more hydrogen bonding groups to a drug molecule may increase solubility, it is important to take into consideration the fact that hydrogen bonding groups may, sometimes, form intramolecular hydrogen bonds which may lead to decreased aqueous solubility.[38]

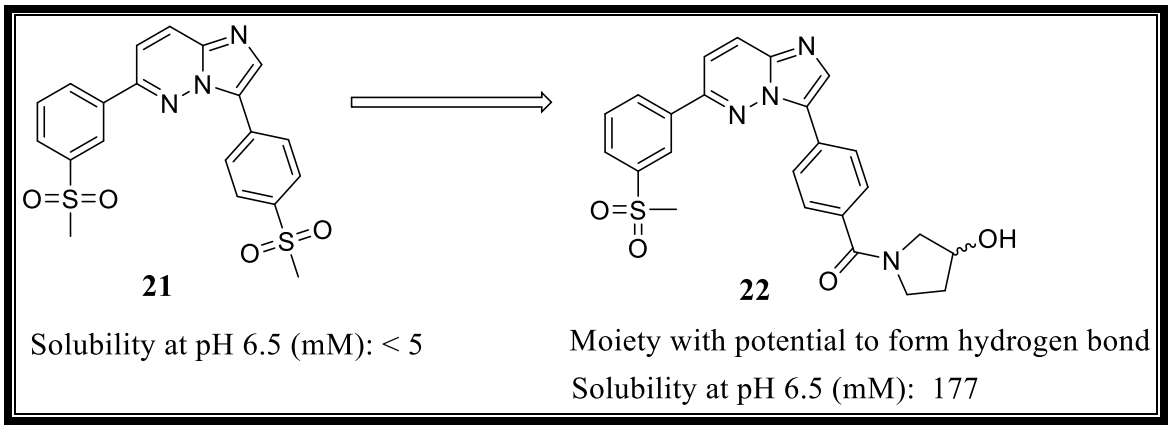

Figure 7: Examples of molecules with potential to form H-bonds.[46]

Figure 8 provides an example of a molecule with an ionisable group that contributes to improved solubility.[46] Compounds that contain ionisable groups such as amines or carboxylic acids, interact with water through ion-dipole interactions once protonated or deprotonated. The cation formed interacts with the electron rich site of the water dipole while the opposite is true for an anion.[38] As ionisable groups are introduced into the drug molecule, the distance between the resulting two ionized unlike charges should be considered. If two oppositely charged groups are too close to each other, then intramolecular interactions are favoured thereby negatively impacting solubility.[38]

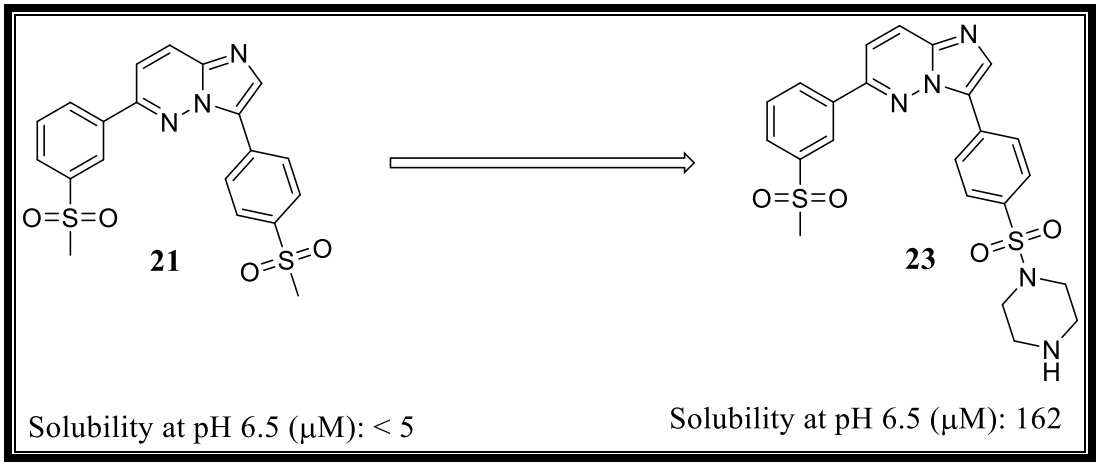

Figure 8: Example of a molecule with ionisable group.[46]

Ishikawa and co-workers have demonstrated that disruption of molecular planarity and symmetry results in an increase in solubility, **Figure 9**. They employed the following strategies to disrupt molecular planarity: increasing the dihedral angle for biaryl systems, introducing a methyl substituent at the benzylic positions and twisting fused rings.[47]

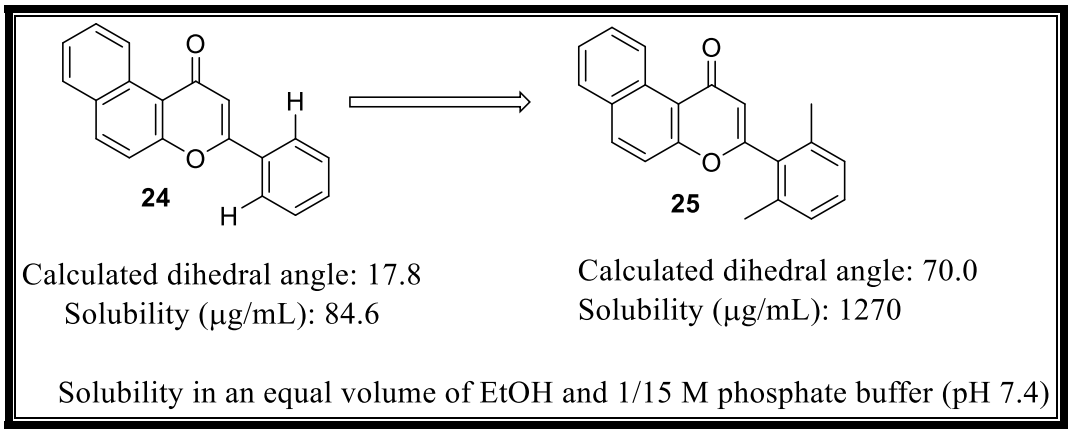

Figure 9: Example showing increase solubility by disrupting of molecular planarity or increase dihedral angle.

Increasing the number of aromatic rings in a molecular structure causes a decrease in aqueous solubility (**Figure 10**).[48] It is important to note that each ring counts as one even if it is from a fused ring system. The increased lattice energy, flatness of aromatic rings which allows greater π-stacking leads to reduced entropic contribution to the free energy of solvation.[49]

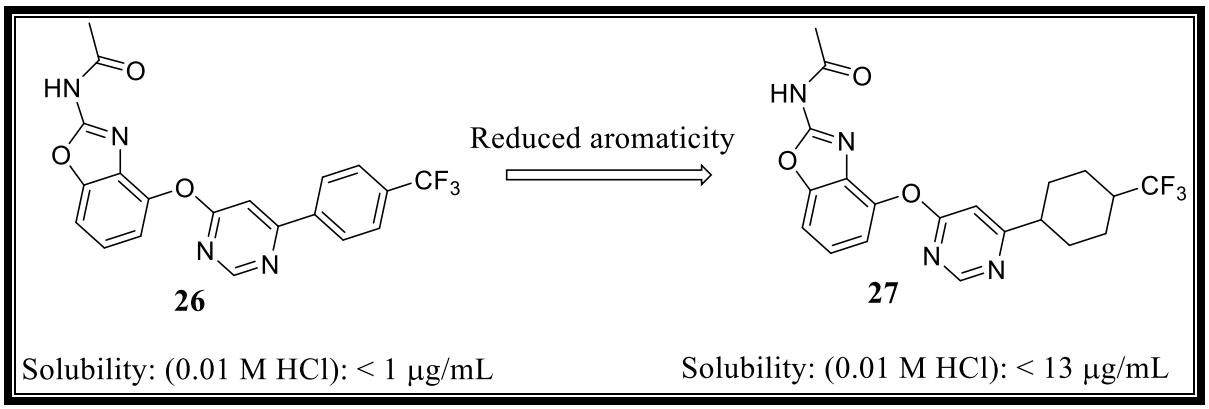

Figure 10: Impact of reducing aromaticity to improve solubility.

Lipophilicity increases as the molecule gets larger and is detrimental to aqueous solubility.[50] Lipophilicity of an unbranched hydrocarbon chain is higher than that of a branched hydrocarbon chain as exemplified in **Figure 11**.[38]

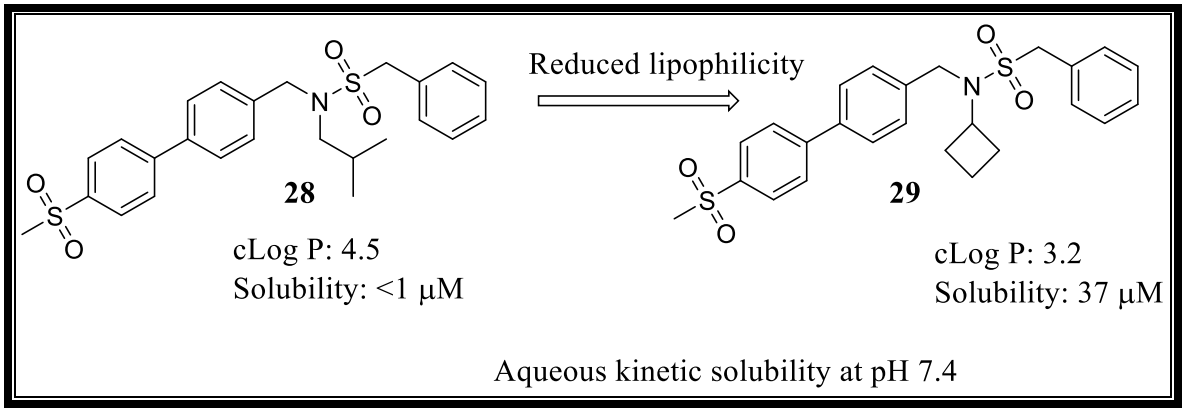

Figure 11: Example of a molecule with decreased lipophilicity.

Incorporating polar or charged groups in a prodrug to improve aqueous solubility has also been used as a strategy. **Figure 12** is an example of prodrug fosphenytoin (**30**), which is the prodrug of phenytoin (**31**).[45]

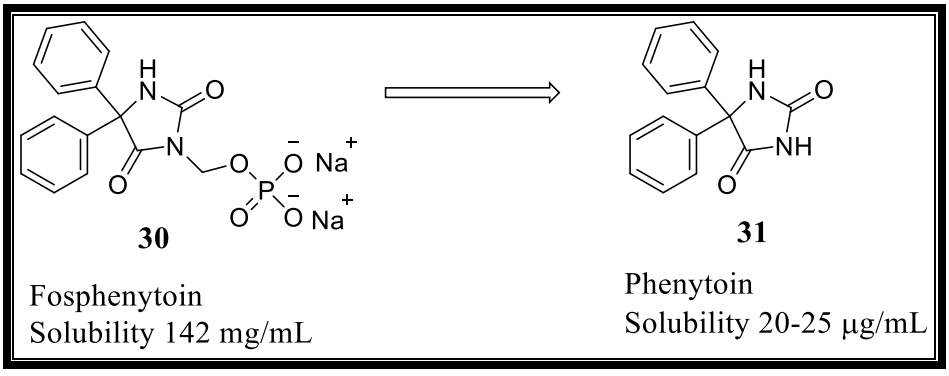

Figure 12: Prodrug strategy to improve aqueous solubility.

Physical approaches: These strategies including particle size reduction, solid depression are used to improve upon the solubility of drugs with the anticipation of not compromising the biological activity. However, with physical methods such as particle size reduction, molecules are likely to decompose/disintegrate due to mechanical stress.[51] Solid dispersion is

another technique that can be applied to improve dissolution, absorption, and therapeutic efficacy.[51] Other physical techniques to improve solubility include the use of super fluid processes, surfactants, solubilizers, cosolvency, hydrotrophy and novel excipients.[51]

1.7 Drug induced cardiotoxicity

1.7.1 The human *ether-a go-go*-related gene (hERG) K+ ion channel and its inhibition

The human *ether-a-go-go*-related gene (hERG) K^+ ion channel controls potassium current in the heart.[52] The hERG channels are inside the heart and are responsible for coordinating the electrical activity of the heart, thus controlling the heartbeat. Undesirable drug interactions with the hERG channels can cause tachyarrhythmia (torsades depointes) which can lead to sudden cardiac death.[53] This cardiac death is a consequence of the blockade of I_{Kr} current in the heart.[54,55] Drug molecules that cause the blockade of I_{Kr} are associated with elongation of the QT interval in the electrocardiogram. A number of drugs have been reported to cause abnormal cardiac muscle repolarisation and have been withdrawn from the market. Examples of such drugs include ((**32**, astemizole),(**33**, sertindole), (**44**, grepafloxacin), and (**35**,terfenadine) (**Figure 13**).[52] It is important to note that other hERG disorders are caused by mutations which may lead to long or short QT intervals.[56,57]

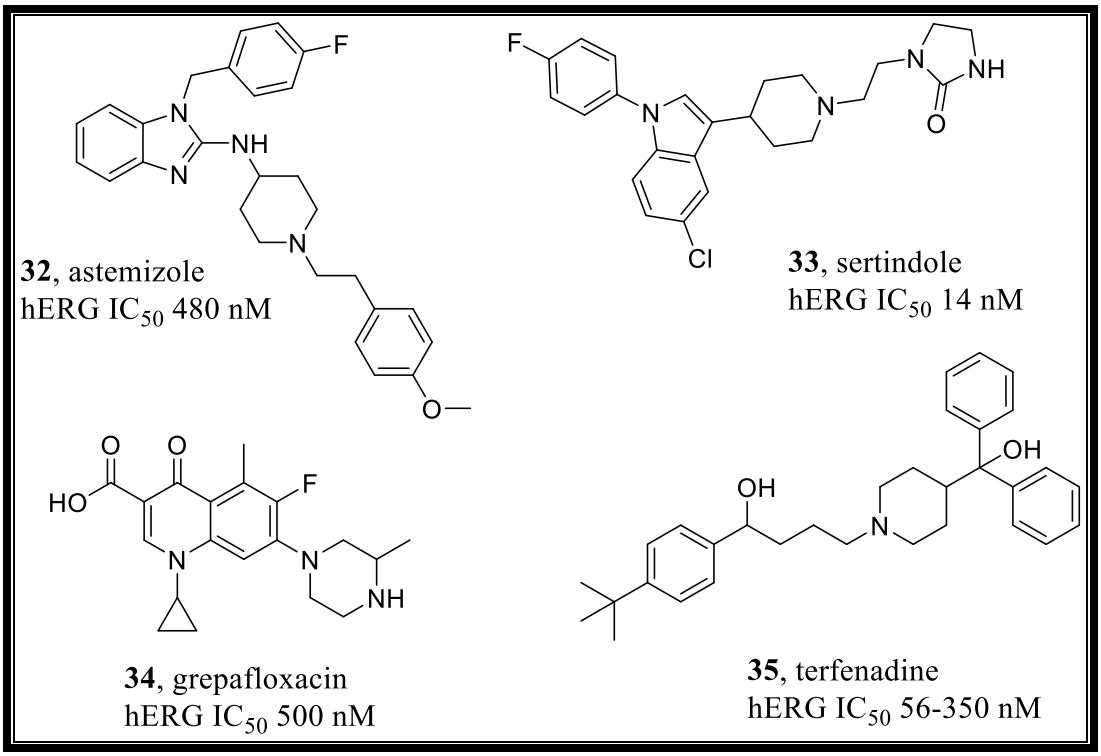

Figure 13: Drugs withdrawn from market because of hERG liability.

1.7.2 Strategies to reduce hERG potency

Compounds containing a basic nitrogen are likely to get protonated at physiological pH. The resulting ammonium cations can potentially interact with π-electrons of the aromatic residues inside the cavity of the hERG channel.[58] Therefore, decreasing the basicity of the basic nitrogen can substantially decrease the proportion of drug molecules which get protonated at physiological pH. This may disrupt π-cation interactions with the hERG channel (examples in **Figure 14**).[52] The presence of basic nitrogen is not the only pharmacophore necessary for hERG binding. The most contributing interactions to hERG activity are π-stacking and hydrophobic interactions between aromatic amino acid residues (F656 and 652) in the hERG channel and aromatic moieties in the drug molecule. Thus, it is important to consider strategies that decrease the lipophilicity of a compound. Structural changes, small or big, can disrupt these interactions and affect hERG liability. The structural changes could include introducing distal aryl rings, decreasing the flexibility of the molecule and incorporating

different stereochemistry. Incorporation of zwitterions in a molecular structure is also known to counteract hERG activity.[58] Furthermore, increasing the polarity of a molecule has the potential to decrease hERG activity since lipophilic interactions get destabilized by such changes.[52]

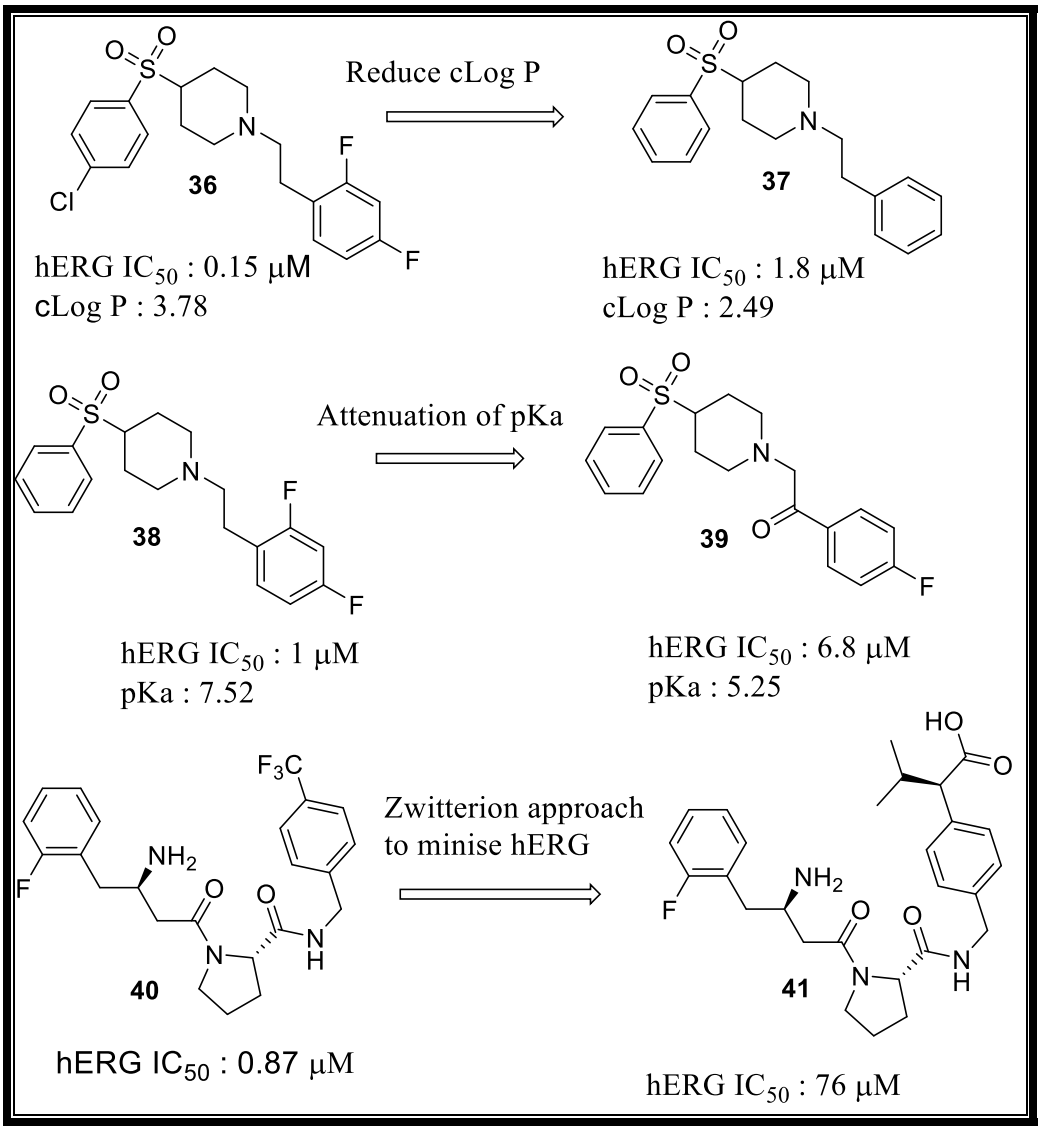

Figure 14: Examples of strategies to reduce hERG activity.

1.8 Imidazopyridazines

1.8.1 Introduction and background

Early stages of drug discovery programmes have discovered applications of imidazopyridazine-based compounds in different therapeutic areas as potential treatments for

diseases such genetic disorders, viral infections, and anxiety. In studies conducted by Sacchi and co-workers, it was demonstrated that imidazopyridazines possess anti-inflammatory, analgesic and ulcerogenic activities.[59] Identified imidazopyridazines compound **43** and **44** in **Figure 15** have been shown to inhibit key kinases including tropomyosin receptor kinase (TRK) and mammalian target of rapamycin (mTOR), which are drivers for growth, proliferation, survival, and differentiation of cancerous cells.[60,61] Proviral integration site of moloney (Pim) murine leukaemia kinases are important for cell survival and cell reproduction including other cell functions such as signal transduction pathways.[62–64] In studies conducted by Wurz *et al*, imidazopyridazine (**42**) with inhibitory effects on the Pim kinase with IC_{50} values less than 10 nM was identified.[65] Also, imidazopyridazines have demonstrated potent activity against picornaviruses (**45**) in studies conducted by Hamdouchi and co-workers.[66]

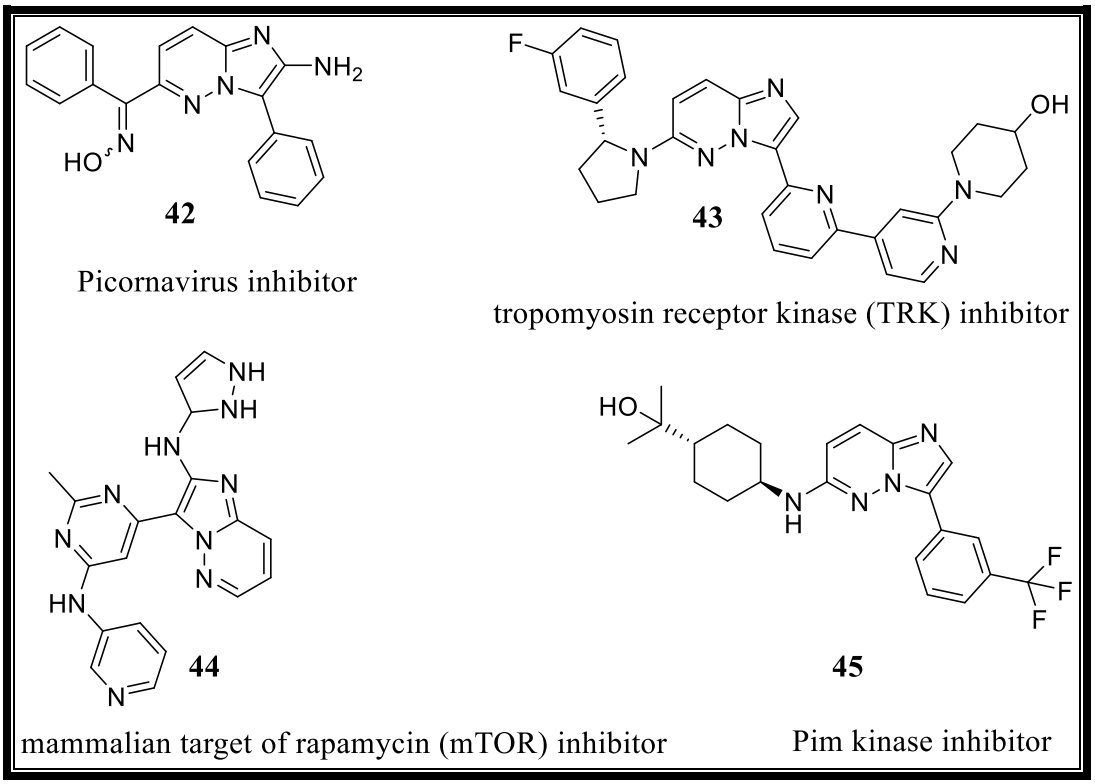

Figure 15: Examples of imidazopyridazines with other biological activities.

1.8.2 Imidazopyridazines as antimalarial agents

Imidazopyridazines have been recently reported to have activity against *P. falciparum* malaria parasites.[46,67,68] Studies conducted by McNamara, and co-workers have reported a class of derivatives of imidazopyridazines related to compound **46** (**Figure 16**) which are able to inhibit any stage of intracellular development of the *Plasmodium* parasite. They have concluded that this class of molecules are able to exert their effect by inhibiting the interaction of the natural substrate with the adenosine triphosphate (ATP)-binding pocket of phosphatidylinositol-4-OH kinase (PI(4)K).[68] Bendjeddou and co-workers have synthesized a series of imidazopyridazines to target inhibition of eukaryotic kinases, including mammalian and protozoan kinases.[69] In this study, it was found that imidazopyridazine derivatives exemplified by compound **47** (**Figure 16**) showed potent inhibition of *P. falciparum* cyclin-dependent kinase-like kinase 1 (*Pf*CLK1).[69] A target-based screening of imidazopyridazines conducted by Judith and co-workers identified a class of compounds exemplified by compound **48** (**Figure 16**), which kills the parasite at two different stages, the late schizogony stage and trophozoite stage.[70] These imidazopyridazines break the life cycle of the parasite by inhibiting cyclic guanosine monophosphate (cGMP)-dependent protein kinase (PKG) and small heat shock protein (HSP29).[70] *P. falciparum* calcium-dependent protein kinase 1 (*Pf*CDPK1) plays a crucial role in the life-cycle of the parasite. It is critical when the parasite invades red blood cells and is responsible for its motility.[71,72] In this regard, structure-activity relationships (SAR) conducted by Chapman and co-workers on a series of imidazopyridazines show selective and potent inhibition of *Pf*CDPK1.[73]

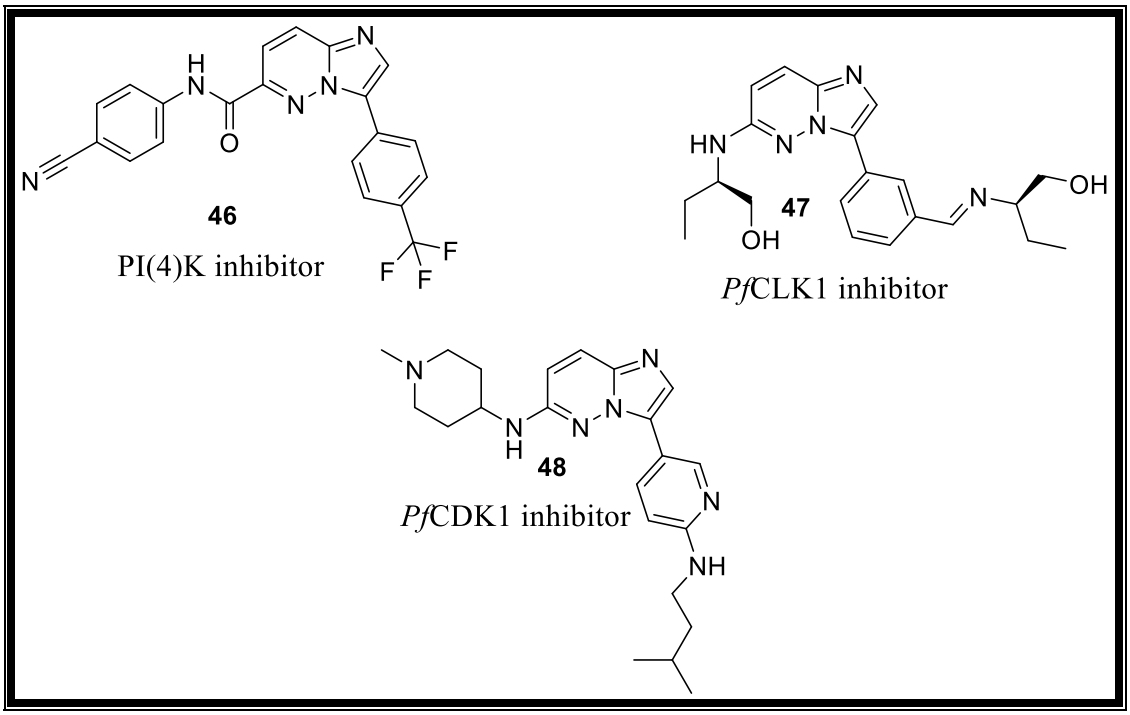

Figure 16: Selected imidazopyridazines which are kinase inhibitors of *P.f* kinases.

In studies performed by Le Manach, *et al*, antimalarial imidazopyridazines were discovered through whole cell high throughput screening (HTS) of a SoftFocus library. In a sub-library named SFK52 and 488 diaryl-imidazopyridazines hits were identified (**Figure 17**).[67] Hit compounds that showed potency at a screening concentration of 1.82 μM were selected and resynthesized. The compounds were tested for activity against the sensitive (NF54) and resistant (K1) strains of *P. falciparum* and compounds showing potency (IC_{50}) between 15 nM to 25 nM were identified. The three hit compounds displayed undesirable *in vitro* ADME properties, and were also found to have high human hepatic extraction ratio (E_H) > 0.8. Compounds **49** and **50** were chosen as starting points for medicinal chemistry optimization. The optimization of potency through SAR led to the discovery of the lead compound (**MMV652103**) shown in **Figure 17**. However, this compound was characterized by poor solubility at pH 6.5 (< 5 μM) although slight improvement was observed under acidic conditions.[46] Moreover, the lead compound showed a hERG (IC_{50} = 0.9 μM) inhibition

liability. In an attempt to increase solubility and de-risk hERG binding, Le Manach, *et al*., synthesized analogues with decreased lipophilicity by replacing phenyl rings with pyridyl rings after which the compounds showed weakly improved solubility. Solubility was also found to substantially improve after introducing substituents containing amide groups and other water solubilising H-bonding groups. Some analogues also displayed high solubility (> 100 μM) while maintaining high activity against the *Pf*NF54 strain (IC_{50} < 35 nM). Solubility was also found to increase when the sulfones was substituted with sulfoxides, which are strongly involved in hydrogen bonding compared to the former and led to the discovery of compound **52** which showed improved solubility and improved *in vivo* efficacy. Selected compounds, which were evaluated for hERG inhibition were found to be highly potent on this channel with IC_{50} containing value of 0.3-0.4 μM.

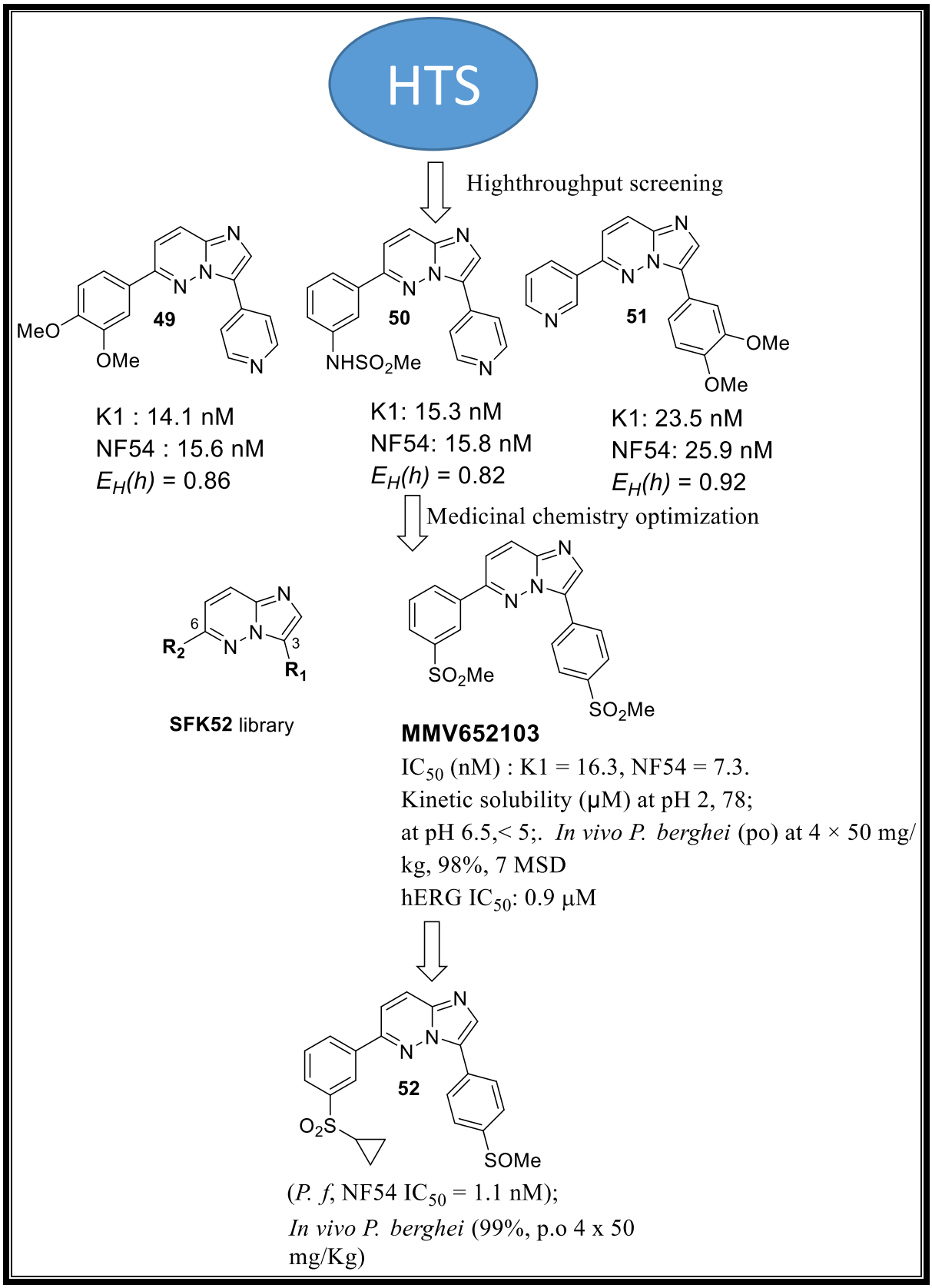

Figure 17: General structure of hit compounds identified from an SKF52 sub-library and the lead compound **52** resulting from medicinal chemistry optimization.

1.9 Research programme

1.9.1 Study justification

Naturally, parasites evolve. This evolution has led to the development of resistance to many once effective antimalarials such as chloroquine and sulfadoxine-pyrimethamine as already described in the introduction part of this dissertation.[74] Recently, emerging resistance to the current frontline treatment option, the ACTs, has been reported on the Thai-Cambodia boarder and Vietnam.[75,76] Additionally, resistance to amodiaquine, one of the partner drugs in ACTs has been reported in South America, Asia and East Africa.[77] The parasite's resistance to available drugs necessitates efforts to find new drugs with a different mechanism of action. Furthermore, antimalarials with multistage activity on different stages of parasite development are needed. These could potentially offer prophylaxis, block transmission, prevent relapse and relieve clinical symptoms. The search for new antimalarials is also motivated by the need to find medicines that could cure malaria in a single dose thereby avoiding patient compliance issues associated with prolonged multiple dosing regimens.[9]

Imidazopridazines have shown diverse range of pharmacological properties and, are structurally novel compared to clinically used antimalarials. As already mentioned, studies conducted by Le Manach *et al*, have identified imidazopyridazine compounds with potent antiplasmodium activity but with liabilities, including strong off target activities such as hERG inhibition and poor aqueous solubility.[46,67] This project was designed to address the poor aqueous solubility and cardiotoxicity risk that could arise from hERG inhibition of imidazopyridazine compounds identified by Le Manach *et al*.

1.9.2 Research hypothesis

The research question is whether it will be possible to identify imidazopyridazine-based antimalarial drug leads with favourable solubility and hERG properties.

1.9.3 Objective

To optimise the solubility and cardiotoxicity risk profile of antimalarial imidazopyridazines.

1.9.4 Specific aims

i) Synthesis and characterization of antimalarial imidazopyridazines designed to improve solubility and hERG inhibition profiles.

ii) Profiling of synthesized compounds with respect to antiplasmodium activity and solubility.

iii) Derivation of antiplasmodium structure-activity relationship (SAR) as well as solubility structure property relationship (SPR) profiles.

iv) Investigation of factors (e.g. melting point, calculated dihedral angle by single X-ray and/or Density Functional Theory calculations, CLogP, and retention time on reversed-phase HPLC) affecting solubility and deduce relationships.

v) Submission of the selected frontrunner compounds with potent antiplasmodium activity for cytotoxicity and hERG profiling.

Chapter Two

2.1 Introduction

This chapter describes the design, synthesis and spectroscopic characterisation of imidazopyridazine analogues. **Figure 18** shows the core scaffold of imidazopyridazines. Previous studies conducted by Le Manach, *et al* have identified substituent positions around the core-scaffold which are optimal for potent antiplasmodium activity.[67] In this regard, a series of compounds were synthesized to further expand the SAR at positions 3 and 6 of the scaffold. ^{1}H-NMR, ^{13}C-NMR, Correlation Spectroscopy (COSY), Heteronuclear Single Quantum Coherence (HSQC) spectra and LCMS were used to confirm the molecular structure. LCMS was also used to determine purity.

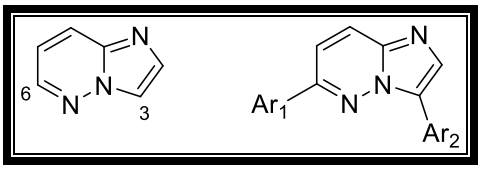

Figure 18: Imidazopyridazine core scaffold.

2.2 Rationale and design

Target compounds were designed with structural modifications aimed at improving solubility, and decreasing hERG channel inhibition activity while potentially retaining and/or improving good antiplasmodium activity.

In their previous studies, Le Manach and co-workers, reported imidazopyridazine-derived analogues that are *meta*-substituted on the phenyl ring at position R_2 (**Figure 19**), which retained good antiplasmodium activity. Where the *meta*-substituent was a sulfoxide, solubility was also improved.[46] Based on these observations, a *meta*-substituted phenyl ring with a sulfoxide group at position R_2 was fixed, while making modifications on the right hand side (RHS) of the molecule. On the RHS portion at R_1, amide functionalities at the *para*

position of the phenyl ring were incorporated. This was guided by prior SAR findings by Le Manach and co-workers who established that the *para* position on the RHS phenyl ring was optimal for potency. Introduction of the amide functionality was also inspired by the need to introduce hydrogen bonding groups to potentially enhance solubility by forming hydrogen bonding interactions with water molecules.[46] It was also observed previously that compounds containing amide bonds had reduced hERG inhibition activity.[46]

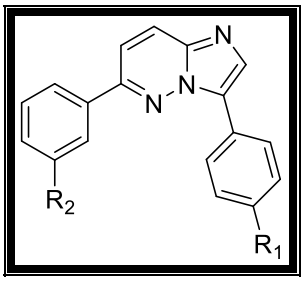

Figure 19: Diarylated imidazopyridazine scaffold showing a fixed substistuent R_2 and point of derivatization R_1.

In this project, an array of different amido compounds was proposed for synthesis in order to expand the scope of SAR studies (**Figure 20**). Such (amide bond) water solubilizing molecular features in the proposed compounds would be expected not only to improve water solubility but potentially discourage lipophilic drug-hERG binding interactions. In addition, some polar analogues **57**, **58, 60**, **62**, **66**, **67**, **68**, **69**, and **70** incorporated additional water solubilising groups on the amidated side chain and ring. The sulfoxide version of analogue **74** has been found to be highly potent (NF54: IC_{50} < 50 nM) in recent work (unpublished data). In this regard, the sulfone was synthesized since sulfoxides are expected to be converted to sulfones *in vivo*.

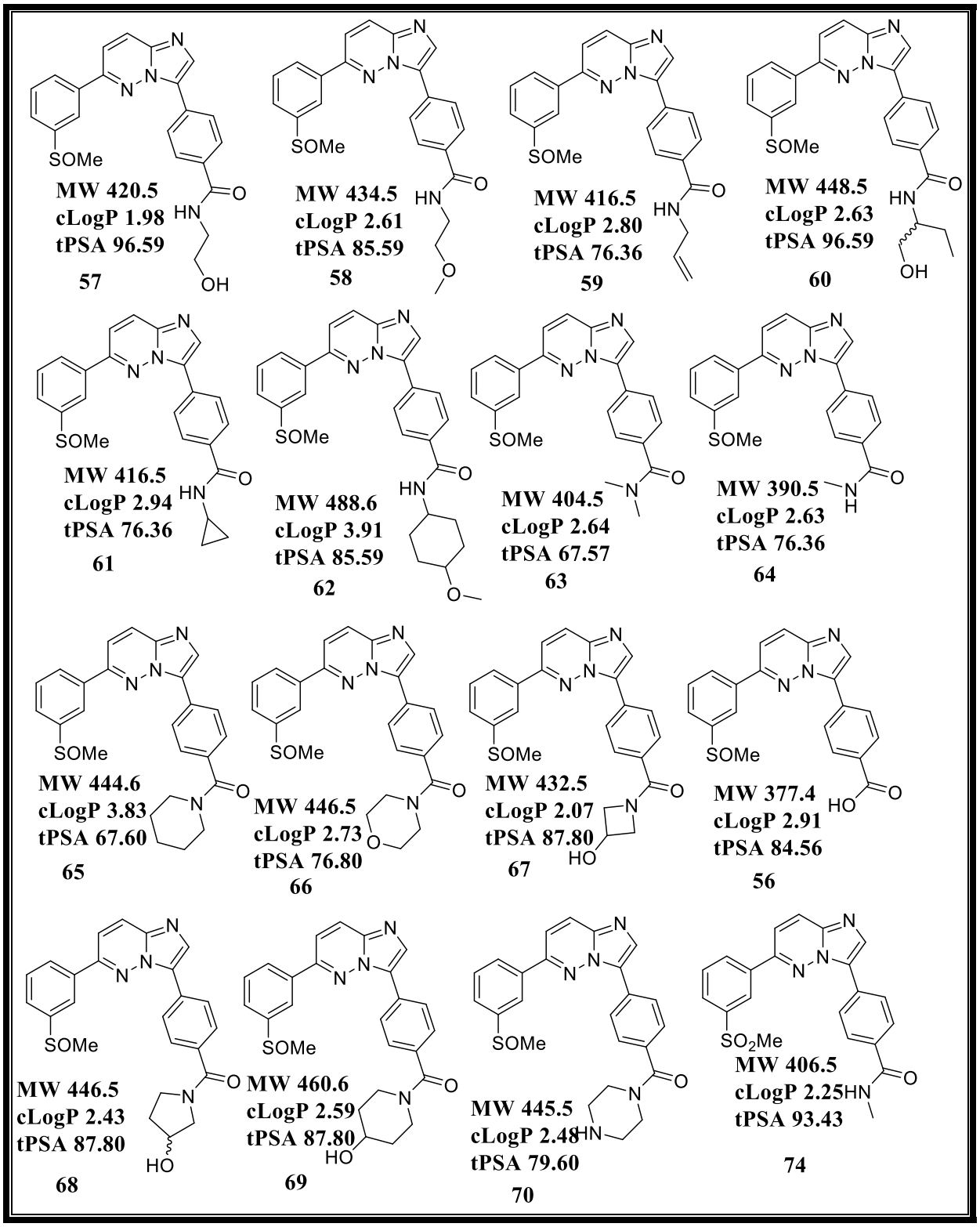

Figure 20: Analogues synthesized for Series 1 studies. MW, molecular weight (g/mol); tPSA, total polar surface area (Å^2); cLogP, calculated partion coefficient.

The results from Series 1 were used as a guide towards structural modifications executed in Series 2 (**Figure 21**). In this regard, structural modifications from Series 1 that preserve potent antiplasmodium activity, lower hERG activity and improved solubility were implemented in the next generation analogues of Series 2.

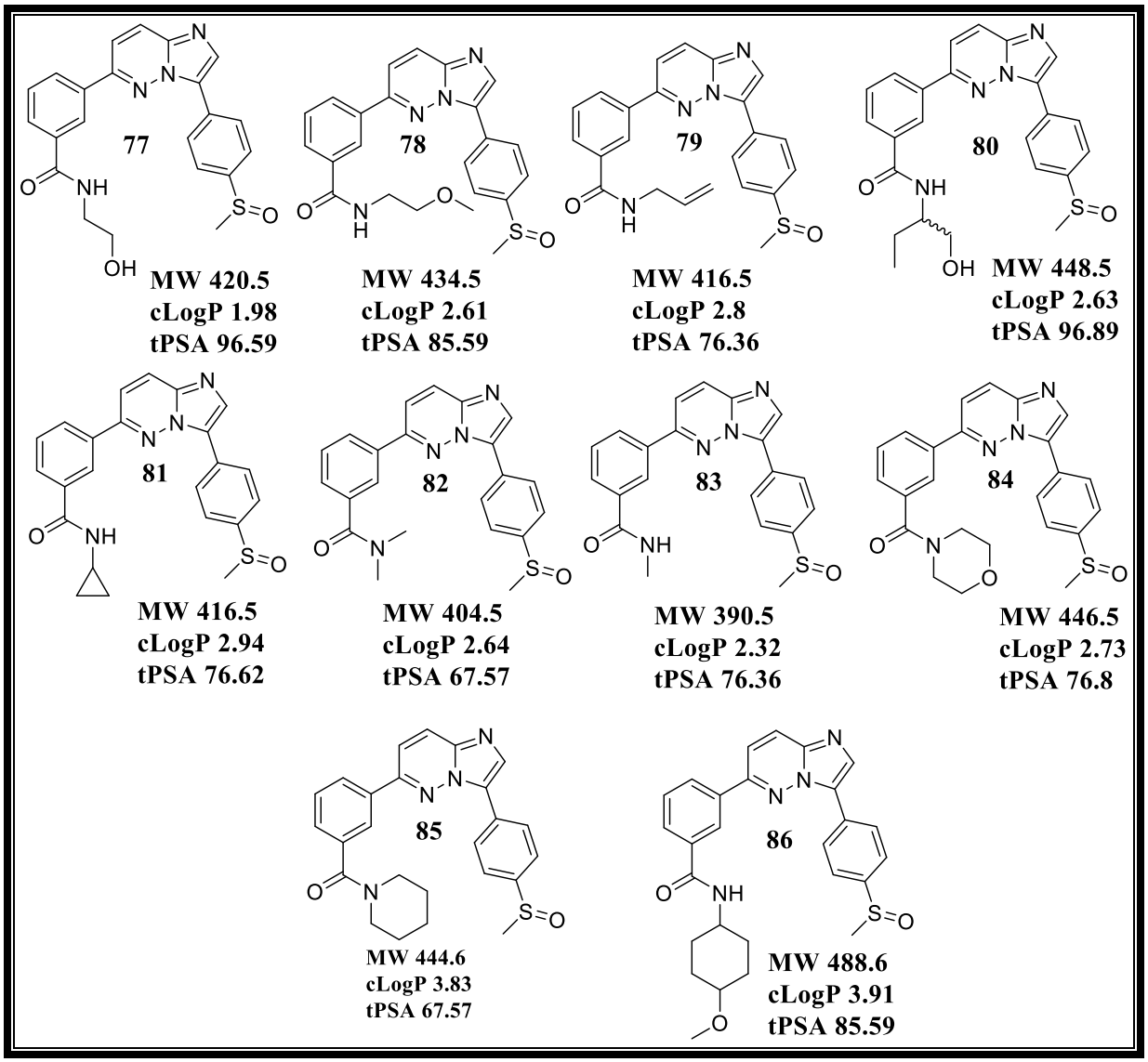

Figure 21: Analogues synthesized for Series 2 studies. MW, molecular weight (g/mol); tPSA, total polar surface area (Å^2); cLogP, calculated partion coefficient.

2.3 Chemistry for Series 1

Intermediate **53** was prepared by a condensation/cyclization reaction of commercially available 3-amino-6-chloropyridazine with bromoacetaldehyde diethyl acetal in the presence of aqueous HBr **(Scheme 1)**.[67] A regioselective iodination was performed with *N*-iodosuccinimide (NIS) to give **54** in good yield. The iodinated compound was then subjected to a regioselective Suzuki-Miyaura coupling reaction with 4-carboxyphenylboronic acid to afford **55** in moderate yield. A second Suzuki-Miyaura reaction with (3-(methylsulfinyl)phenyl)boronic acid gave the sulfoxide-substituted intermediate **56** in reasonable yield.[67] A final acid catalyzed amide coupling step in the presence of propylphosphonic anhydride (T3P) to give the target compounds for Series 1.

The sulfone-deravative analogue **74** was synthesized via a different intermediate **73** in **Scheme 2**. Where the chloro-substituted pyridazine intermediate **53** was subjected to a Suzuki-Miyaura reaction with (3-(methylsulfonyl)phenyl)boronic acid to obtain the intermediate **71**, which was then iodinated in the presence of NIS to give **72** in good yield. A second Suzuki-Miyaura coupling on this intermediate then delivered the benzoic acid intermediate **73** in low yield. An amide coupling in the presence of T3P gave **74** in poor yield. The final target compounds with their respective yields are summarised in **Table 2**.

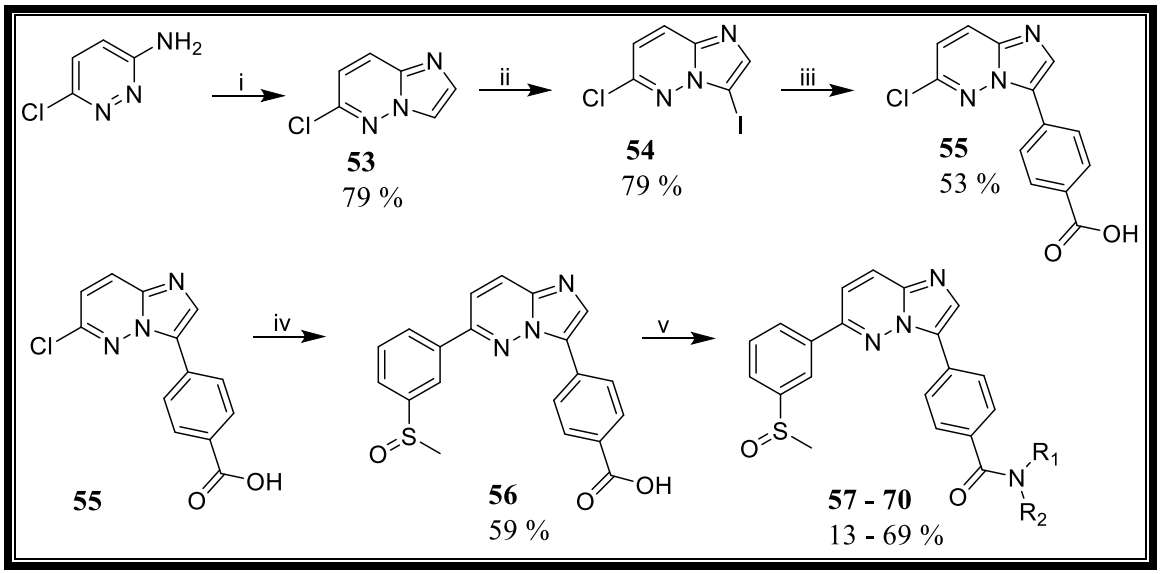

Scheme 1: Synthetic scheme for the synthesis of amidated imidazopyridazine analogues **57–70**: *Reagents and conditions* (i) $BrCH_2CCH(OEt)_2$, HBr, EtOH/H_2O, 103 °C , 16 h; (ii) NIS, DMF, 30 °C, 6 days; (iii) 4-carboxyphenylboronic acid, $Pd(PPh_3)_2Cl_2$, 1M K_2CO_3, DMF, 80 °C, 12 h; (iv) 3-methylsulfinylphenylboronic acid, $Pd(PPh_3)_2Cl_2$, 1M K_2CO_3, DMF, 100 °C, 16 h; (v) appropriate amine or amine hydrochloride salt, 50 % T3P in EtOAc, DIPEA, DMF, 0–50 °C, 3–16 h;

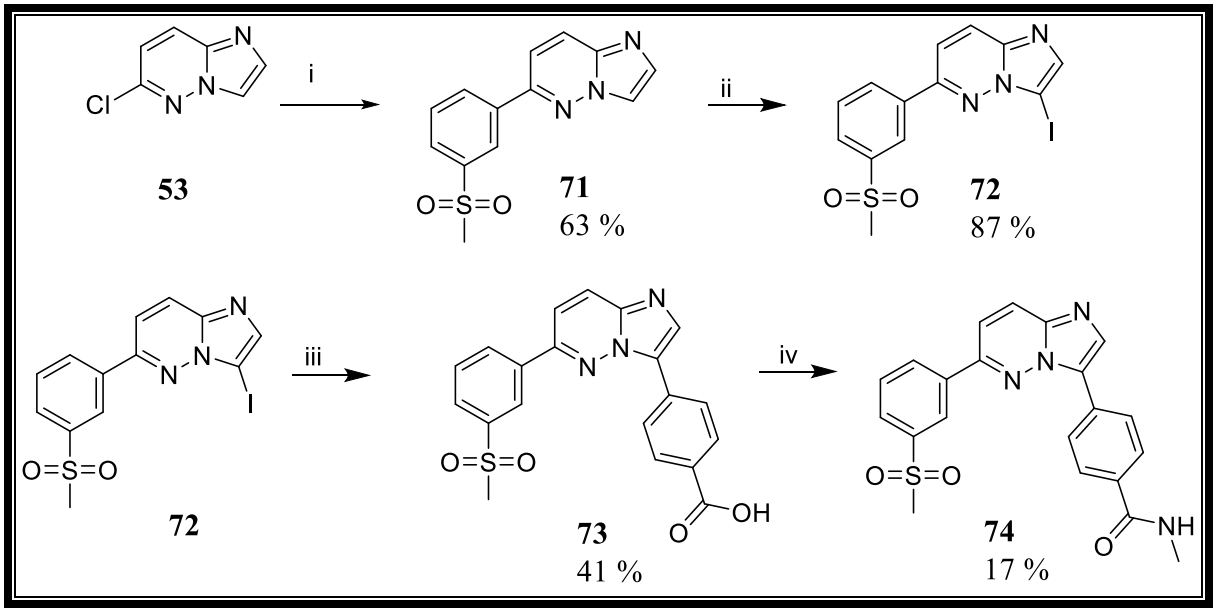

Scheme 2: Synthetic scheme for the synthesis of amidated imidazopyridazine analogue **74**: *Reagents and conditions* (i) 3-methylsulfonylphenylboronic acid, $Pd(PPh_3)_2Cl_2$, 1M K_2CO_3, DMF, 100 °C, 19 h; (ii) NIS, DMF, 35 °C, 3 days; (iii) 4-carboxyphenylboronic acid, $Pd(PPh_3)_2Cl_2$, 1M K_2CO_3, DMF, 80 °C, 15 h; (iv) methyl amine hydrochloride salt 50 % T3P in EtOAc, DIPEA, DMF, 50 °C, 3 h.

Table 2: Series 1 derivatives with respective % yields.

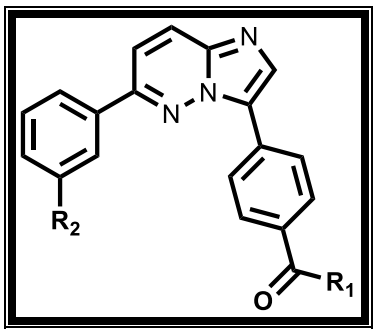

Compound code	R_2	R_1	Yield (%)
56	SOMe		59
57	SOMe	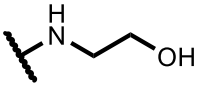	13
58	SOMe	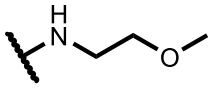	69
59	SOMe	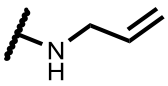	14
60	SOMe	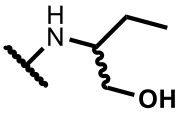	38
61	SOMe	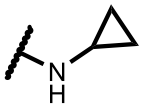	43
62	SOMe	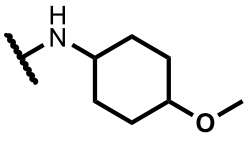	40
63	SOMe		40
64	SOMe		29

65	SOMe	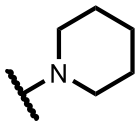	27
66	SOMe	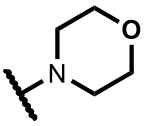	47
67	SOMe	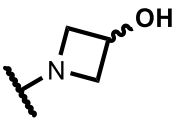	13
68	SOMe	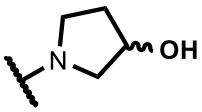	20
69	SOMe	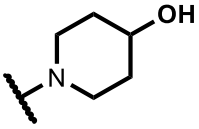	9
70	SOMe	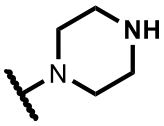	5
74	SO_2Me		17

2.3.1 ^{1}H-NMR, ^{13}C-NMR interpretation

The one-dimensional ^{1}H-NMR and ^{13}C-NMR spectra were processed using MestReNova v10.0.2-15465. Multiplicity patterns are reported using the following abbreviations s = singlet, d = doublet, t = triplet, m = multiplet, dd = doublet of doublets, br s = broad singlet, br m = broad multiplet, t = triplet, dt = doublet of triplets, dq = doublet of quartet. Coupling constants (*J* values) are reported in Hertz (Hz). Where assignment of ^{1}H-NMR and ^{13}C-NMR signals was ambiguous, two-dimensional NMR spectra from COSY, and HSQC spectroscopy were acquired to facilitate accurate assignments. The Attached Proton Test (APT) was

employed to identify negative and positive carbons. All final compounds were subjected to purity check experiments using LC-MS to ensure an acceptable level of purity (≥ 95%).

2.3.2 Mechanism and characterisation for the cyclization of bromoacetaldehyde diethyl acetal with 6-chloropyridazin-3-amine (Step I, Scheme 1)

The reaction mechanism involved in the generation of intermediate **53** begins with protonation of bromoacetaldehyde diethyl acetal by a Brønsted acid to produce a resonance-stabilized oxonium ion with elimination of EtOH (**Scheme 3**).[78] The stabilized oxonium ion is attacked by a water molecule whereafter intramolecular proton transfer and loss of EtOH leads to the formation of the protonated aldehyde. A nucleophilic addition of 6-chloropyridazin-3-amine to the protonated aldehyde then affords a hydroxyl intermediate which upon intramolecular proton transfer undergoes elimination of water to form an iminium ion intermediate, which is then converted to the corresponding imine intermediate upon deprotonation by the water molecule. An intramolecular attack by the pyridazine nitrogen onto the alkyl bromide then leads to a cyclized intermediate from which water abstracts a proton leading to the aromatized product **53.**

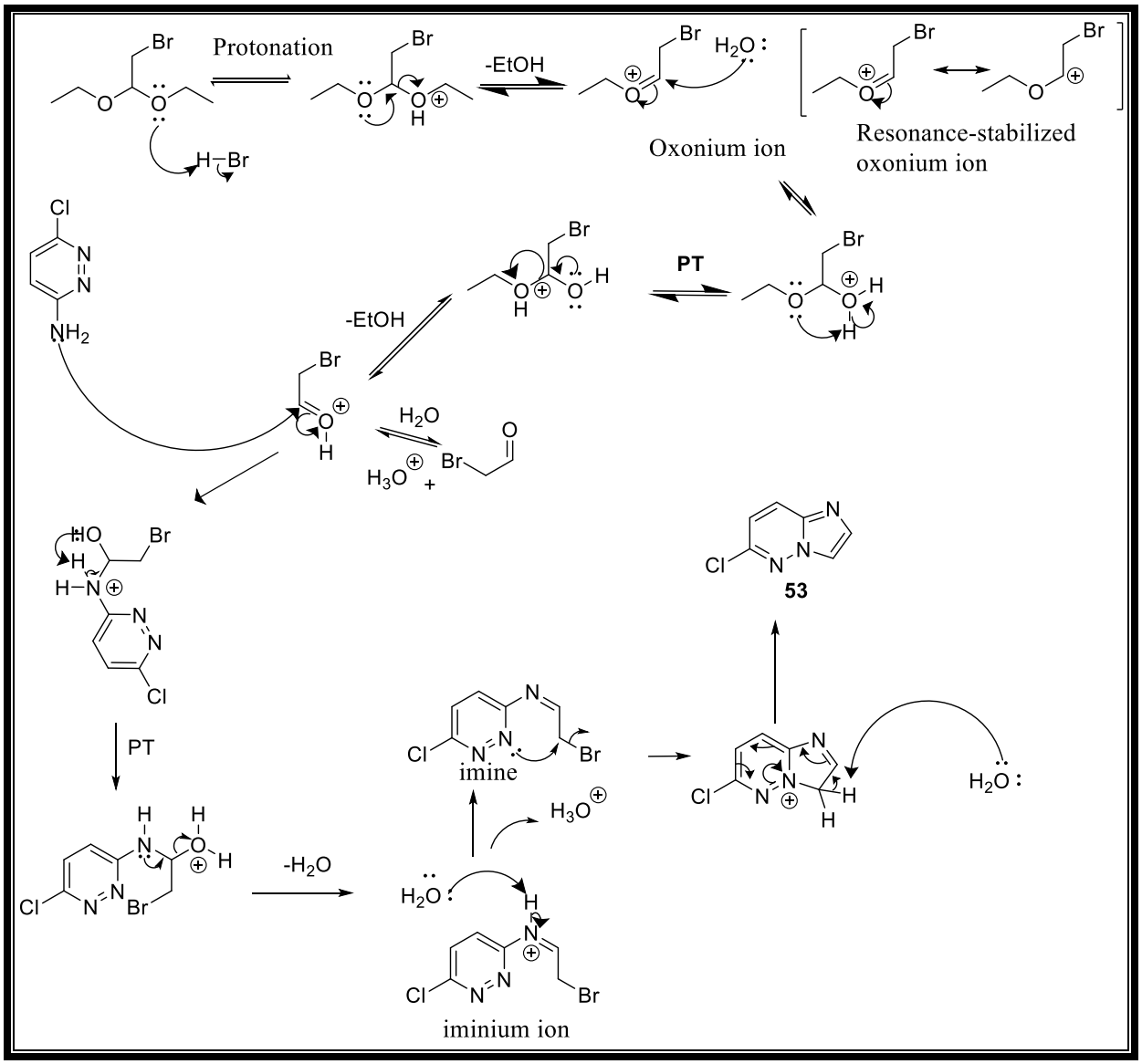

Scheme 3: Mechanism for the formation of the intermediate **53** from 6-chloropyridazin-3-amine in the presence of HBr.

The structure of intermediate **53** was confirmed by ^{1}H-NMR spectroscopy as shown in **Figure 22.I**. A broad peak at δ 8.12–8.10 ppm was assigned to H7, which integrates for 1H. Typically this broad peak is observed as a doublet. However, due to the sensitivity of the NMR instrument, peak broadening was observed, resulting in the doublet coalescing to form a broad peak. Two doublets resonating at 8.02 ppm (J = 9.5 Hz) and 7.78 ppm (J = 1.3 Hz) integrating for 1H each were assigned to H6 and H8, respectively. Lastly, a relatively shielded doublet integrating for 1H, was observed at 7.28 ppm with a J-value of 9.5 Hz and

was assigned to the aromatic proton H1. Six carbon peaks in the ^{13}C-NMR spectrum of **53** were observed (**Figure 22.II**) and an LC-MS of the pseudomolecular ion was observed at *m/z* $[M + H]^+$ = 154.1 shown in **Figure 22.III**.

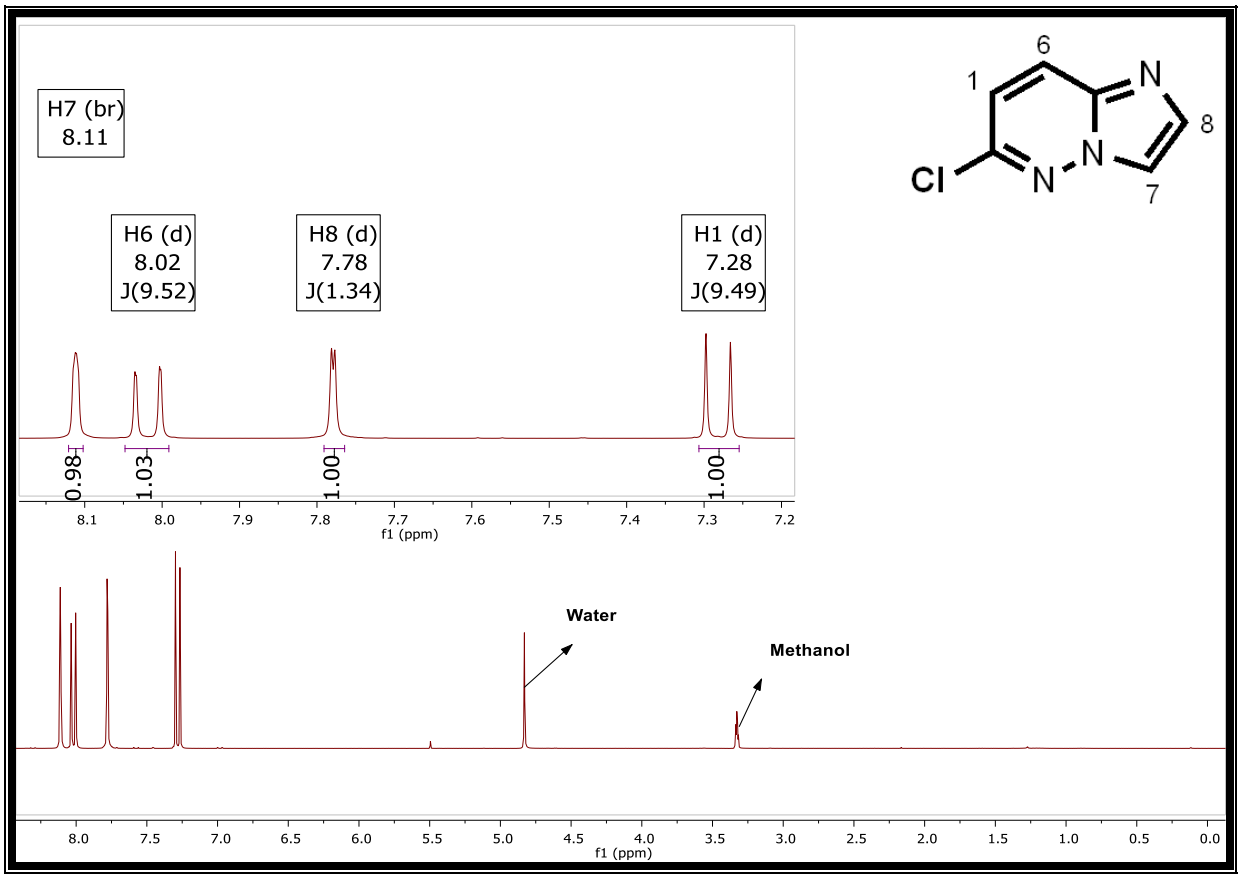

Figure 22.I: ^{1}H-NMR spectrum of **53** at 300 MHz in methanol-d_4.

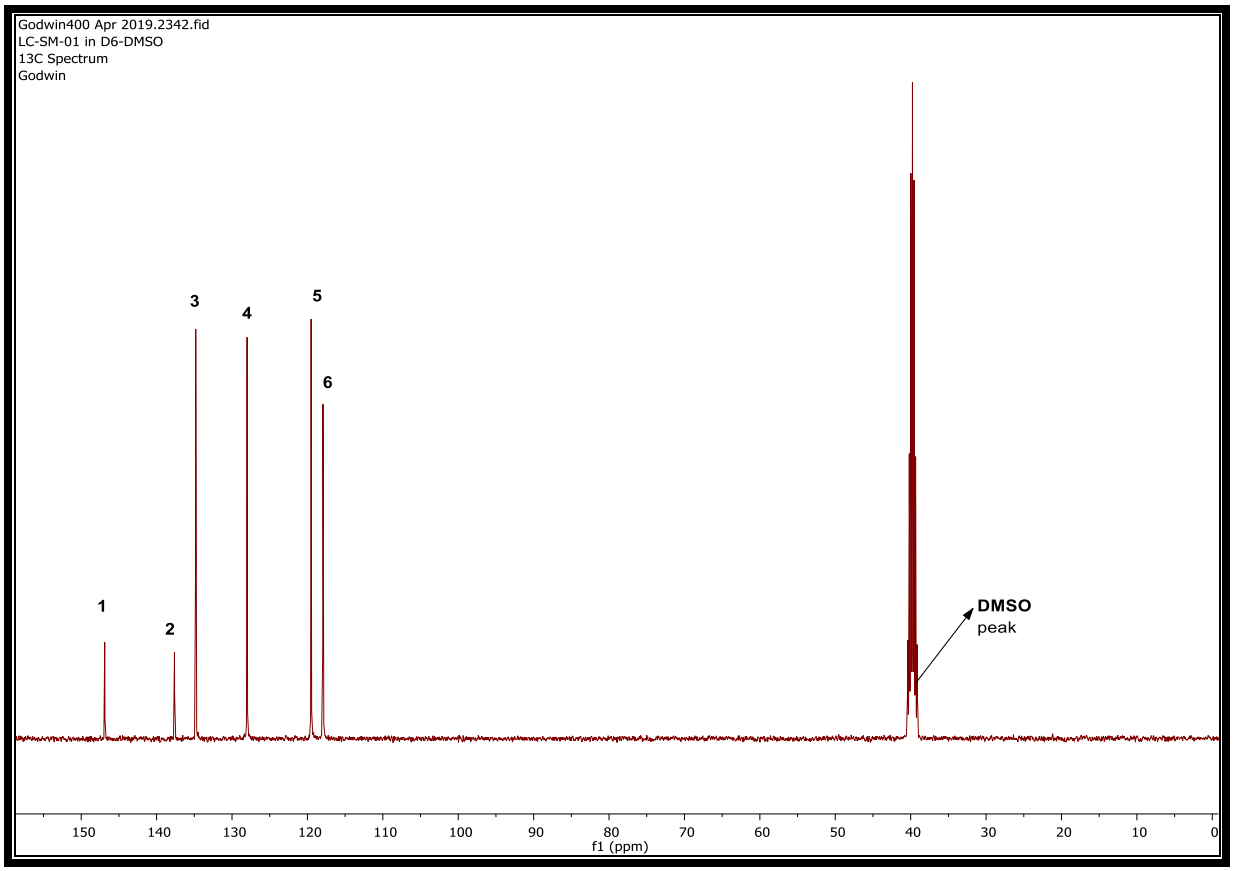

Figure 22.II: ^{13}C-NMR spectrum of **53** at 300 MHz in DMSO-d_6.

Method Info : Standard 2.2min method with 254nm, 280nm and 290nm and positive ESI mode 100-800m/z

Additional Info : Peak(s) manually integrated

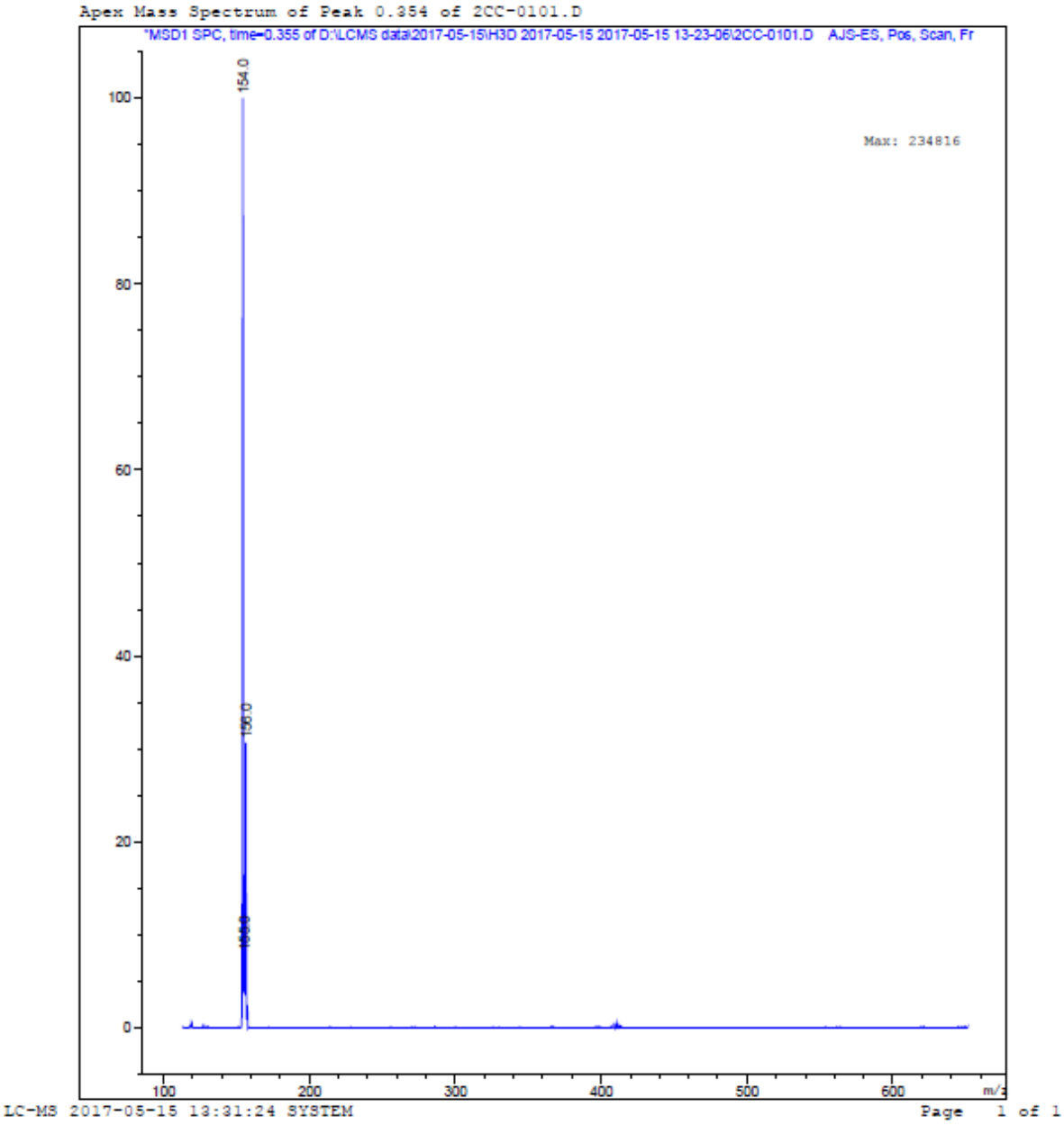

Figure 22.III: LC-SM chromatogram of compound **53**.

2.3.3 Mechanism and characterisation for the iodination of 53 (Step II, Scheme 1)

Iodination of intermediate **53** was regiospecific with only the most nucleophilic carbon being iodinated.[79] NIS was used as a source of electrophilic iodine, whilst the electron rich π-bond from the five-membered ring in compound **53** acted as the nucleophile (**Scheme 4**).

Iodination on the six-membered ring of **53** is not possible as the carbons on this ring are less nucleophilic compared to the carbons on the five-membered ring. The second carbon in the five-membered ring does not undergo iodination because electrophilic attack at this carbon would lead to an unstable arenium intermediate with highly unstable resonance contributors.

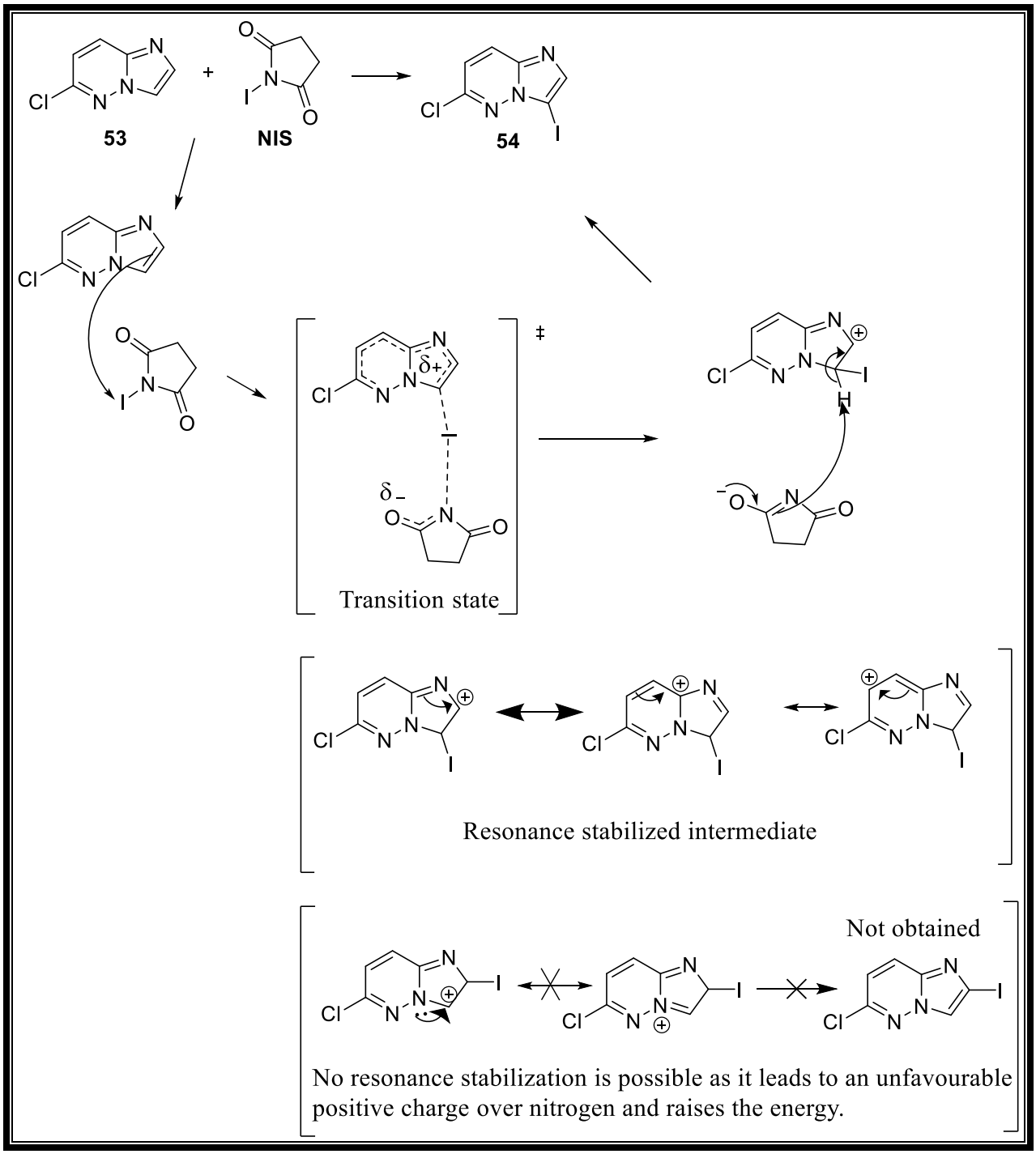

Scheme 4: The mechanism of reaction for the formation of **54** in the presence of NIS.

Successful iodination of compound **53** to obtain compound **54** was confirmed by ^{1}H-NMR spectroscopy. The ^{1}H-NMR spectrum (**Figure 23**) shows the iodinated product **54** with the disappearance of a doublet and appearance of a new singlet peak in the aromatic region. A singlet was observed at 7.87 ppm, integrating for 1H and was assigned to H8. The two doublets at 8.02 (J = 9.5 Hz) and 7.34 (J = 9.5 Hz) ppm were assigned to H6 and H1, respectively. Five carbon peaks in the ^{13}C-NMR spectrum of **54** were observed, and on LC-MS, a pseudomolecular mass ion was observed at m/z $[M + H]^{+}$ = 279.7.

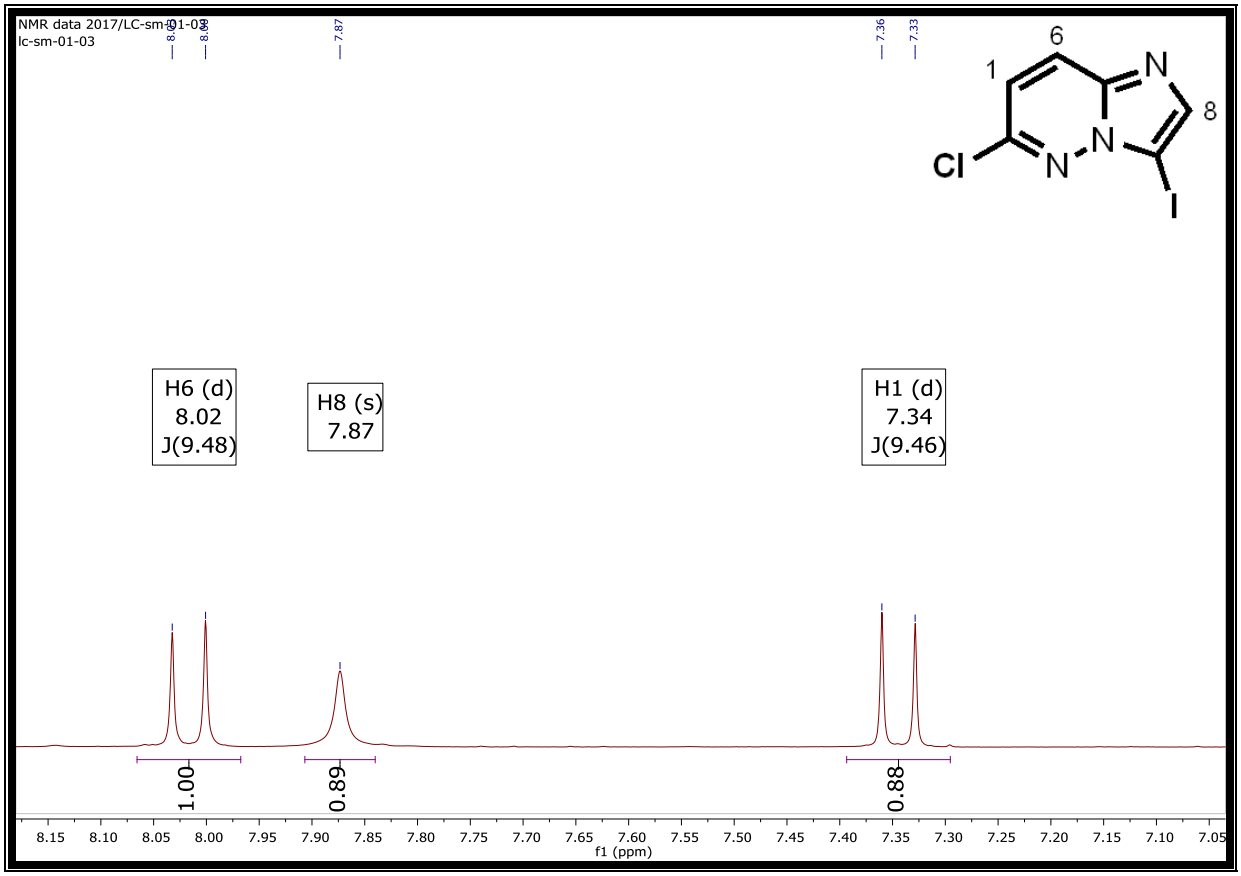

Figure 23: ^{1}H-NMR spectrum of **54** at 300 MHz, in methanol-d_4.

2.3.4 Mechanism and characterisation for formation of compound 55 (Step III, Scheme 1)

The Suzuki-Miyaura cross coupling reaction mechanism is shown in **Scheme 5**. Suzuki-Miyaura reactions are highly regioselective and this selectivity depends on the nature of the

carbon-halogen bond strength.[78,80] The carbon-halogen bond strength tends to decrease down the halogen group in the periodic table and this effect makes oxidative addition (first step in the catalytic cycle) difficult for the chlorine while iodine undergoes oxidative addition relatively easily.[80] The halogen-carbon bond strength decreases down the group hence the carbon-iodo bond requires less energy for oxidative addition to occur compared to the carbon-chloro bond, which requires high temperature reaction conditions for oxidative addition to occur. Hence, the reaction for the substitution of chloro was carried out at a much higher temperature of 100 °C (in the preparation of **56**) while iodine substitution was carried out at 80 °C (in the preparation of **55**). In the first step, oxidative addition of the iodo-derived substrate **54**, generates a palladium (II) intermediate. The second step of the catalytic cycle is transmetalation which is known to be slow, hence the base (K_2CO_3) was used to speed up this step.[78] The ligands around the Pd(II) complex then rearrange into a *cis* orientation for reductive elimination to occur which regenerates the palladium (0) catalyst.

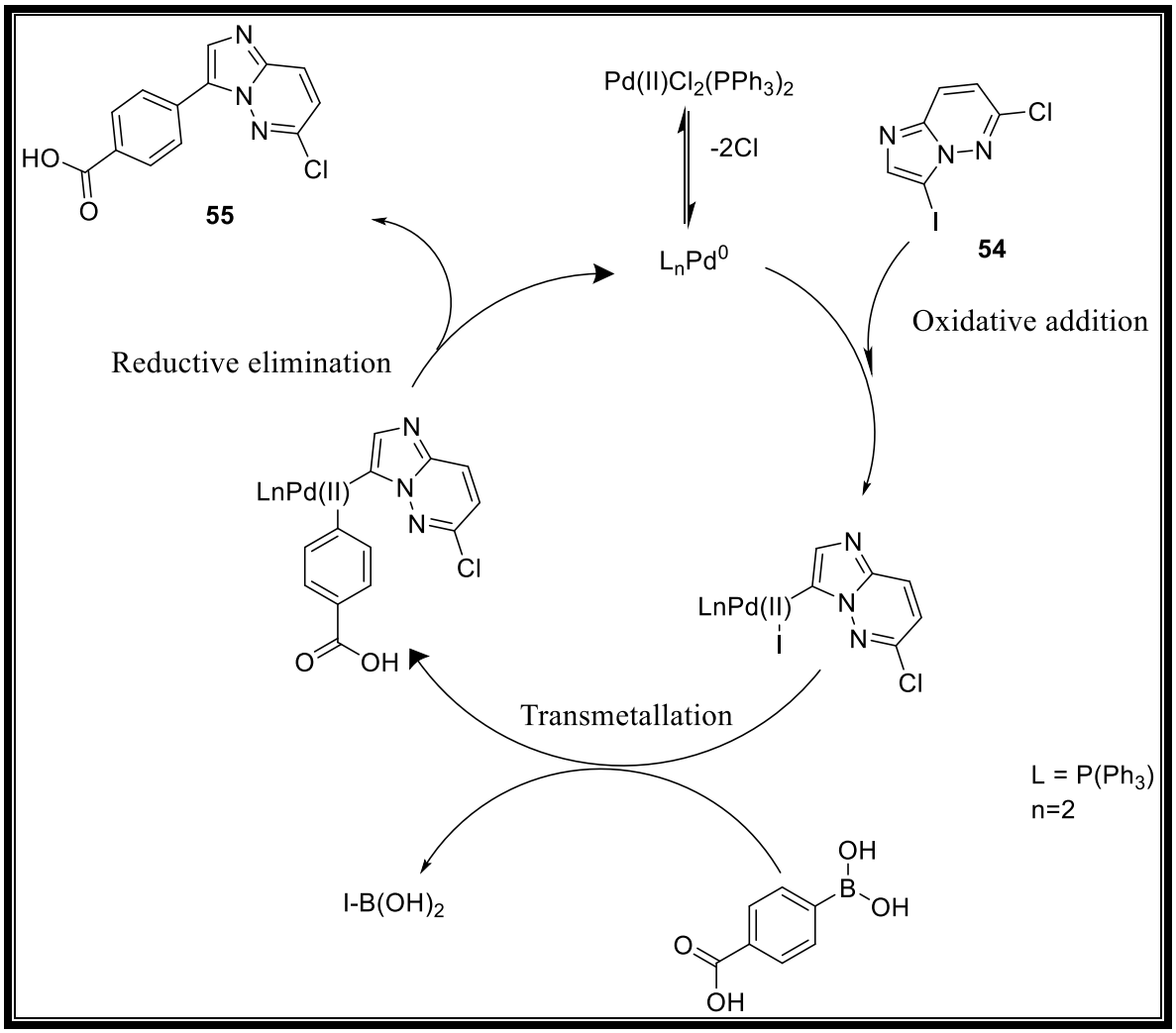

Scheme 5: Catalytic cycle of the Suzuki-Miyaura coupling reaction catalysed by $PdCl_2(PPh_3)_2$.

The successful formation of compound **55** was confirmed by ^{1}H-NMR spectroscopy. As shown in **Figure 24**, 5 peaks in the aromatic region were observed in the ^{1}H-NMR spectrum of **55**. A sharp singlet at δ 8.43 ppm was assigned to proton H8 and integrates for 1H. A relatively deshielded doublet arising at 8.32 ppm (J = 9.4 Hz) integrating for 1H was assigned to H6. A doublet appearing at 8.23 ppm (J = 8.8 Hz) and integrating for 2H was assigned to H12 and H14. A second doublet resonating at 8.08 ppm (J = 8.8 Hz) and integrating for 2H was assigned to H11 and H15. A doublet assigned to H1 and appearing at 7.46 ppm (J = 9.5

Hz) integrated for 1H. Eleven carbon peaks in the ^{13}C-NMR spectrum were observed while a pseudomolecular mass ion *m/z* $[M + H]^+$ = 273.87 was observed on LC-MS.

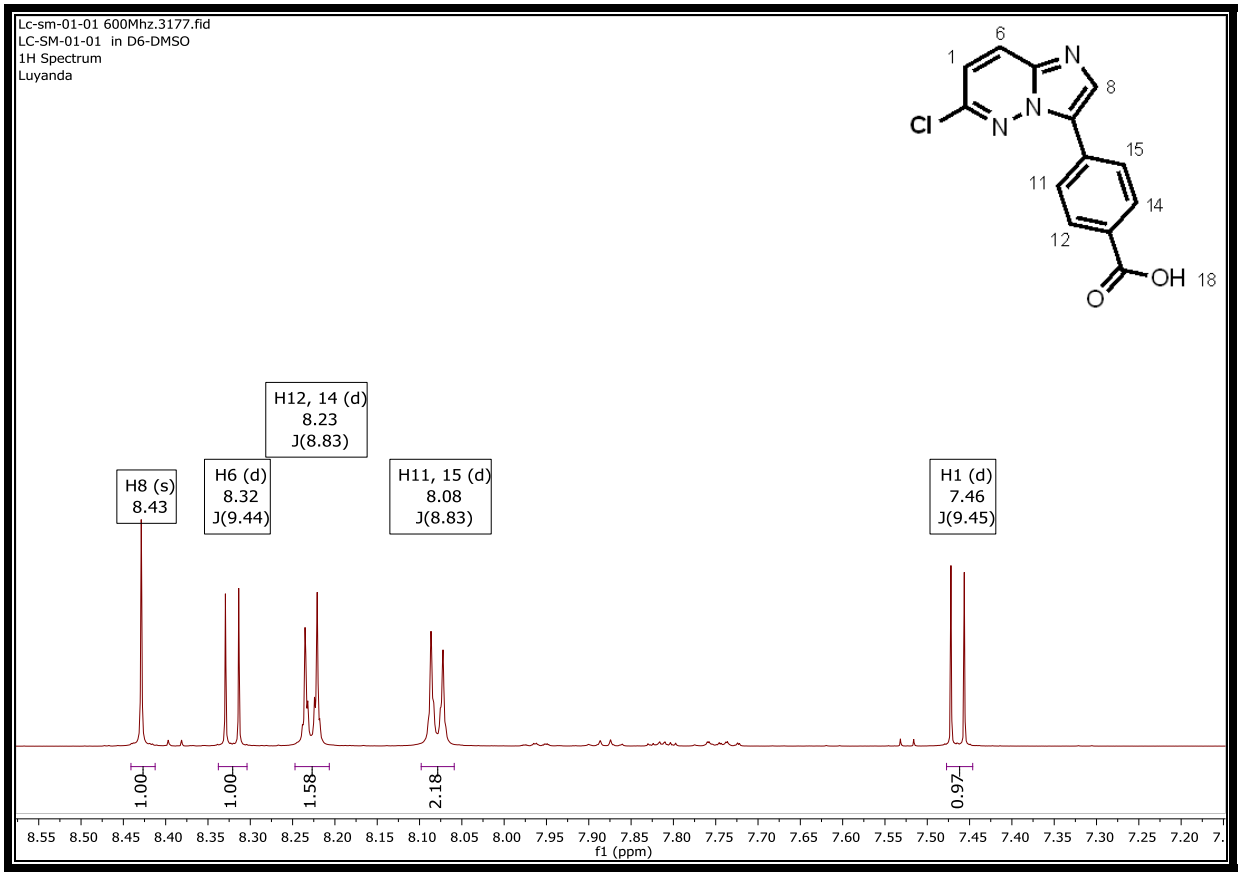

Figure 24: ^{1}H-NMR spectrum of **55** at 600 MHz in DMSO-d_6.

2.3.5 Characterisation of the sulfoxide common intermediate 56 (Step IV, Scheme 1)

The sulfoxide-substituted common intermediate **56** was obtained through a Suzuki-Miyaura cross coupling reaction. The ^{1}H-NMR spectrum is shown in **Figure 25**. Focusing on the left-hand side portion of the molecule, a triplet at 7.81 ppm (J = 7.7 Hz) was assigned to H13 and integrates for 1H. A multiplet at 8.36–8.29 ppm which integrates for 3H was assigned to H6, H8 and H12. A doublet signal at 7.96 ppm (J = 9.5 Hz), which was assigned to H1 integrates for 1H. A sharp singlet at 2.86 ppm, which integrates to 3H was assigned to H27. A triplet at 8.43 ppm (1.8 Hz) was assigned to H16 and integrates for 1H. Two doublets of an AB spin system are observed at 8.18 (J = 8.4 Hz) and 8.05 (J = 8.3 Hz) ppm with each doublet integrating for 2H, attributed to H18, H20 and H17, H21, respectively. A doublet of triplet

resonating at 7.87 ppm (J = 6.8, 1.2 Hz) and integrates for 1H was assigned to H14. Overall, 17 peaks in the ^{13}C-NMR spectrum were observed with some carbons co-resonating at the same chemical shift. LC-MS analysis revealed a pseudomolecular ion mass m/z $[M + H]^+$ = 377.8.

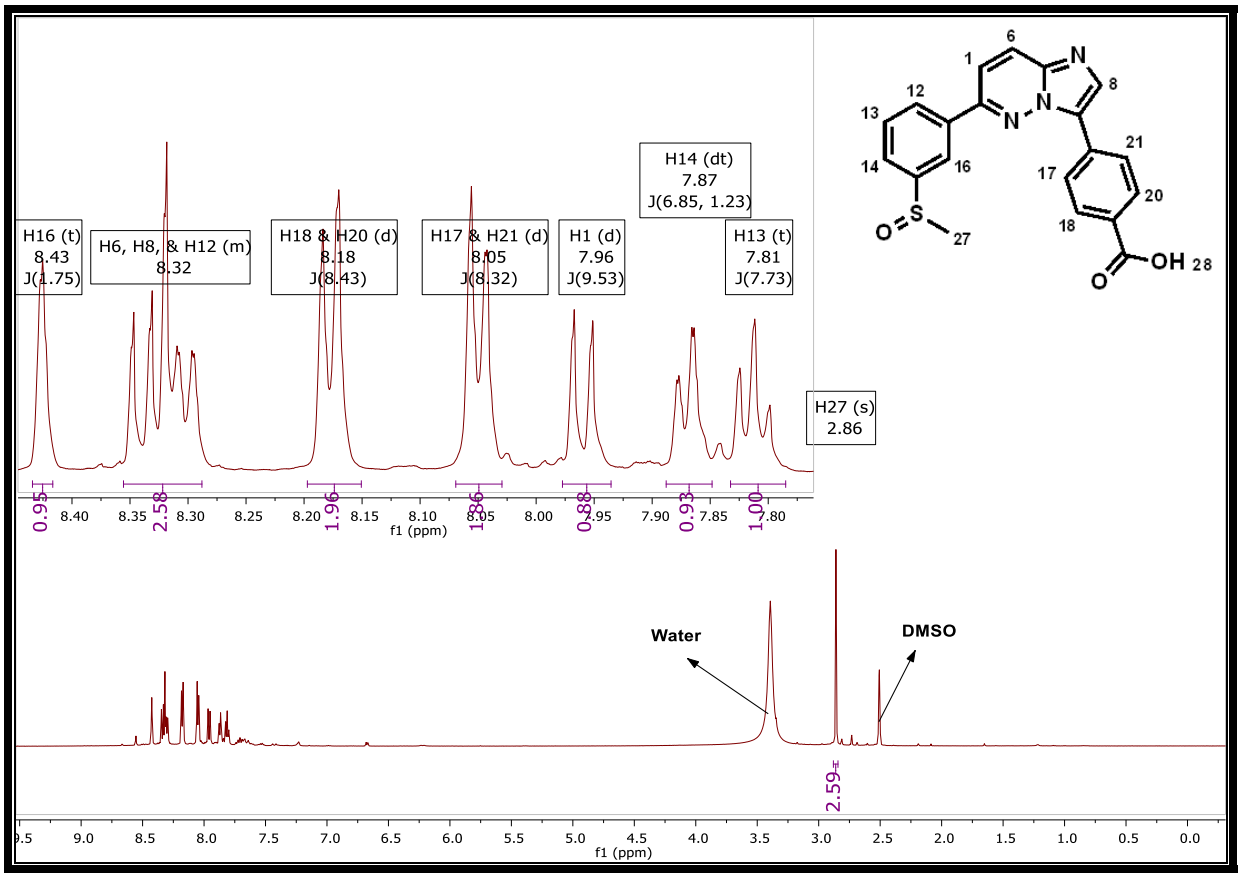

Figure 25: ^{1}H-NMR spectrum of **56** at 600 MHz in DMSO-d_6.

2.3.6 Characterisation of the sulfone-substitued intermediate 71 (Step I, Scheme 2)

Intermediate **53** was subjected to a Suzuki-Miyaura cross coupling reaction with [3-(methylsulfonyl)phenyl]boronic acid to afford compound **71**. The ^{1}H-NMR spectrum of **71** is shown in **Figure 26**. A triplet observed at 8.54 ppm (J = 1.9 Hz) was assigned to H15 and integrates for 1H. The H15 triplet is caused by long range coupling with H11 and H13. A multiplet at 8.41–8.35 ppm, which integrates for 2H was observed and was assigned to H8 and H11. A doublet resonating at 8.23 ppm (J = 9.5 Hz) was assigned to H6 and integrates

for 1H. A doublet of triplets at 8.07 ppm (J = 12.9, 1.2 Hz) was assigned to H13, which integrates for 1H. A doublet observed at 7.88 ppm (J = 9.8 Hz) which integrates for 1H was assigned to H1. A multiplet at 7.8–7.81 ppm was assigned to H12 and H7 which integrates for 2H. A sharp singlet at 3.29 ppm integrating for 3H was assigned to H18. The intermediate was further confirmed by LC-MS which showed a pseudomolecular ion at, *m/z* $[M+H]^+$ = 273.9. 13 distinct peaks in the ^{13}C-NMR spectrum attributable to the 13 carbons in the structure were observed.

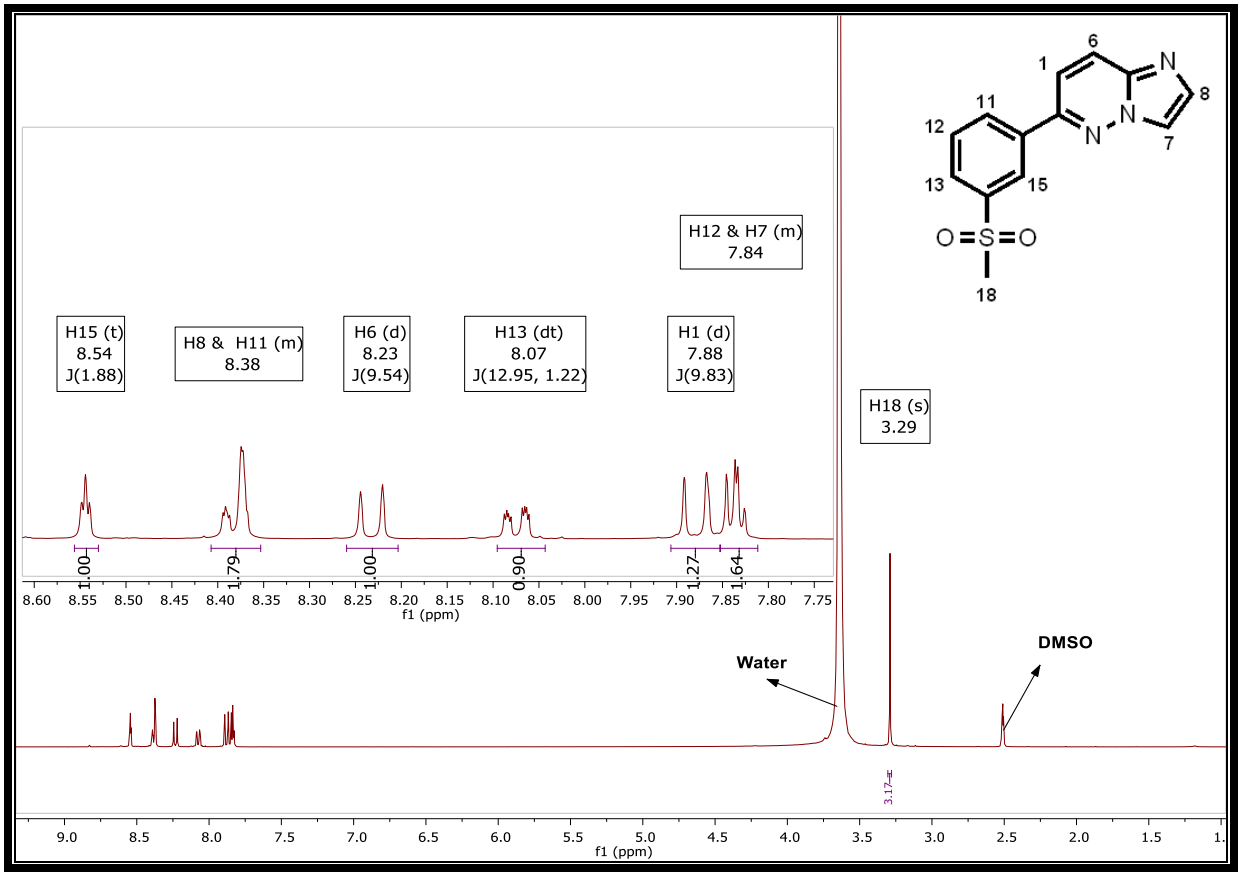

Figure 26: ^{1}H-NMR spectrum of **71** at 400 MHz in DMSO-d_6.

2.3.7 Characterisation of 72 intermediate (Step II, Scheme 2)

The intermediate **71** was iodinated with NIS to afford compound **72**. The ^{1}H-NMR spectrum (**Figure 27**) of **72** shows a triplet at 8.65 ppm (J = 1.9 Hz) integrating for H1 which was assigned to H15. A doublet of triplets integrating for H1 at 8.48 ppm (J = 7.9, 1.8 Hz) was

assigned to H11. A doublet resonating at 8.29 ppm (J = 9.5 Hz) was assigned to H6 and integrates for 1H. A doublet of triplets observed at 8.13 ppm (J = 7.8, 1.8 Hz), which integrates for 1H was assigned to H13. A multiplet signal at 8.03–7.97 ppm, which integrates for 2H was assigned to H8 and H1. A triplet observed at 7.90 ppm (J = 7.9 Hz), which integrates for 1H, was assigned to H12. A sharp singlet at 3.34 ppm was assigned to H18 and integrates for 3H. Furthermore, a pseudomolecular ion, *m/z* $[M+H]^+$ = 399.6, for this intermediate was observed upon LC-MS analysis while 13 peaks in the ^{13}C-NMR spectrum were observed which corresponded to the 13 carbons of this intermediate.

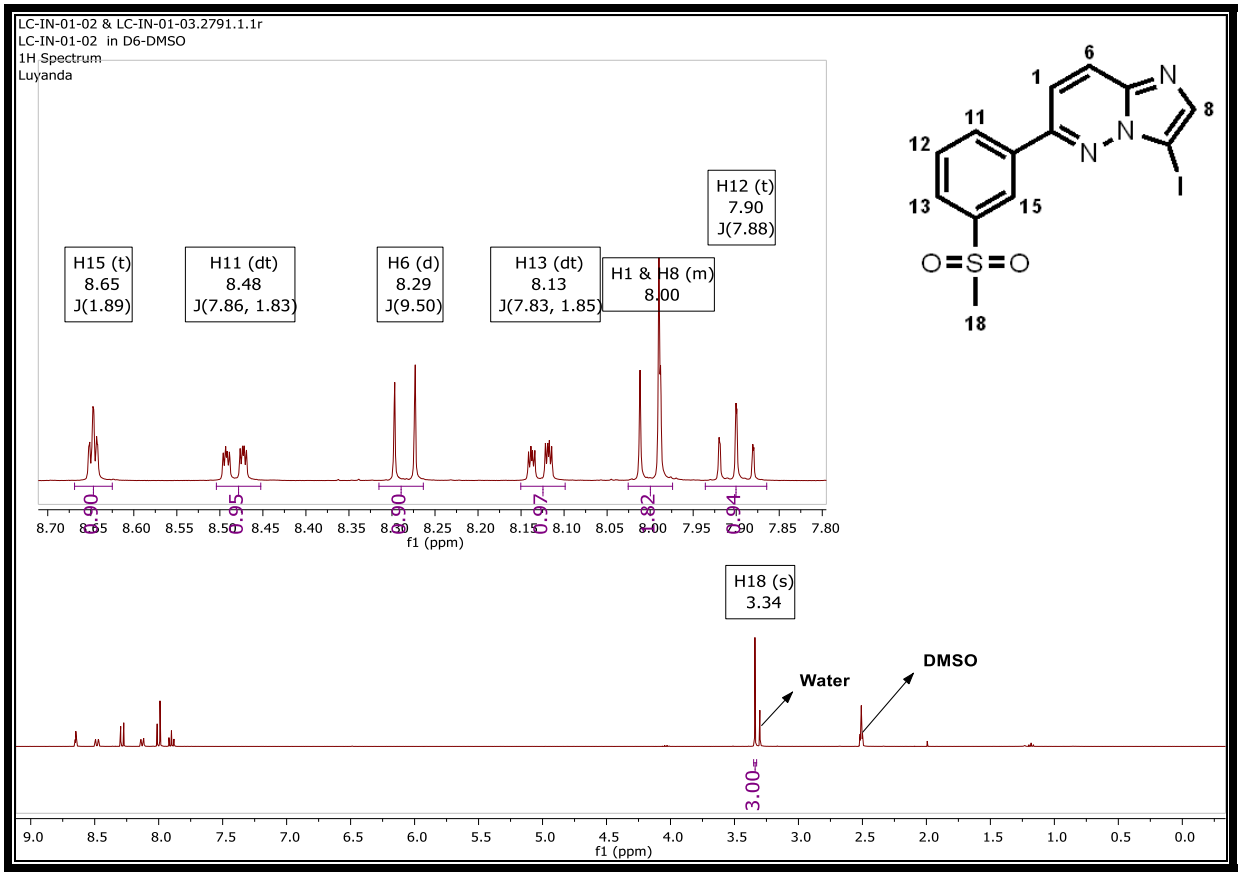

Figure 27: ^{1}H-NMR spectrum of **72** at 400 MHz in DMSO-d_6**.**

2.3.8 Characterisation of intermediate 73 (Step III, Scheme 2)

The sulfone compound **73** was synthesized by coupling 4-carboxyphenylboronic acid with the intermediate **72** through a Suzuki-Miyaura cross coupling reaction. The ^{1}H-NMR

spectrum of **73** is shown in **Figure 28**. The introduction of the 4-carboxyphenyl group was accompanied by the appearance of extra signals in the spectrum. A doublet observed at 8.34 ppm (J = 8.7 Hz), which integrates for 2H was assigned to H22 and H24. A doublet at 8.09 ppm (J = 8.3 Hz), which integrates for 2H was assigned to H21 and H25. A triplet integrating for 1H observed at 8.67 ppm (J = 1.8 Hz) was assigned to H15. A doublet of triplets at 8.52 ppm (J = 7.9, 1.9 Hz) was assigned to H11 and integrates for 1H. A singlet at 8.43 ppm, which integrates for 1H was assigned to H8. A doublet resonating at 8.40 ppm (J = 9.5 Hz) was assigned to H6 and integrates for 1H. A doublet of triplets, which integrates for 1H, was observed at 8.12 ppm (J = 7.8, 1.9 Hz) was assigned to H13. The doublet observed at 8.05 ppm (J = 9.6 Hz) and integrates for 1H was assigned to H1. A triplet observed at 7.91 ppm (J = 7.9 Hz) integrating for 1H was assigned to H12. Lastly, a sharp singlet at 3.35 ppm was assigned to H19 and integrates for 3H. When subjected to further analysis by LC-MS, **73** exhibited a pseudomolecular ion (ESI/APCI: *m/z* $[M+H]^+$ = 393.8). Additionally, 17 peaks in the ^{13}C-NMR spectrum with some carbons co-resonating at the same chemical shift.

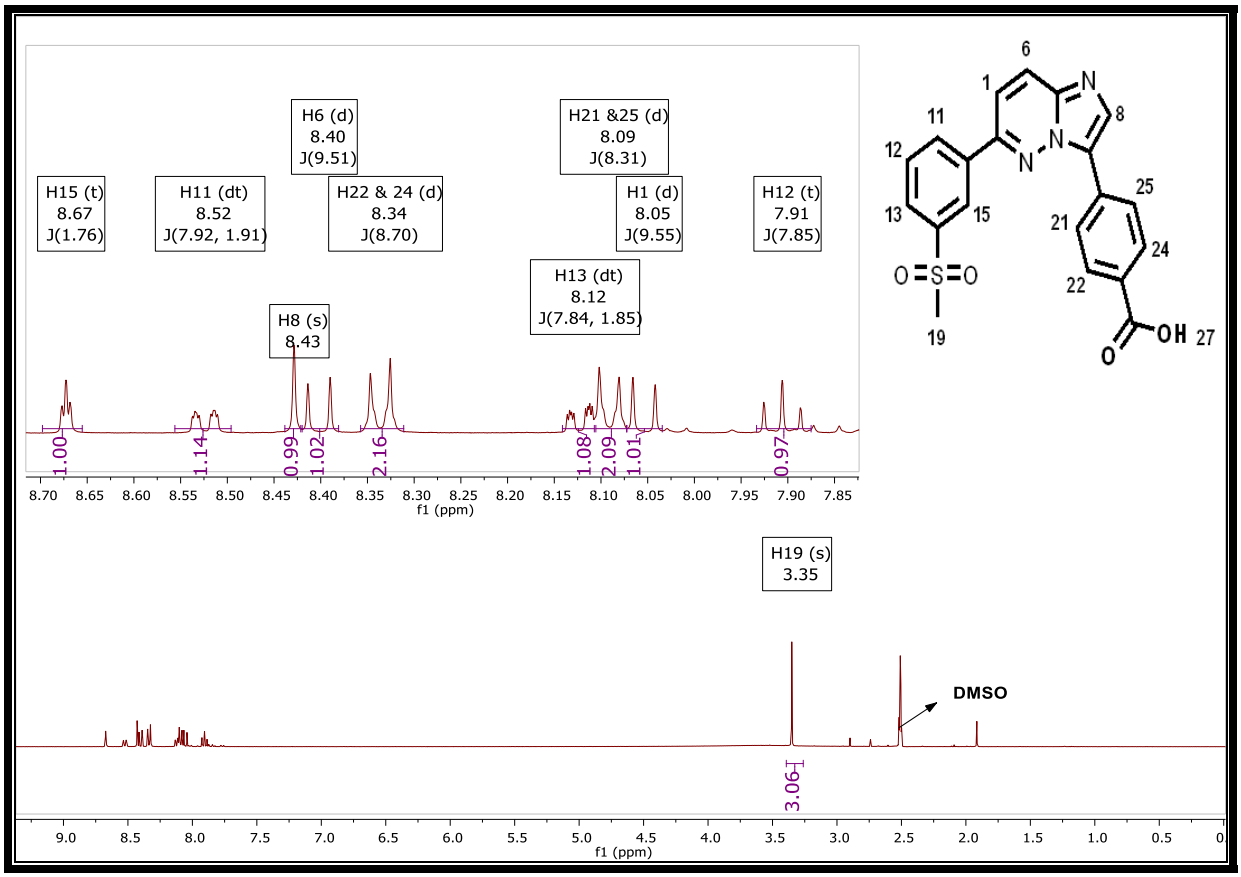

Figure 28: ^{1}H-NMR spectrum of **73** at 600 MHz in DMSO-d_6.

2.3.9 Mechanism for formation, and characterisation, of final amide target compounds (Step V in Scheme 1 and Step IV Scheme 2)

In the first step of the mechanism, DIPEA depronate the acidic proton of the carboxylic acid to form a carboxylate ion (**Scheme 6**). The carboxylate ion then attacks the phosphorus atom of T3P in the second step. The intermediate formed now contains a good leaving group. The primary or secondary amine then attacks the carbonyl carbon to expel the T3P moiety resulting in the target compound after protonation.

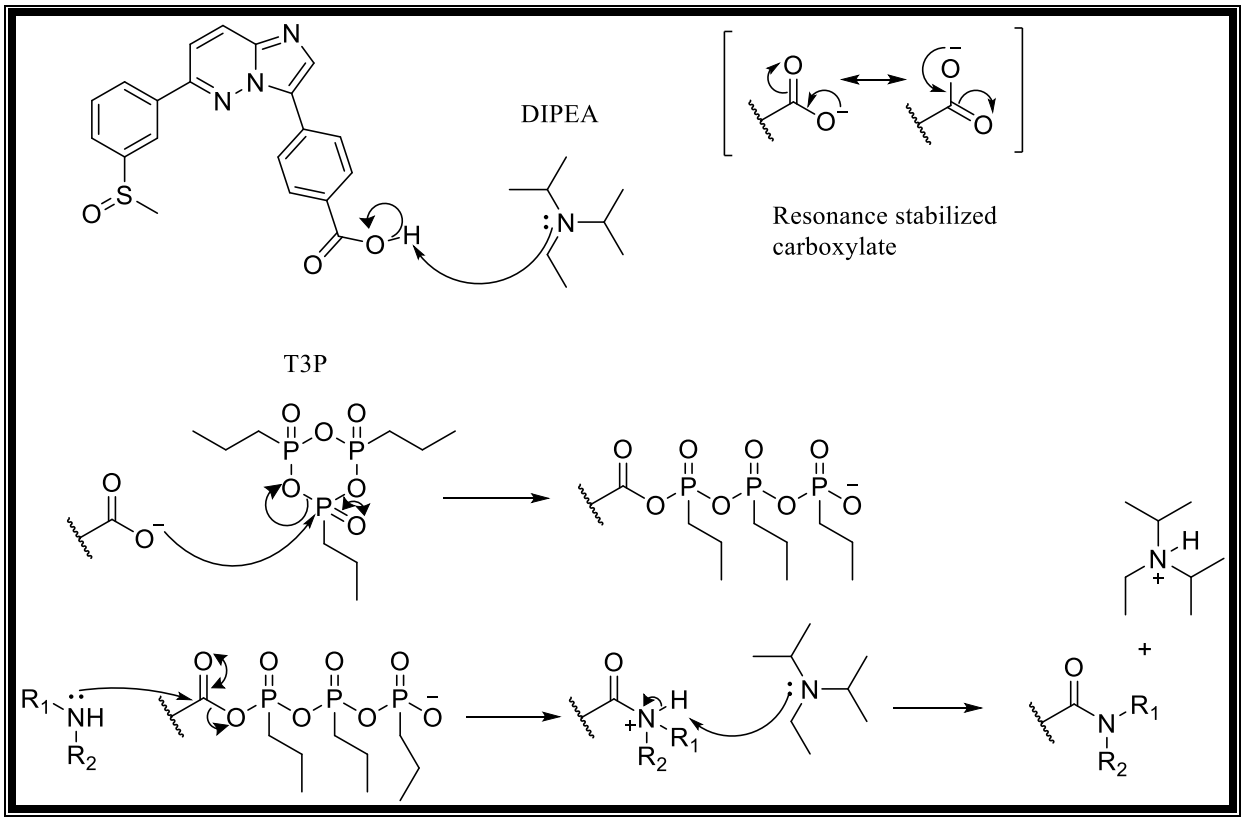

Scheme 6: Mechanism of T3P-mediated acid-amine coupling.

The ^{1}H-NMR spectrum of target compound **59** is shown in **Figure 29.I**. The proton H15 was assigned to a peak appearing as a triplet at δ 8.41 ppm (J = 1.8 Hz), which integrates for 1H. The relatively small J-value indicates long range coupling with H11 and H13. The two doublets observed at 8.26 (J = 8.6 Hz) and 7.98 (J = 8.5 Hz) ppm each integrating for 2H were assigned to H19, H21 and H18, H22, respectively. A doublet of triplets resonating at 8.23 ppm (J = 5.2, 1.3 Hz) was assigned to H11 which integrates for 1H. A singlet at 8.18 ppm was assigned to H8 and integrates for 1H. A doublet at 8.13 ppm (J = 9.5 Hz) which integrates for 1H was assigned to H6. A multiplet arising at 7.86–7.81 ppm and integrating for 2H was assigned to H1 and H13. A triplet observed at 7.75 ppm (J = 7.9 Hz) was assigned to H12 and integrates for 1H. A doublet of doublets of triplets at 6.00 ppm (J = 17.2, 10.3, 5.6 Hz) was assigned to H33 and integrates for 1H. Two doublet of quartet signals at 5.30 and 5.18 ppm were assigned to two geminal protons H31 and H32, respectively. H31 is

trans to H33 and has a larger *J*-value of 17.2 Hz and is more deshielded relative to H32. On the other hand, H32 is *cis* to H33 and has a lower *J*-value of 10.3 Hz. H28 was assigned to a doublet of triplet (J = 5.6, 1.7 Hz) at 4.06 ppm and integrates for 2H. A sharp singlet in the aliphatic region was assigned to H27 and integrates for 3H. In **Figure 29.II** and **Figure 29.III** are COSY spectra of **59**, which were used to identify protons that are corelating. The solid black lines in COSY spectra of **59** indicate protons that are correlating. In the MS chromatogram (**Figure 29.IV**), acquired by LC-MS, ESI/APCI, an *m/z* value of 416.8 corresponding to pseudomolecular ion $[M+H]^+$ of the target compound was observed. Additionally, the ^{13}C-NMR spectrum showed 21 distinct signals attributable to the 23 carbons of the compound as shown in **Figure 29.V**. Carbons (C18, C22,) and (C19, C21) are co-resonating at the same chemical shifts as indicated in **Figure 29.V**. The asterics in the carbon spectrum indicates carbons that do not have protons attached and double asteric indicates a carbonyl carbon, which resonates at 167.97 ppm. **Figure 29.VI** is HSQC spectrum of **59**, which was used to match proton to its carbon.

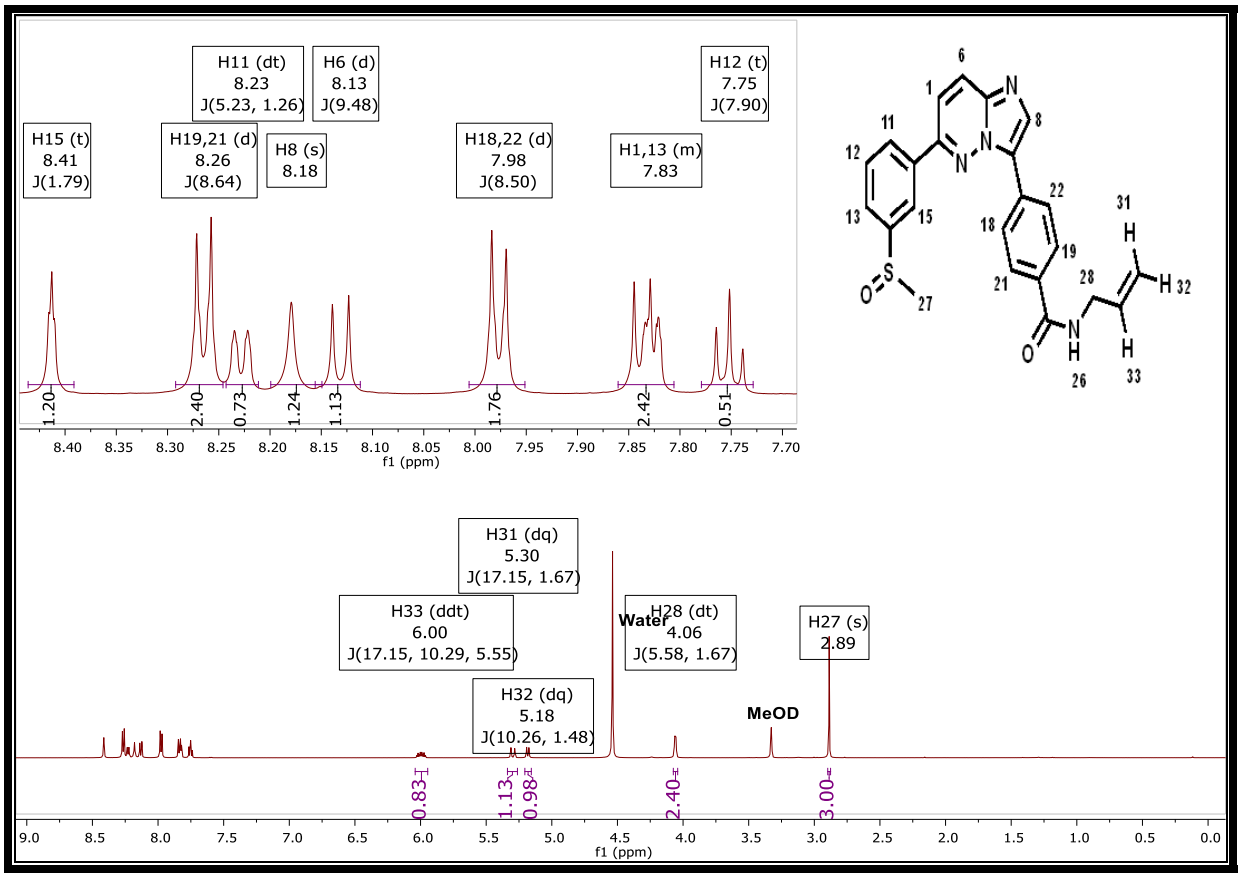

Figure 29.I: ^{1}H-NMR spectrum of **59** at 600 MHz in Methanol-d_4.

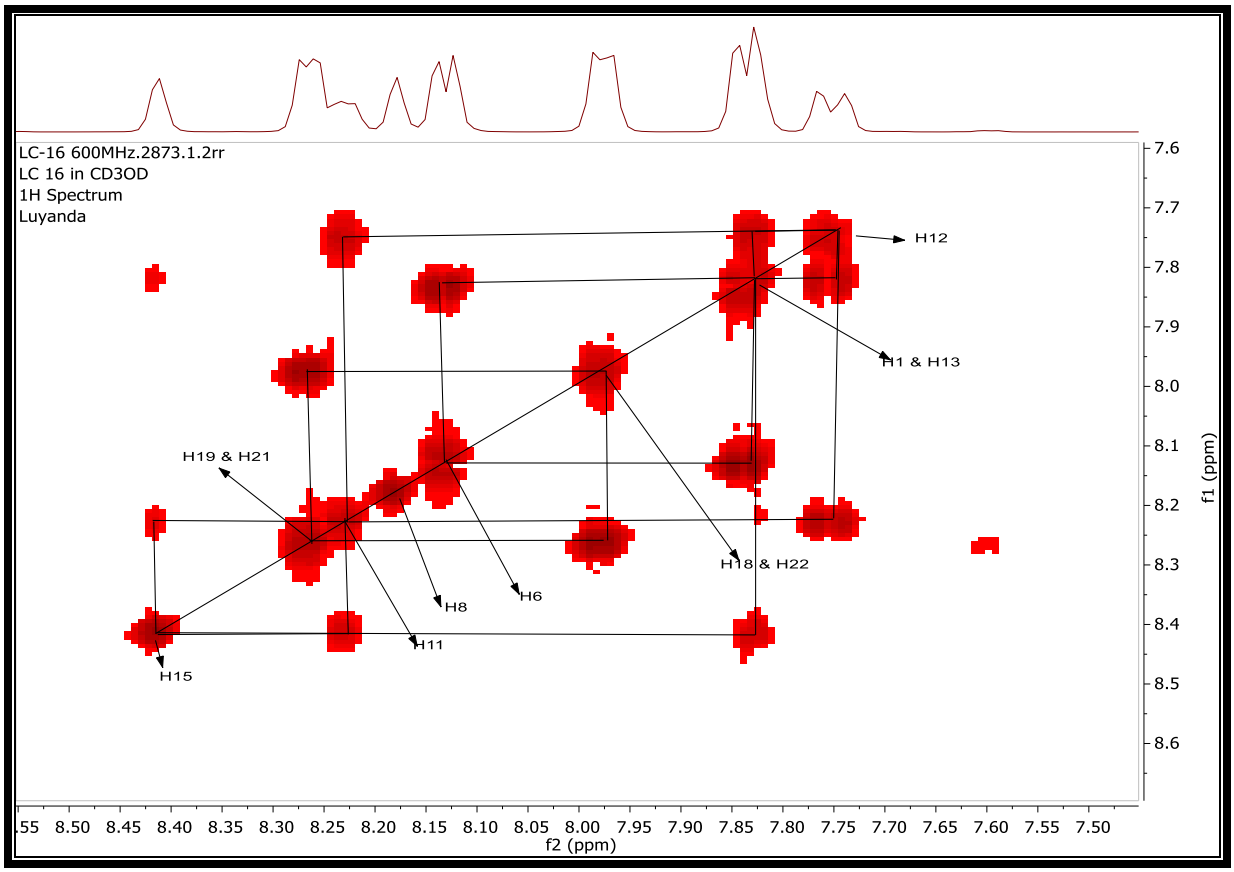

Figure 29.II: COSY spectrum of **59** aromatic regions downfield at 600 MHz in Methanol-d_4.

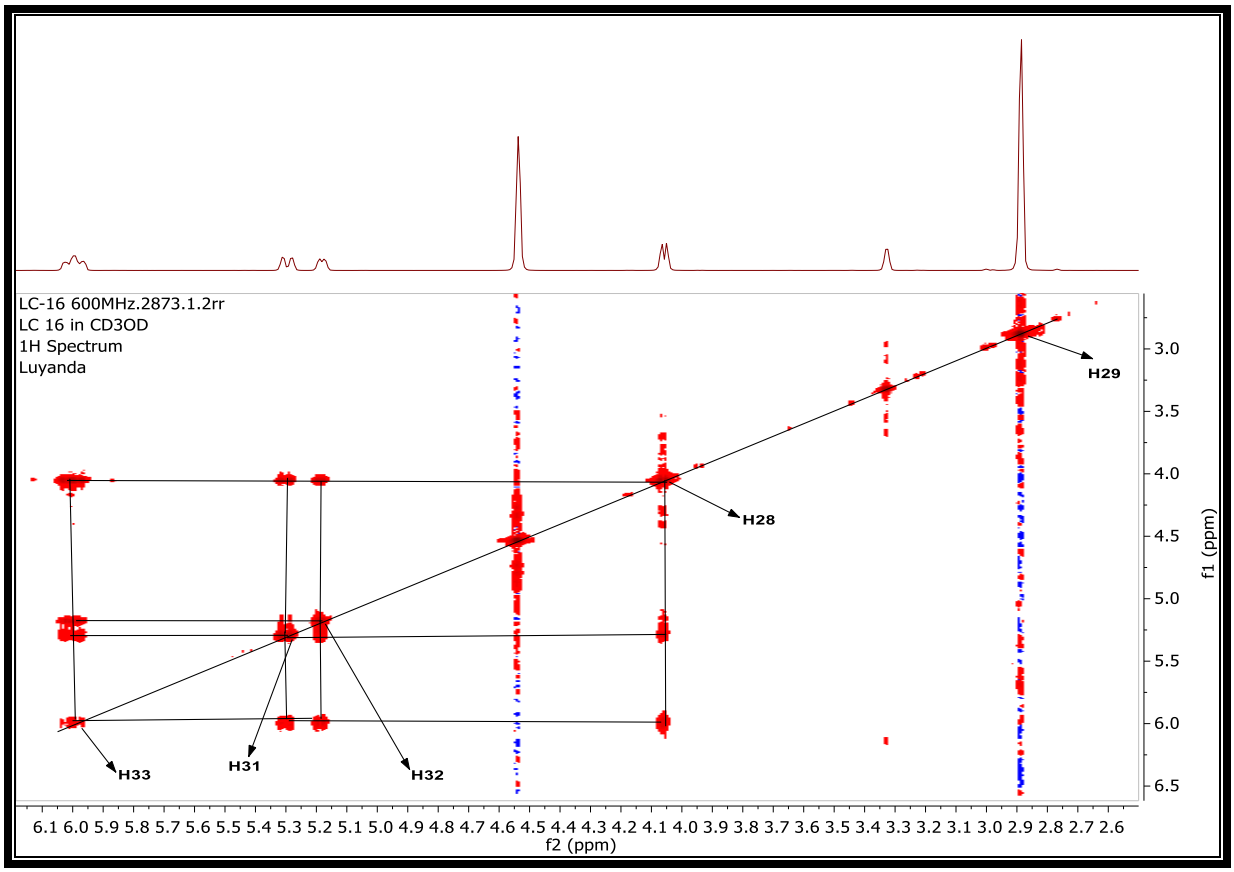

Figure 29.III: COSY spectrum of **59** upfield aliphatic regions at 600 MHz in Methanol-d_4.

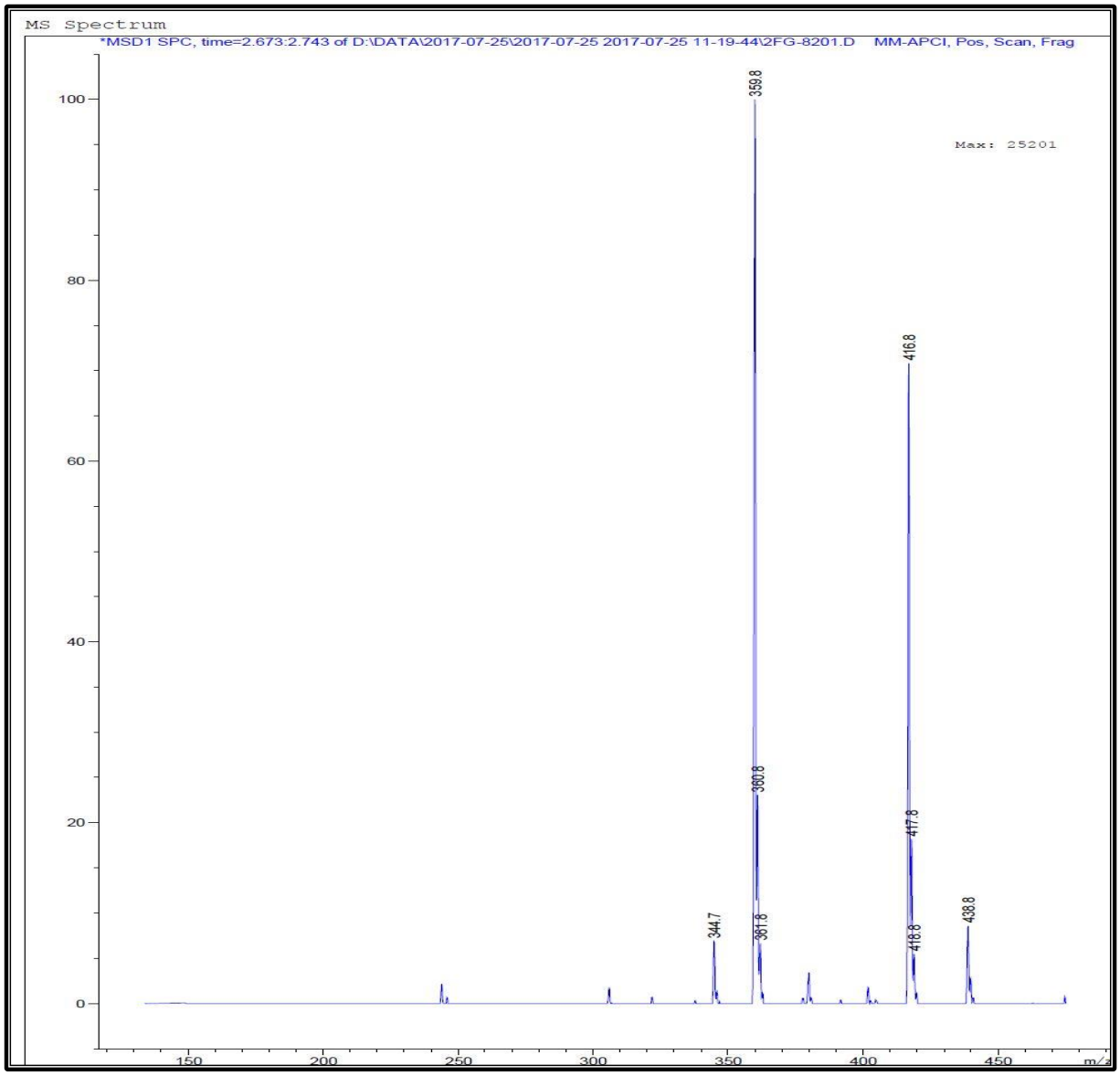

Figure 29.IV: MS spectrum of **59**.

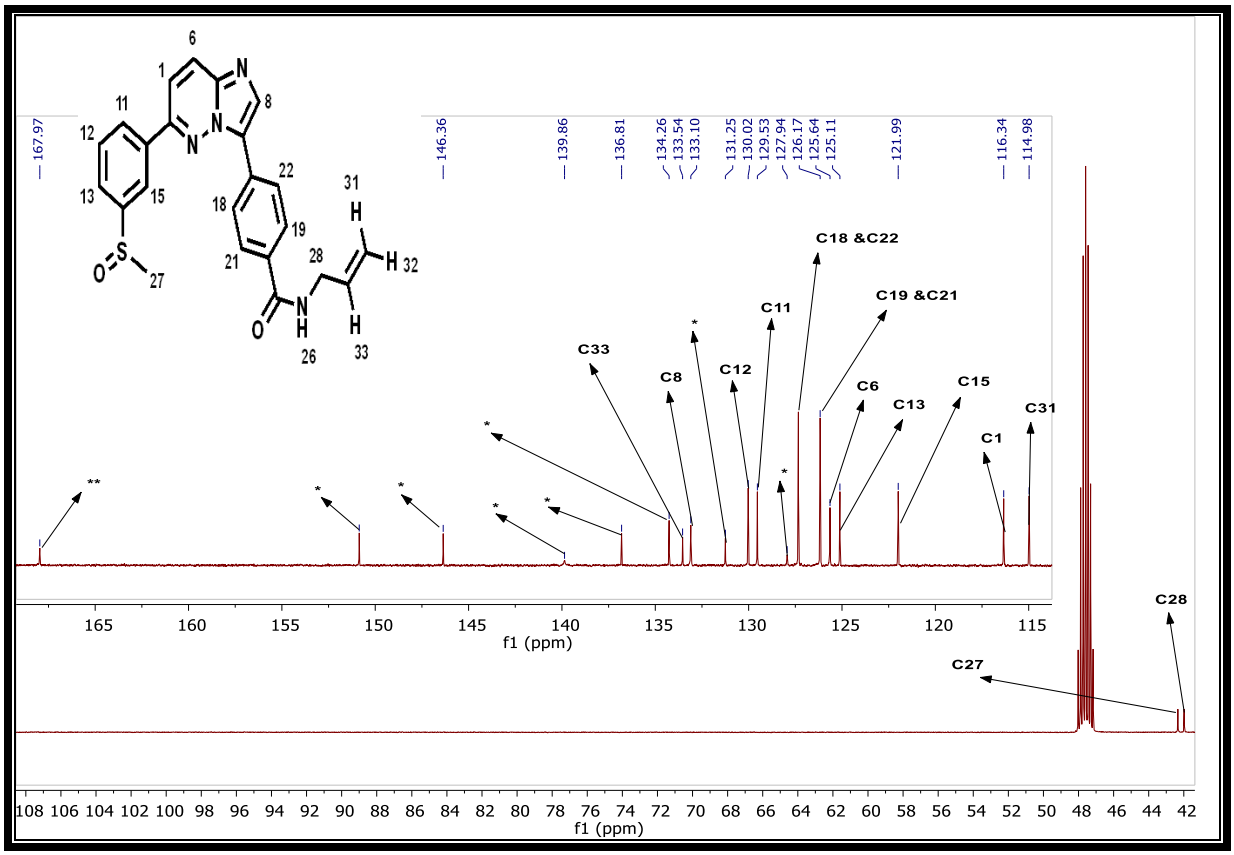

Figure 29.V: ^{13}C-NMR spectrum of **59** at 600 MHz in Methanol-d_4.

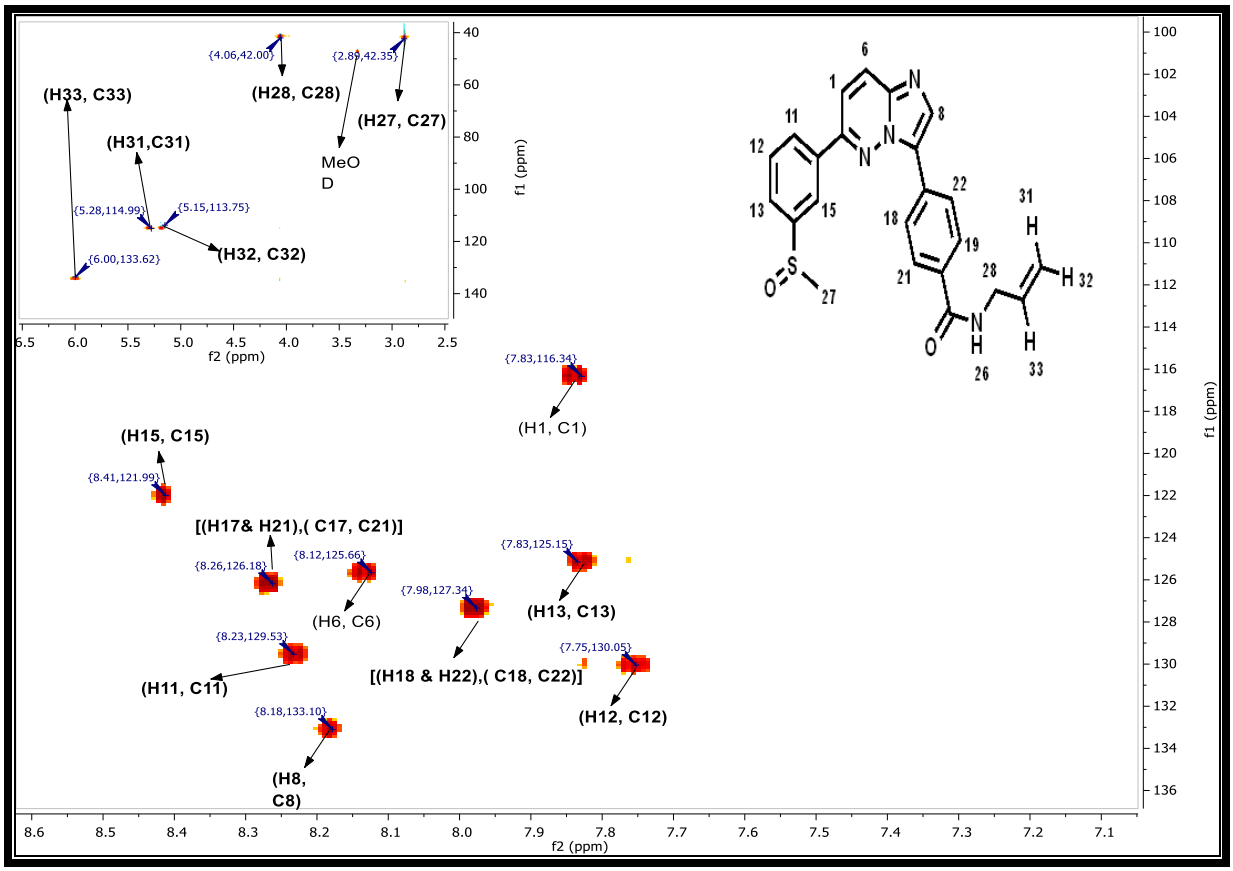

Figure 29.VI: HSQC spectrum of **59** at 600 MHz in Methanol-d_4.

For target compounds **58**, **60**, and **61,** only ^{1}H-NMR peaks arising from newly introduced amide substituents will be discussed in addition to LC-MS confirmation.

The ^{1}H-NMR spectrum of compound **58** is shown in **Figure 30.I**. A sharp singlet integrating for 4H at 3.63 ppm was assigned to H26 and H27. An attached proton test (APT) experiment, whose spectrum is shown in **Figure 30.II**, shows two CH_2 groups at 39.4 and 70.7 ppm in the aliphatic region and CH_2 belongs to protons H27 and H26. H31 was assigned to a sharp singlet resonating at 3.43 ppm and integrating to 3H. A pseudomolecular ion *m/z* $[M+H]^+$ = 434.8, was also observed upon LC-MS analysis.

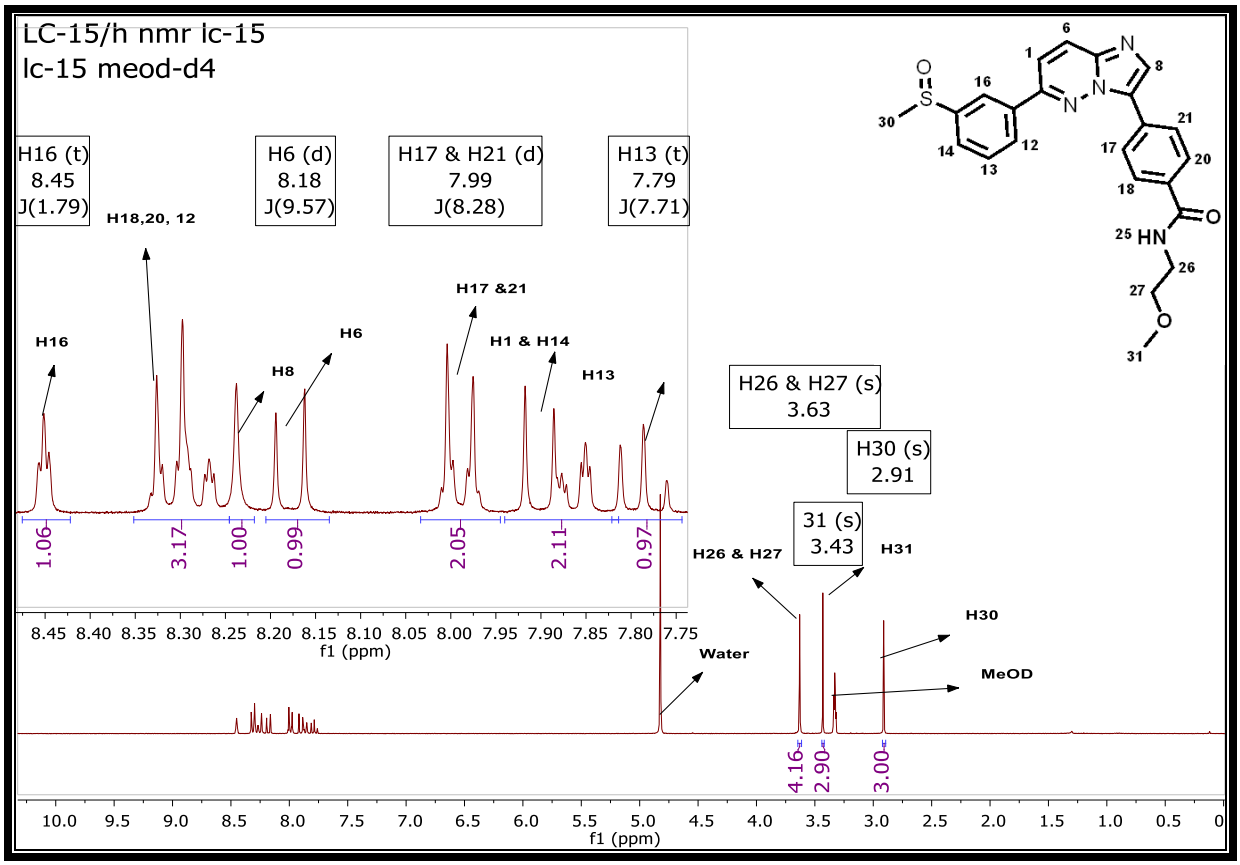

Figure 30.I: ^{1}H-NMR spectrum of **58** at 300 MHz in methanol-d_4.

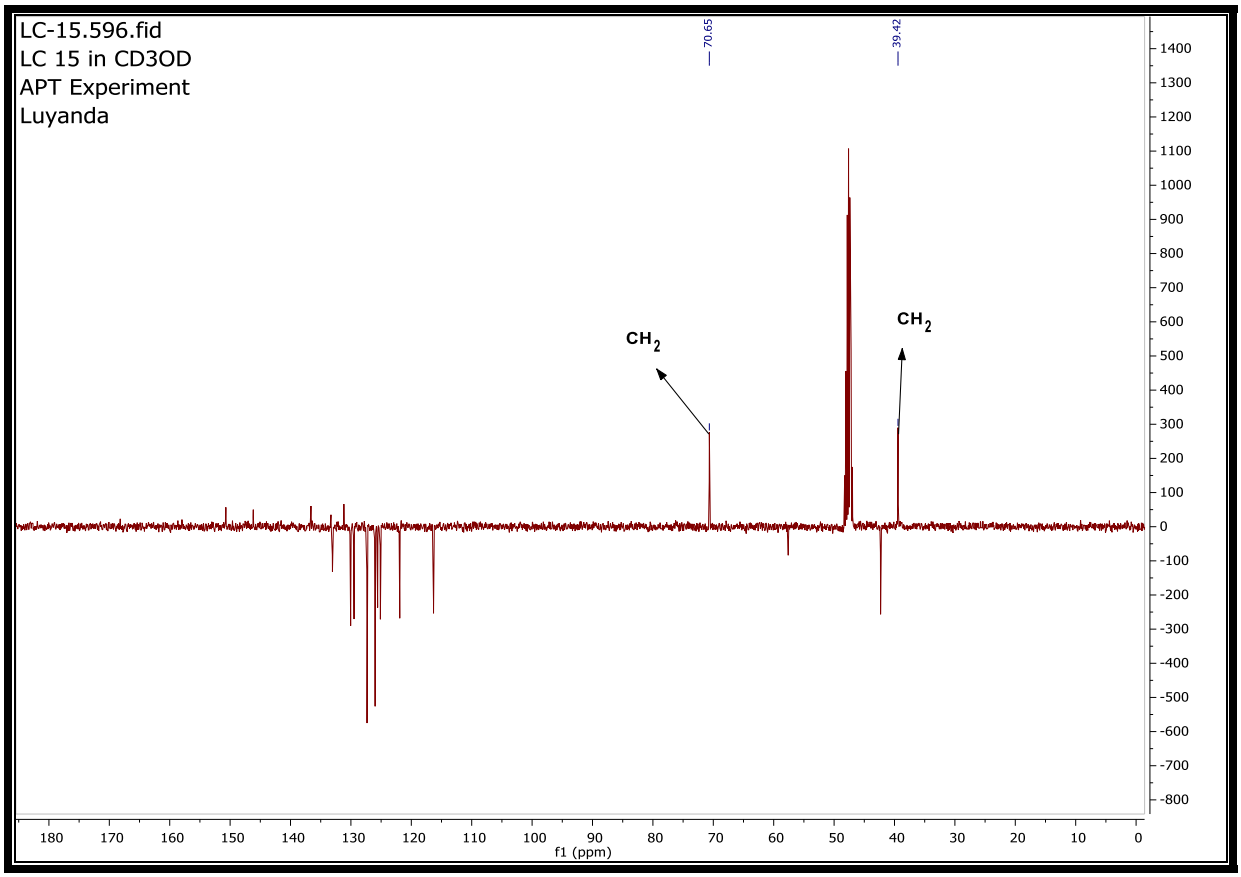

Figure 30.II: ^{13}C-APT spectrum of **58** in methanol-d_4.

For compound **60**, whose ^{1}H-NMR spectrum is shown in **Figure 31**, a triplet observed at 0.92 ppm (J = 7.4 Hz) was assigned to H29 and integrates for 3H. Multiplet signals appearing at 1.78–1.63 and 1.57–1.42 ppm were assigned to diastereotopic protons H28a and H28b, which integrates for 1H in each multiplet. The diastereotopic protons, H27a and H27b were assigned to two multiplets appearing at 3.55–3.48 and 3.48–3.41 ppm, respectively, with each peak integrating for 1H. A multiplet which appears at 3.93 ppm was assigned to H26 and integrates for 1H. A triplet signal at 4.65 ppm (J = 5.8 Hz) was assigned to H30 and integrates for 1H. Additionally, a pseudomolecular ion, m/z $[M+H]^+$ = 449.0, was observed upon LC-MS analysis.

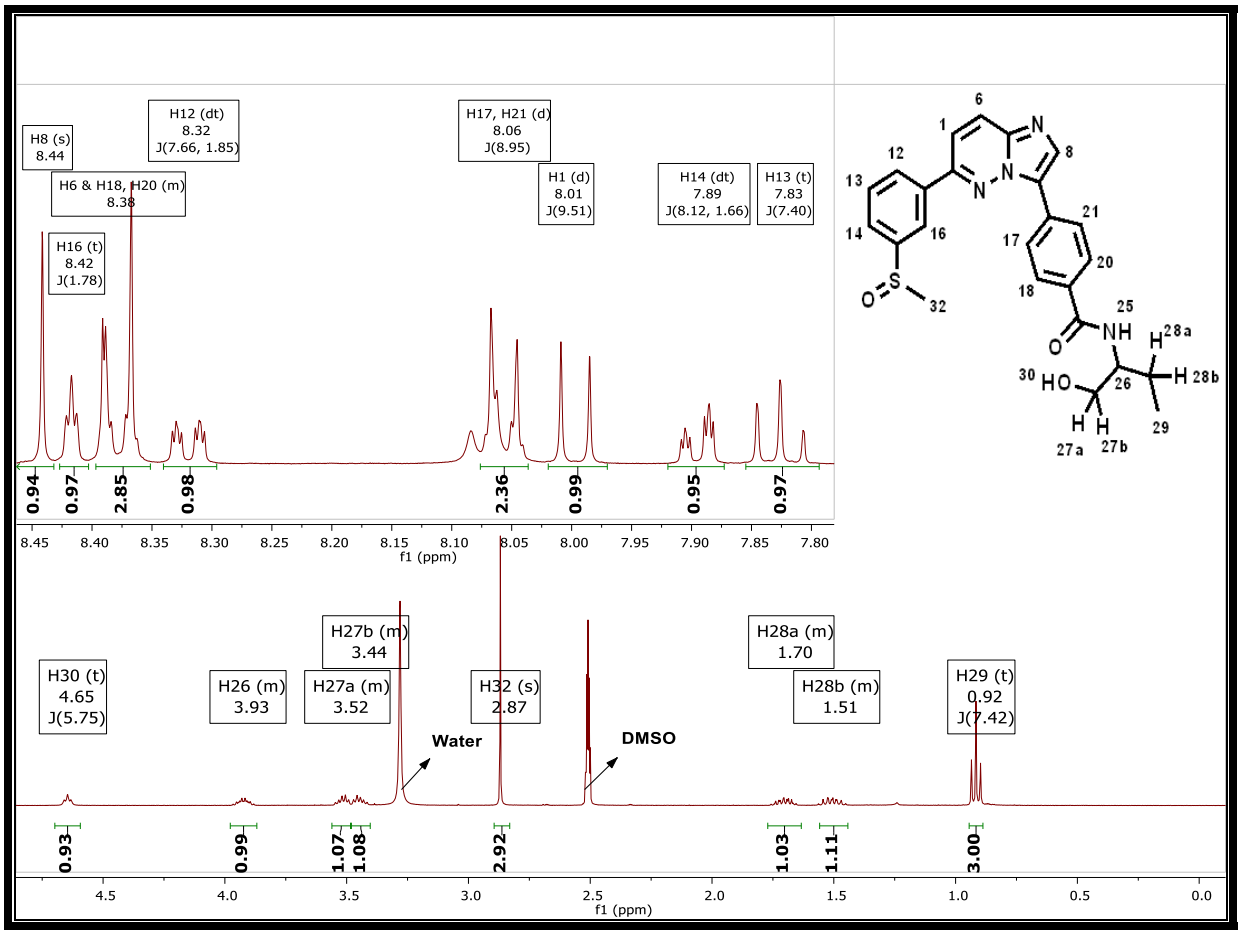

Figure 31: ^{1}H-NMR spectrum of **60** at 300 MHz in DMSO-d_6.

Figure 32 shows the ^{1}H-NMR spectrum of compound **61**. The spectrum shows that the signals for H30 and H29 protons were resolved into those corresponding to protons above and below the ring. $H30_a$ indicates a proton above the surface of the ring while $H30_e$ indicates the one below the ring. In this regard $H30_a$ and $H29_a$ are equivalent as are $H30_e$ and $H29_e$. A multiplet signal resonating at 0.66–0.58 ppm was assigned to $H30_a$ and $H29_a$ while the multiplet at 0.77–0.68 ppm was assigned to $H30_e$ and $H29_e$ both of which integrate for 2H each. The H28 proton was assigned to a multiplet at 1.30–1.22 ppm, which integrates for 1H. A doublet at 8.53 ppm (J = 4.2 Hz) which integrates for 1H was assigned to H18. A pseudomolecular ion mass, *m/z* $[M+H]^+$ = 417.0, for this compound was also observed upon LC-MS analysis. Additionally, 20 peaks in the ^{13}C-NMR spectrum were observed with some carbons co-resonating at the same chemical shifts.

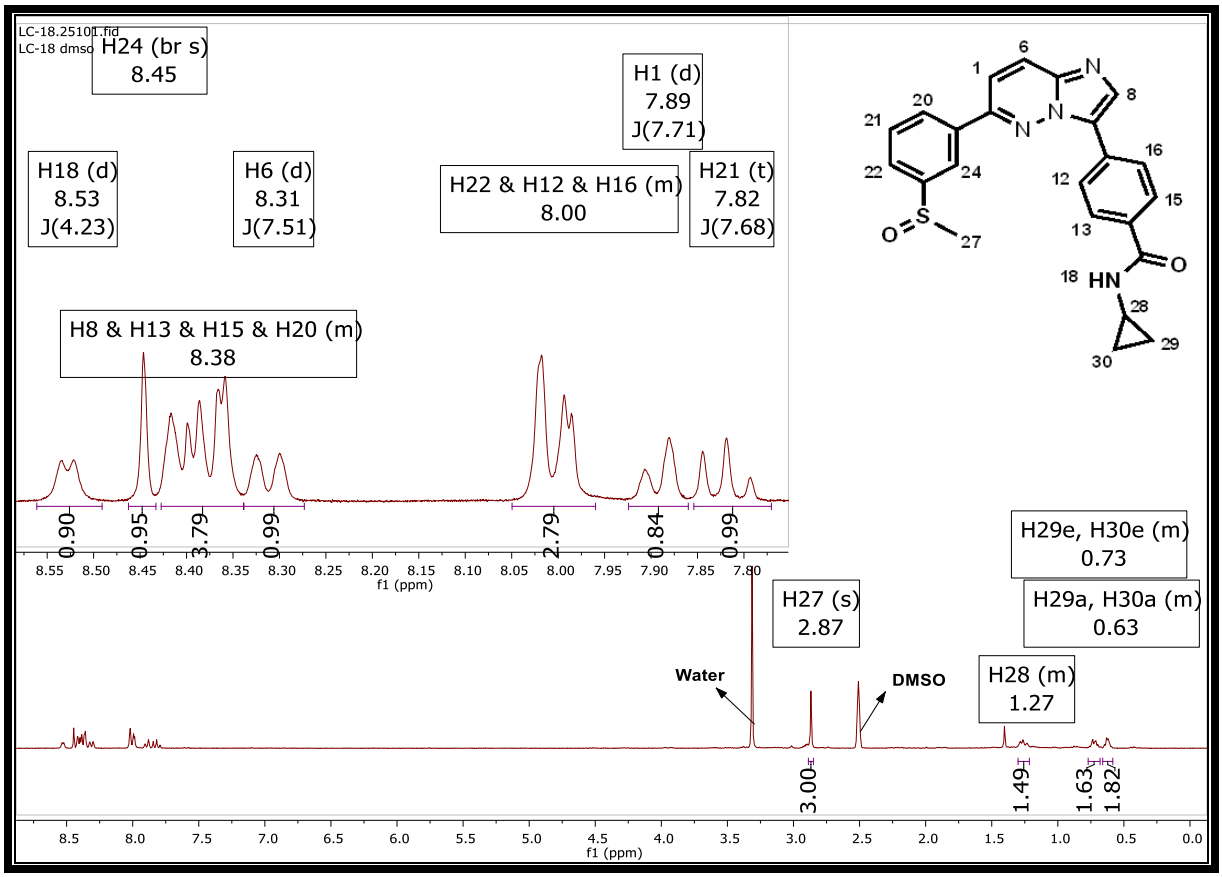

Figure 32: ^{1}H-NMR spectrum of **61** at 300 MHz in DMSO-d_6.

The compound **74** was prepared from the sulfone-substituted intermediate **73** in a T3P mediated acid-amine reaction. The ^{1}H-NMR spectrum of **74** is shown in **Figure 33**. A multiplet observed at 8.39 ppm, which integrates for 3H was assigned to H6, H13 and H15. A multiplet at 8.03 ppm, which integrates for 3H was assigned to H1, H12 and H16. A triplet observed at 8.65 ppm (J = 1.8 Hz) was assigned to H21, and integrates for 1H. A doublet of triplets at 8.50 ppm (J = 7.8, 1.9 Hz) was assigned to H17 which integrates for 1H. A singlet at 8.46 ppm, which integrates for 1H was assigned to H8. A doublet of triplets observed at 8.13 ppm (J = 7.8, 1.8 Hz), which integrates for 1H was assigned to H19. A triplet observed at 7.90 ppm (J = 7.9 Hz) integrating for 1H was assigned to H18. A sharp singlet at 3.35 ppm was assigned to H25 and integrates for 3H. A doublet at 2.84 ppm which integrates for 3H was assigned to H29. On LC-MS analysis, **74** showed a pseudomolecular ion at *m/z* $[M+H]^+$

= 406.8 while 19 peaks were observed in the ^{13}C-NMR spectrum with some carbon atoms co-resonating at the same chemical shifts.

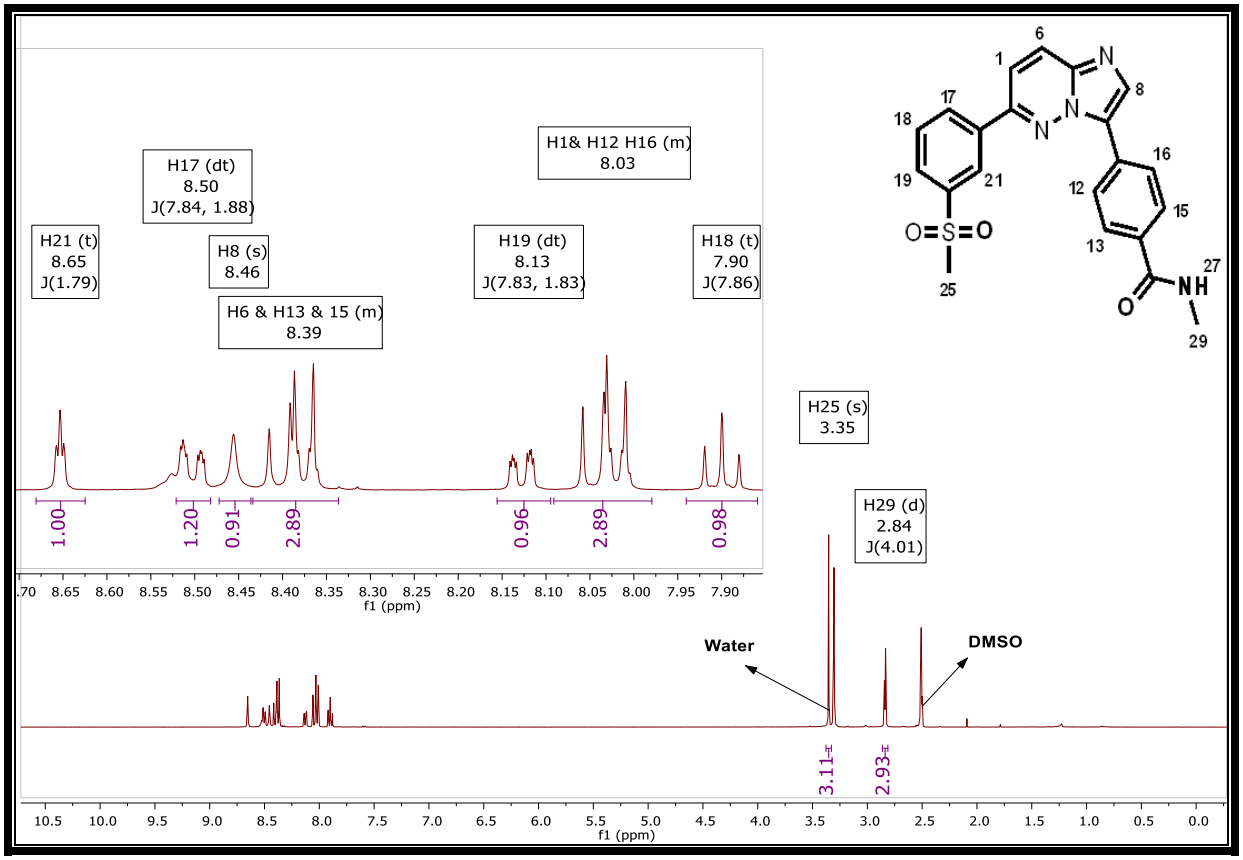

Figure 33: ^{1}H-NMR spectrum of **74** at 600 MHz in DMSO-d_6.

2.4.1 Chemistry for Series 2 analogues

The iodinated intermediate **54** was subjected to a regioselective Suzuki-Miyaura coupling reaction with (4-(methylsulfinyl)phenyl)boronic acid to afford the sulfoxide-substituted intermediate **75** as shown in **Scheme 7**. A second Suzuki-Miyaura coupling reaction with 3-carboxyphenylboronic acid gave the benzoic acid common intermediate **76**. This intermediate was then subjected to an acid catalyzed amide coupling mediated by T3P to give the desired target compounds **77-86**. The final amide target compounds and yields obtained via this synthetic scheme are summarized in **Table 3**.

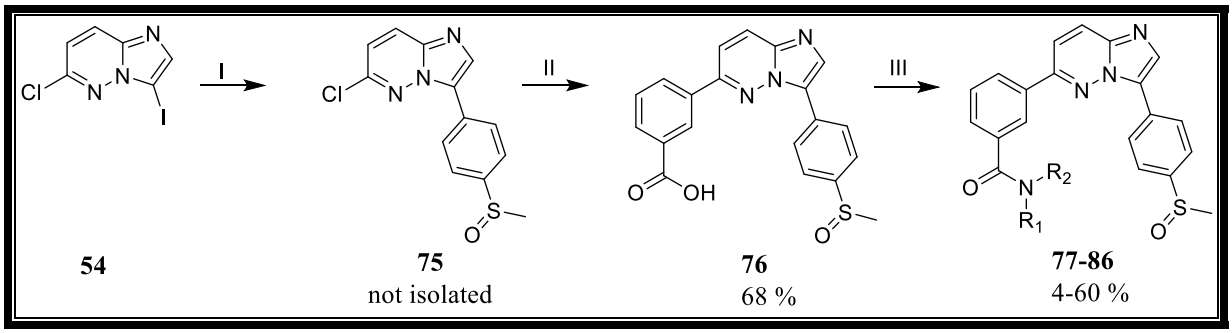

Scheme 7: Synthetic scheme for the synthesis of amidated imidazopyridazine analogues **77- 86**: *Reagents and conditions* (I) 4-methylsulfinylphenylboronic acid, $Pd(PPh_3)_2Cl_2$, 1M K_2CO_3, 1,4-dioxane, 80 °C, 14 h; (II) 3-carboxyphenylboronic acid, $Pd(PPh_3)_2Cl_2$, 1M K_2CO_3, 1,4-dioxane, 100 °C, 15 h ; (III) appropriate amine or amine hydrochloride salt, 50 % T3P in EtOAc, DIPEA, 1,4-dioxane, 0–30 °C, 1-3 h.

Table 3: Series 2 derivatives with respective % yields.

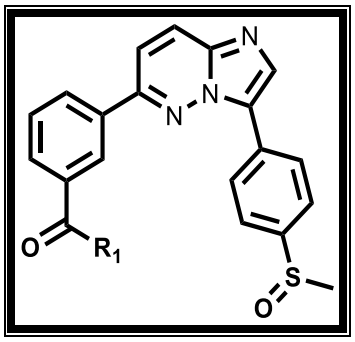

Compound code	R_1	Yield (%)
77	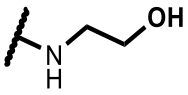	4%
78	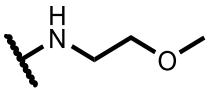	43
79	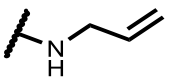	60
80	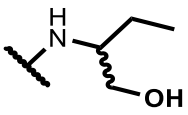	13

81	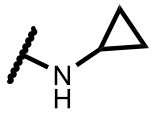	4
82		11
83		18
84	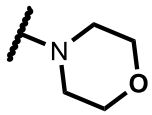	51
85	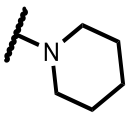	36
86	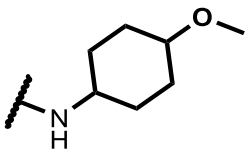	50

2.4.2 Characterisation of compound 77 (Step II, Scheme 7)

A ^{1}H-NMR spectrum of **76** is shown in **Figure 34**. A broad peak at 8.64–8.60 ppm was assigned to H16 and integrates for 1H. A sharp singlet at 2.83 ppm, which integrates for 3H was assigned to H26. A singlet was also observed at 8.40 ppm, integrating for 1H and was assigned to H8. Two 2-proton doublets of an AB spin system are observed at 8.46 (J = 8.81 Hz) and 7.83 ppm (J = 8.8 Hz) and were assigned to H17, H21 and H18, H20, respectively. A triplet integrating for 1H and observed at 7.63 ppm (J = 7.7 Hz) was assigned to H13. A relatively deshielded doublet at 8.31 ppm (J = 9.5 Hz) integrating for 1H was assigned to H6. A doublet appearing at 7.92 ppm (J = 9.5 Hz) and integrating for 1H was assigned to H1. Two doublet of triplets at 8.25 (J = 7.8, 2.0 Hz) and 8.08 ppm (J = 7.7, 1.9 Hz) each integrating for 1H were assigned to H12 and H14, respectively.

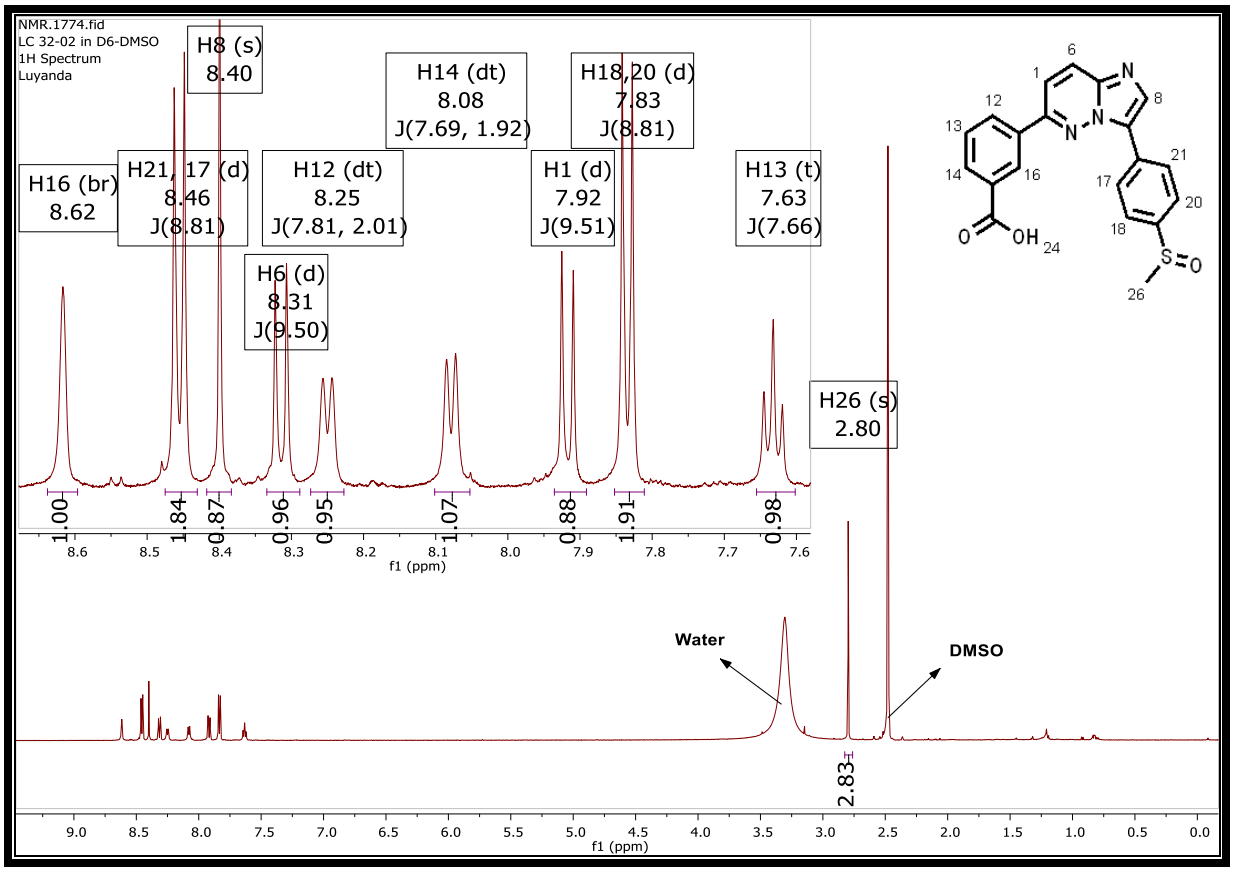

Figure 34: ^{1}H-NMR spectrum of **76** at 600 MHz in DMSO-d_6.

2.4.3 Characterisation of the final target compounds (Step III, Scheme 7)

For the target compounds in this portion of SAR, analogue **77** is used as a representative for ^{1}H-NMR interpretation (**Figure 35**). A triplet at 8.67 (J = 5.5 Hz) integrating for 1H was assigned to H30. H26 was assigned to a peak appearing as a triplet at δ 4.76 ppm (J = 5.6 Hz). Two quartets at 3.58 (J = 5.9 Hz) and 3.41ppm (5.8 Hz) each integrating for 2H were assigned to H28 and H27, respectively.

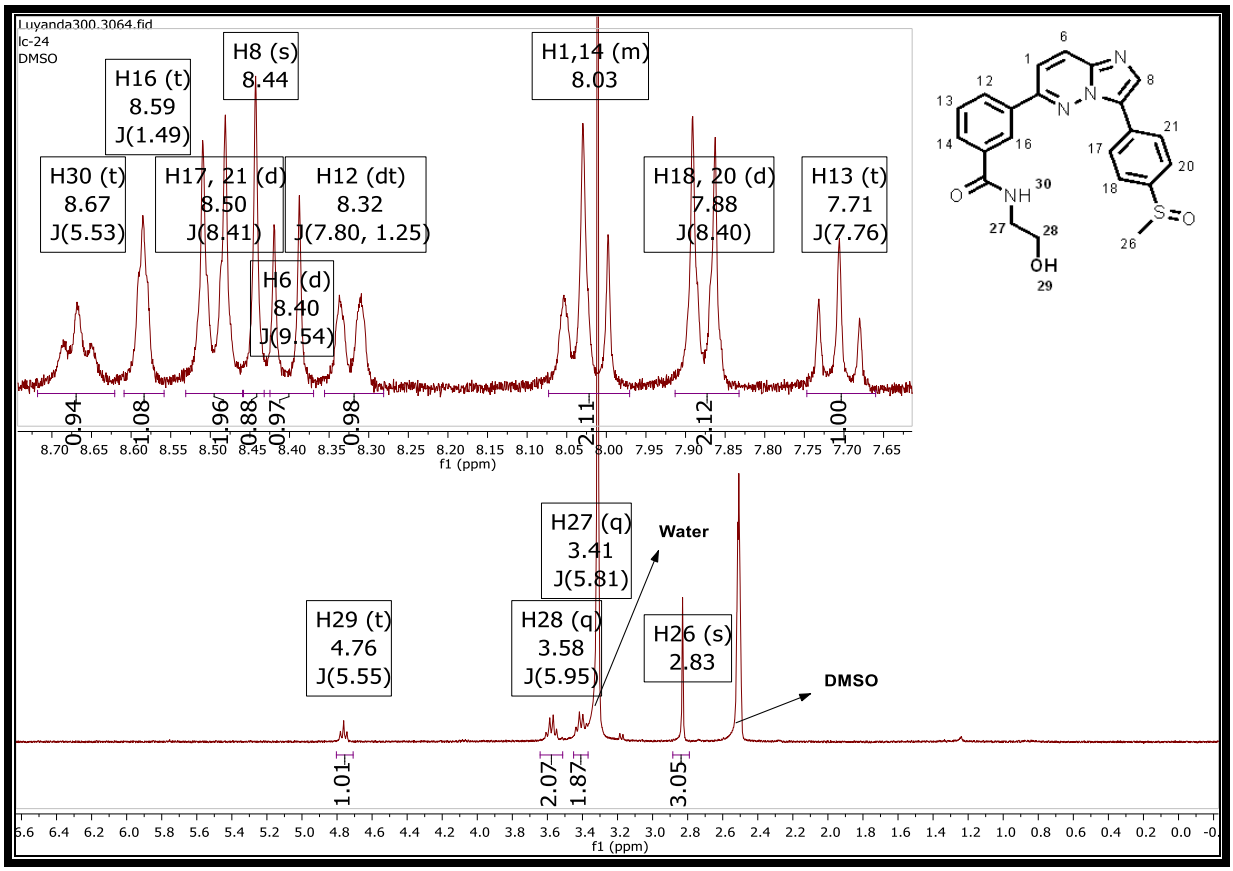

Figure 35: ^{1}H-NMR spectrum of **77** at 300 MHz in DMSO-d_6.

Chapter three

Pharmacological activity Evaluation of target compounds

3.1 Overview

All synthesized molecules were submitted for *in vitro* antiplasmodium activity testing against a chloroquine (CQ)-sensitive strain of *P. falciparum* (NF54). The potency of each molecule was measured as the concentration required to cause 50 % inhibition of the parasite's growth (IC_{50}). A low IC_{50} value is preferred to minimize undesirable side effects. A transgenic parasite line was employed in the luciferase assay, NF54-*Pf*S16-GFP-Luc, for gametocyte viability determination. The gametocytocidal assay allows the determination activity of each compound at both late and early stage of gametocyte development. Compounds were also evaluated for hERG inhibition activity against the hERG potassium channel and was determined using *in vitro* IonWorks patch-clamp electrophysiology.[81,82] The same compounds evaluated for hERG inhibition activity were evaluated for cytotoxicity.

3.2 Series 1 pharmacological evaluation: *in vitro* antiplasmodium activity against asexual blood stage parasites

Among the 16 compounds in **Table 4**, four (**64**, **67**, **68**, and **74**) were highly potent with IC_{50} value less than 100 nM. The compounds with larger cyclic substituent **65** (IC_{50} = 301 nM), **66** (IC_{50} = 136 nM), **69** (IC_{50} = 105 nM), **70** (IC_{50} = 521 nM), and **62** (IC_{50} = 590 nM) were found to be relatively less potent. Compounds with a hydroxyl group on the heterocyclic amide substituent **67** (IC_{50} = 18 nM), **68** (IC_{50} = 66 nM), and **69** (IC_{50} = 105 nM) were found to be more potent than those lacking the hydroxyl group **66** (IC_{50} = 136 nM), **65** (IC_{50} = 301 nM) and **70** (IC_{50} = 521 nM). The addition of a methyl substituent to the secondary amino group of **64** (IC_{50} = 67 nM) to form **63** (IC_{50} = 177 nM) was detrimental to activity. Looking at compounds **65** (IC_{50} = 301 nM) and **66** (IC_{50} = 136 nM), and **70** (IC_{50} = 521 nM) potent activity was observed with the morpholino ring and decreases when this ring is replaced by

piperazine and piperidine rings. The sulfone analogue **74 (**IC_{50} = 19 nM) was found to the more active than the corresponding sulfoxide **64** (IC_{50} = 67 nM) revealed that activity was improved. Converting the hydroxyl moiety (**57** IC_{50} = 371 nM) to an ether (**58** , IC_{50} = 144 nM) increased activity. The intermediate carboxylic acid **56** displayed reasonable activity with an IC_{50} value of 114 nM.

Table 4: Antiplasmodium activity of Series 1 analogues against *Plasmodium falciparum* (NF54).

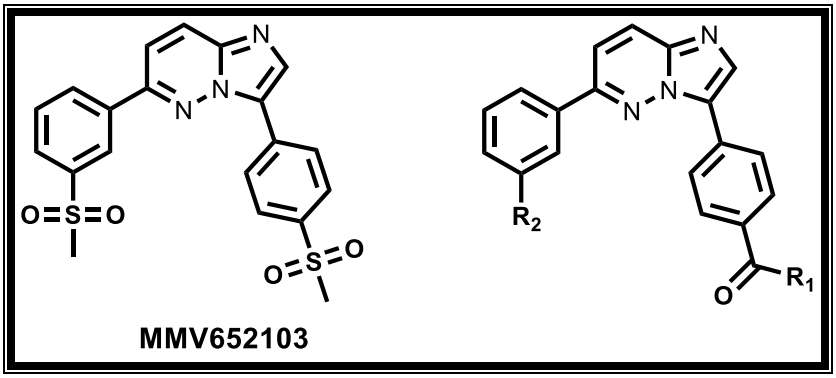

Compound code	R_2	R_1	NF54 IC_{50} (nM)[a,b]
MMV652103			7.3
56	SOMe		114
57	SOMe	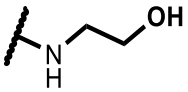	371
58	SOMe	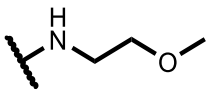	144
59	SOMe	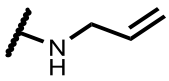	141

60	SOMe	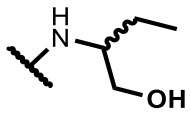	290
61	SOMe	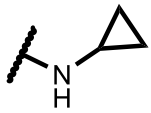	209
62	SOMe	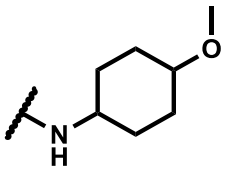	590
63	SOMe		177
64	SOMe		67
65	SOMe	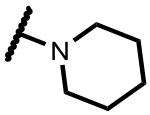	301
66	SOMe	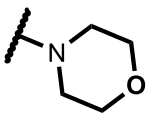	136
67	SOMe		18
68	SOMe	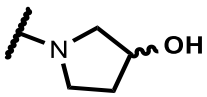	66
69	SOMe	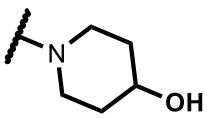	105
70	SOMe	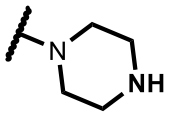	521
74	SO_2Me		19

[a]$IC_{50,}$ 50 % inhibitory concentration and values are average of ≥ 2 independent experiments.

[b]Chloroquine (IC_{50} = 16 nM) and artesunate (IC_{50} = 7 nM) were used as reference drugs.

3.4 Series 2 pharmacological evaluation: *in vitro* antiplasmodium activity

Among the ten compounds synthesized from Series 2 exploration (**Table 5**), five showed high activity with IC_{50} < 100 nM (**77, 79**, **83, 84**, and **85**). Methylation of **83** (IC_{50} = 60 nM) to form the dimethylated analogue **82** (IC_{50} = 131 nM) was detrimental to antiplasmodium activity. The piperidine moiety in **85** (IC_{50} = 3 nM) conferred greater activity than the morpholine moiety in **84** (IC_{50} = 16 nM), indicating that $–CH_2–$ is preferable to –O– in the six-membered ring. Incorporating a more rigid moiety such as cyclopropyl group in **81** (IC_{50} = 284 nM) was detrimental to antiplasmodium activity compared to all other flexible moieties [(**77**, **79–85**) < 201 nM] with exception of compound **86** (IC_{50} = 6000 nM). An amide functionality with large substituent such as in **86** (IC_{50} = 6000 nM) was detrimental to activity.

Table 5: Antiplasmodium activity of Series 2 analogues against *Plasmodium falciparum* (NF54).

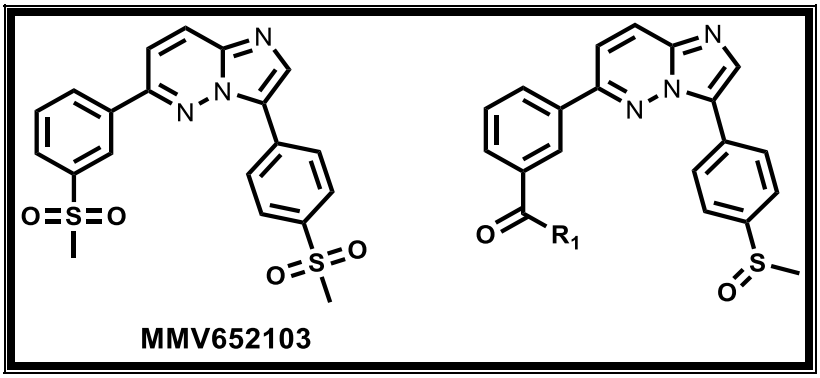

Compound code	R_1	NF54 IC_{50} (nM)[a,b]
MMV652103		7.3

77	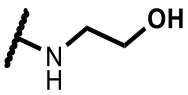	69
78	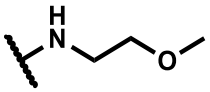	198
79	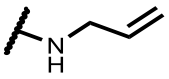	94
80	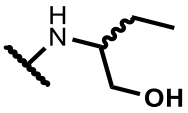	201
81	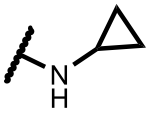	284
82		131
83		60
84	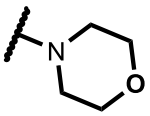	9
85	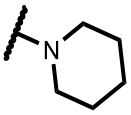	3
86	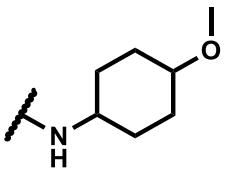	6000

[a]$IC_{50,}$ 50 % inhibitory concentration and values are average of ≥ 2 independent experiments.

[b]Chloroquine (IC_{50} = 16 nM) and artesunate (IC_{50} = 7 nM) were used as reference drugs.

3.5 *In vitro P. falciparum* gametocytocidal activity

As already mentioned, gametocytocidal compounds are of interest as they could block parasite transmission between man and the mosquito. The gametocytocidal activies of 13 compounds were evaluated and ranked accordingly (**Table 6**).

Table 6: Early and late gametocytocidal activity classification.

Criteria	Classification
> 70 % inhibition at 5 μM and > 50 % inhibition at 1 μM	High (IC_{50} < 100 nM)
> 70 % inhibition at 5 μM and < 50 % inhibition at 1 μM < 70 % inhibition at 5 μM and > 50 % inhibition at 1 μM 50–70 % inhibition at 5 μM and < 50 % inhibition at 1 μM	Moderate (100 nM < IC_{50} < 500 nM)
<50 % inhibition at 5 μM and < 50 % inhibition at 1 μM	Minimal (IC_{50} > 500 nM)

Of the 13 compounds tested against early-stage gametocytes, four (**74**, **79**, **84** and **85**), showed high gametocytocidal activity (**Table 7**). Moderate gametocytocidal activity was observed for compounds **57**, **58**, **59**, **78**, **81**, and **83**. Minimal activity was observed from compounds **61**, **62**, and **60**. With regards to late-stage gametocytocidal activity, compounds **60** and **61** displayed moderate activity. Minimal activity was observed from **62** and all other compounds showed high activity**.**

Table 7: *In vitro* evaluation of selected imidazopyridazines compounds for gametocydal activity.

Compound code	Structure	% inhibition in early–stage gametocytes, luciferase		% inhibition in late-stage gametocytes, luciferase	
		1µM	5µM	1µM	5µM
57	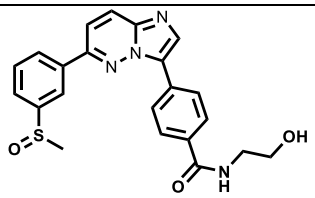	19	62	69	91
58	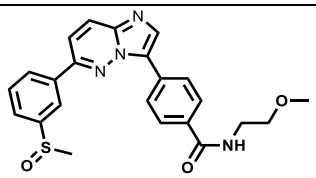	40	58	53	91
59	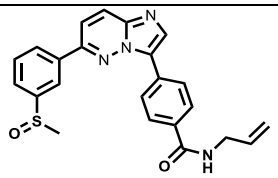	24	17	73	94
60	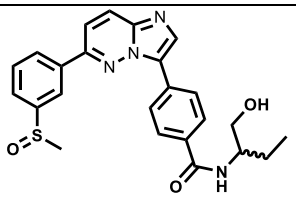	6	42	45	81
61	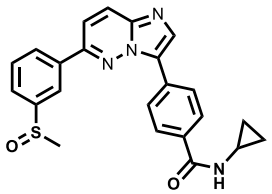	41	49	34	80

62	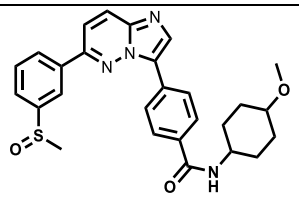	2	4	26	43
74	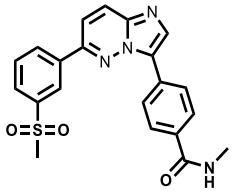	85	96	98	99
78	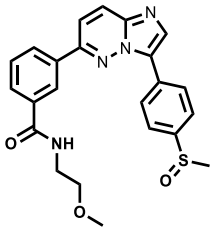	39	70	79	96
79	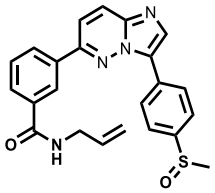	62	72	80	95
81	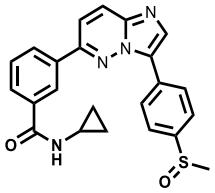	53	67	63	94
83	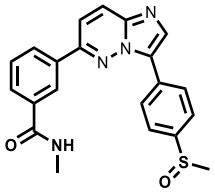	55	58	52	92
84	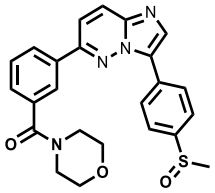	83	79	95	97

85	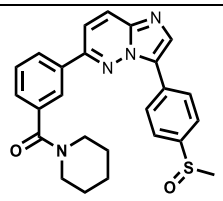	89	86	96	98

3.6 Cytotoxicity and hERG channel inhibition activity

Six selected compounds were evaluated for cytotoxicity using a Chinese Hamster Ovarian (CHO) mammalian cell line and hERG channel inhibition activity. The results are shown in **Table 8**. Compounds are considered to have an acceptable hERG inhibition profile if the *in vitro* hERG IC_{50} exceeds 10 μM and drugs in development are desired to have hERG activity *in vitro* > 30 μM.[83] Amidated analogues displayed an encouraging hERG channel inhibition activity profile except **65** whose hERG IC_{50} was below 10 μM. **Figure 36** depicts a plot of tPSA against hERG activity IC_{50} showing a positive moderate correlation. All compounds were found to have low cytotoxic and the positive values of log(SI) suggest that compounds are more selective towards the *Pf*NF54 strain than the CHO cells.

Table 8. Cytotoxicity and hERG activity results.

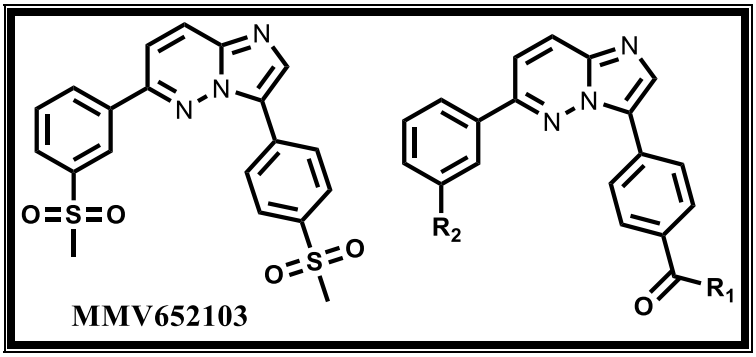

Compound code	R_1	CHO C_{50} (μM)	hERG IC_{50} (μM)	NF54 IC_{50} (μM)[a,b]	SI = CHO C_{50} / NF54 IC_{50}	Log(SI)
MMV652103		> 234	0.9	0.0073	> 30000	4.48
63		165	20.3	0.177	932	2.96
64		75.5	17.9	0.067	1127	3.05
65	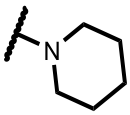	83	9.0	0.301	275	2.44
66	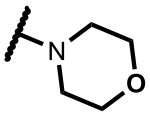	185	23.4	0.136	1360	3.13
67		> 231	20.9	0.018	12833	4.11
68	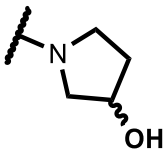	ND	30.4	0.066	ND	ND
69	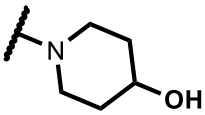	> 217	36.0	0.105	2067	3.32

hERG, human *ether-a go-go*-related gene; ND, no data; SI, selectivity index, [a]$IC_{50,}$ 50 % inhibitory concentration and values are average of ≥ 2 independent experiments;

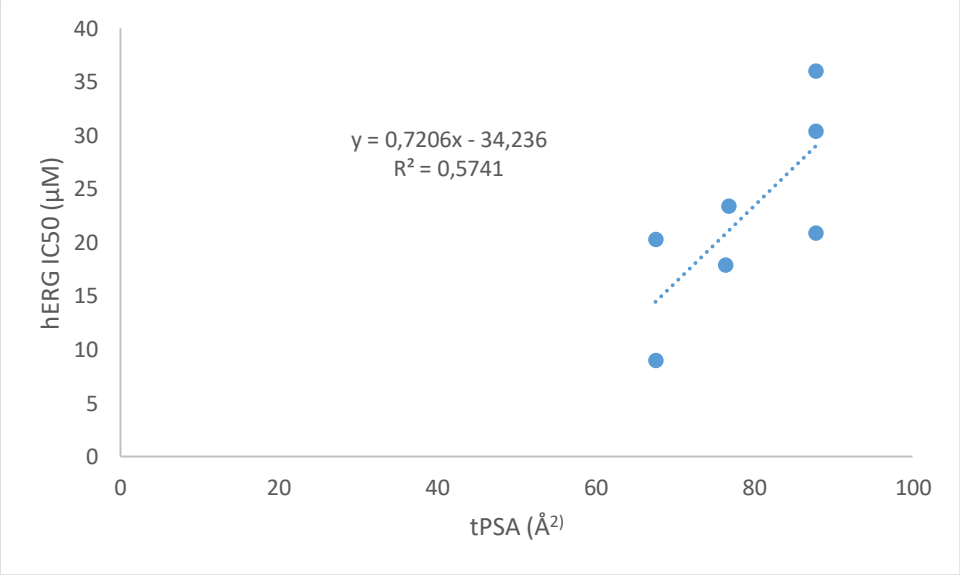

Figure 36: Scatter plot of hERG activity and total polar surface area.

3.7 Conclusions

A total of 26 imidazopyridazines were synthesized and evaluated for their *in vitro* antiplasmodium activities. A selection of the compounds showed superior activity compared with the lead compound **MMV652103** while a number were less potent. Results from testing against sexual gametocyte stage of the parasite suggest that late-stage gametocytes were more sensitive, as many molecules that were moderately or minimally active against early stage gametocytes displayed higher activity against late-stage gametocytes. Amidated analogues generally displayed a promising cytotoxicity and hERG channel inhibition profile.

Chapter four

Physicochemical property evaluation and structure-property relationships

4.1 Overview

The melting points of the compounds were determined experimentally using a Stuart SMP40 melting point apparatus. The commercially available reagent 3-amino-5-methylisozole was used for instrument calibration and the temperature was set to increase at 5 °C per minute. The mean average melting point of each compound using the instrument, and 1 °C was added and subtracted from this to obtain the melting point interval. The solubility of all synthesized compounds was evaluated via turbidimetric and HPLC-based kinetic solubility assays. Solubility assays are discribed fully in experimental section in chapter six.

Solubility results were used to rank the compounds following the classification listed in **Table 9** and **Table 10**.[43,84]

Table 9: Turbidimetric kinetic solubility rankings.

Classification	**Turbidimetric solubility (µM)**
highly insoluble	< 1
Moderately soluble	1-100
Highly soluble	> 100

Table 10: HPLC-based kinetic solubility rankings.

Classification	**HPLC-based solubility (µM)**
High soluble	≥ 150

Moderately soluble	50-150
Low	11-50
Very low	< 11

In an attempt to identify which physicochemical factor contributed to aqueous solubility, the physicochemical parameters were plotted [log(solubility) against melting point, cLogP, and tPSA]. **Table 11** uses Evan's guidelines to determine the degree of correlation strength based on R^2 values.[85]

Table 11: Correlation strength.

R^2	**Classification**
0.0–0.19	Very weak
0.20–0.39	Weak
0.40–0.59	Moderate
0.60–0.79	Strong
0.80–1.00	Very strong

4.2 Structure property relationship of Series 1

4.2.1 Effect of incorporating hydrogen bonding donors and acceptors to improve solubility

The solubility and melting point values of the compounds obtained from Series 1 are listed in **Table 12**. Turbidimetric kinetic solubility results**:** Compounds **58** (200 μM) and **61** (200 μM) were highly soluble, and compound **60** (80 μM) was moderately soluble. Introducing a bulky

cyclic group in **62** (< 5 μM) was detrimental to solubility. Compounds such as **58** (200 μM) with linear alkyl amide substituents and hydrogen bond acceptor moieties conferred greater solubility (200 μM).

HPLC–based solubility results: Compound **58** (155 μM) was highly soluble, while compounds **60** (10 μM) and **61** (10 μM) were very lowly soluble. On the other hand, compound **74** (< 5 μM) was poorly soluble compared to the highly soluble sulfoxide version **64**, indicating that the inclusion of a sulfone moiety lowered the aqueous solubility. High molecular weight is generally detrimental to solubility, as molecular weight increases so does cLogP. The effect of increasing solubility through incorporation of hydrogen bonding donor and acceptor groups is outweighed by high molecular weight [decreasing solubility: **64** (200 μM) > **69** (170 μM) > **62** (< 5 μM)] [increasing molecular weight: **62** (390.5 g/mol) < **69** (460.6 g/mol) < **62** (488.6 g/mol)].

Table 12: Solubility and melting points results of Series 1.

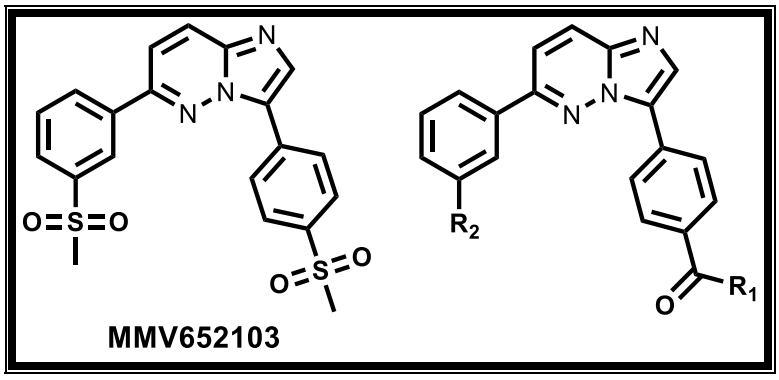

Compound code	R_2	R_1	Solubility (μM)	Melting point (°C)	clogP	tPSA
MMV652103			(<5*)	134.0–136.0	2.50	98.47

56	SOMe		ND	ND	2.91	84.56
57	SOMe	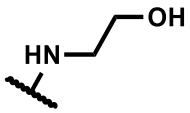	ND	207.0–209.0	1.98	96.59
58	SOMe	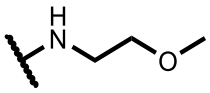	200 (155*)	315.7–317.5	2.61	85.59
59	SOMe	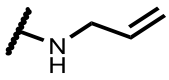	ND	192.6–194.6	2.80	76.36
60	SOMe	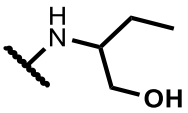	80 (10*)	268.9–270.9	2.63	96.59
61	SOMe	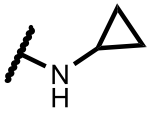	200 (10*)	236.4–238.4	2.94	76.36
62	SOMe	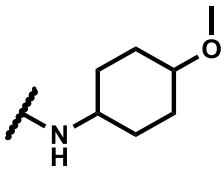	SM	264.0–266.0	3.91	85.49
63	SOMe		200*	ND	2.64	67.57
64	SOMe		195*	241.0–243.0	2.63	76.36
65	SOMe	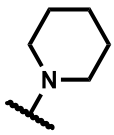	70*	268.0–270.0	3.83	67.60
66	SOMe	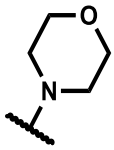	75*	247.8–249.8	2.73	76.80

67	SOMe	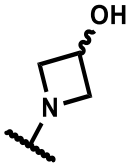	200*	ND	2.07	87.80
68	SOMe	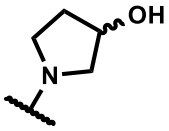	200*	ND	2.43	87.80
69	SOMe	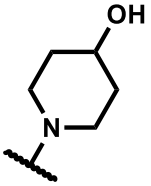	170*	243.2–245.2	2.59	87.80
70	SOMe	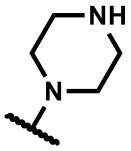	200*	248.0–250.0	2.48	79.60
74	SO_2Me		(<5*)	250.5–252.5	2.25	93.43

ND = not determined; cLogP, calculated log P, determined using StarDrop version 6.4; tPSA, total polar surface area, determined using StarDrop version 6.4; SM, solid material not dissolved after vortexing (< 5 μM);* HPLC-based solubility.

4.2.2 Effect of reducing cLog P to improve solubility

Correlation with cLogP (HPLC-based method): As shown in **Figure 37**, cLogP is very weakly and negatively correlated (R^2 = 0.1275), therefore, the observed changes on solubility was not attributed to cLogP changes.

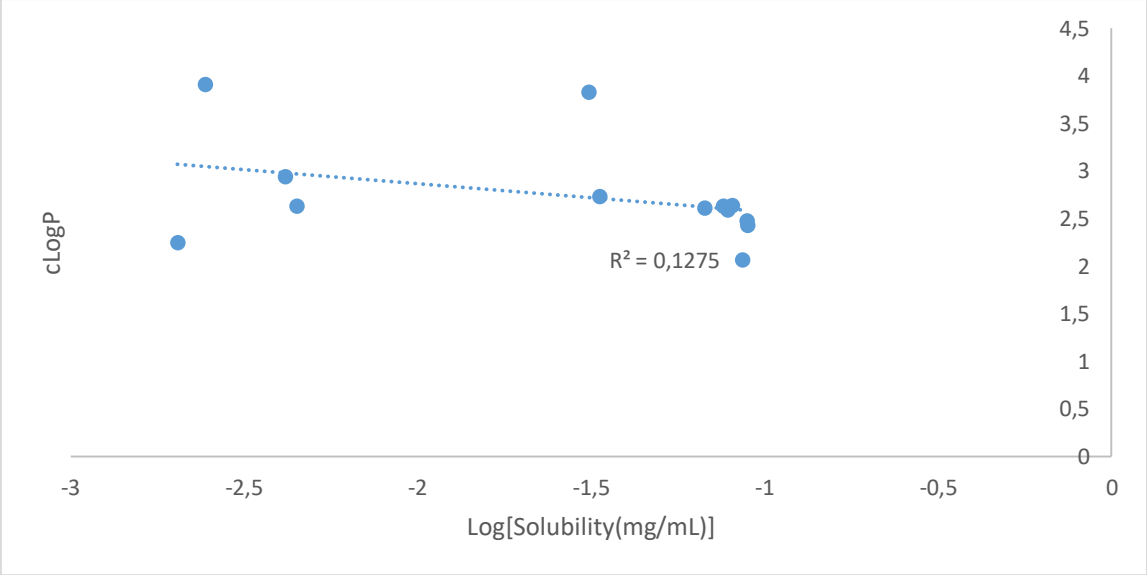

Figure 37: Series 1 log[Solubility (mg/mL)] versus cLogP.

All compounds had higher melting point relative to the parent compound **MMV652103.** The high melting points observed suggests that the compounds had higher crystal lattice energy than the parent compound.[86] However, compounds with low melting points are preferred as they are less likely to have many polymorphs.[87] As shown in **Figure 38**, melting point was very weakly correlated to log (solubility) (R^2 = 0.1827), therefore, melting point was not a causation for the observed changes on solubility.

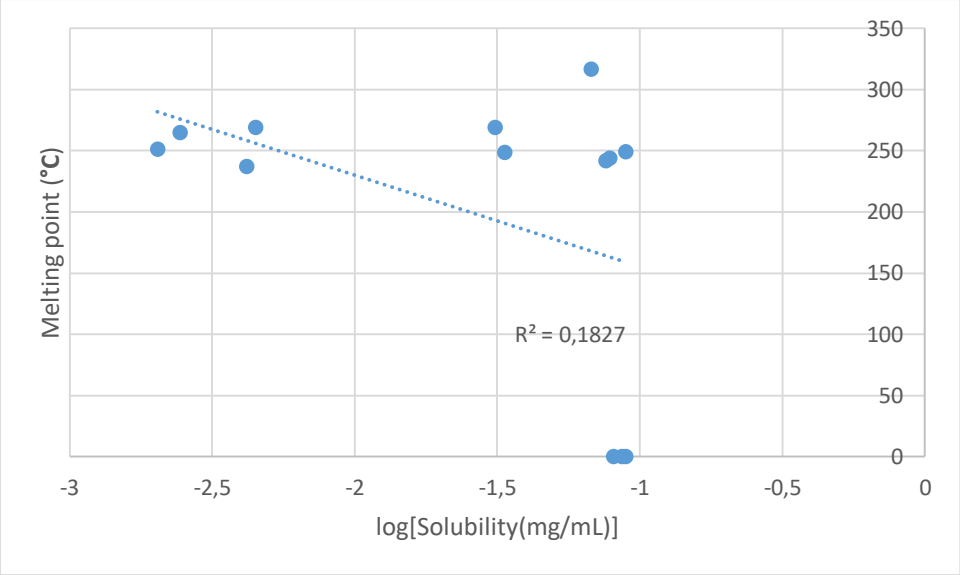

Figure 38: Series 1 log[Solubility (mg/mL)] versus melting point.

tPSA is important for permeation through cells, and is influenced by polar atoms such as oxygen and nitrogen, which also influence solubility. As shown in **Figure 39**, a plot of log(solubility) versus tPSA shows a very weak correlation (R^2 = 0.124), therefore, tPSA was not the causation for the changes observed on solubility.

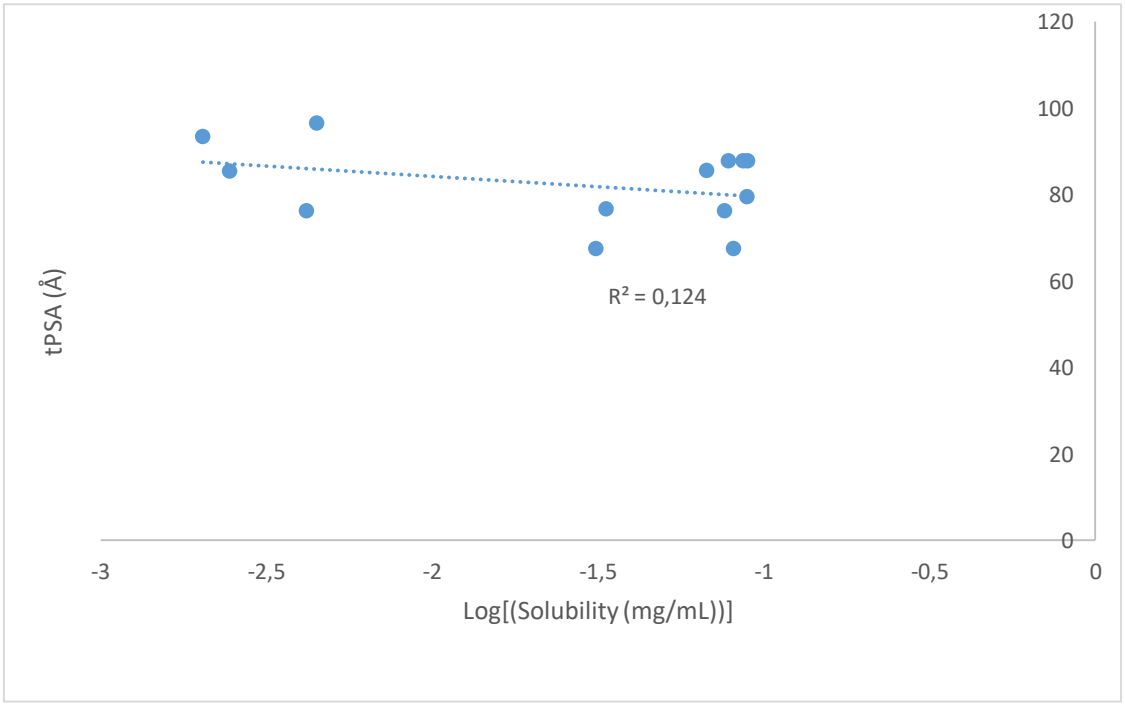

Figure 39: Series 1 log[Solubility (mg/mL)] versus tPSA.

4.3 Structure property relationship of Series 2

4.3.1 Effect of incorporating hydrogen bonding donors and acceptors to improve solubility

Turbidimetric solubility results: All Series 2 compounds were found to be highly soluble over the entire concentration range (0–200 µM) except compound **86** (< 5 µM). Introducing a bulky cyclic group in **86** (< 5 µM) was detrimental to solubility. The solubility and melting points of the compounds obtained from Series 2 are listed in **Table 13**.

Table 13: Solubility and melting points of Series 2 compounds.

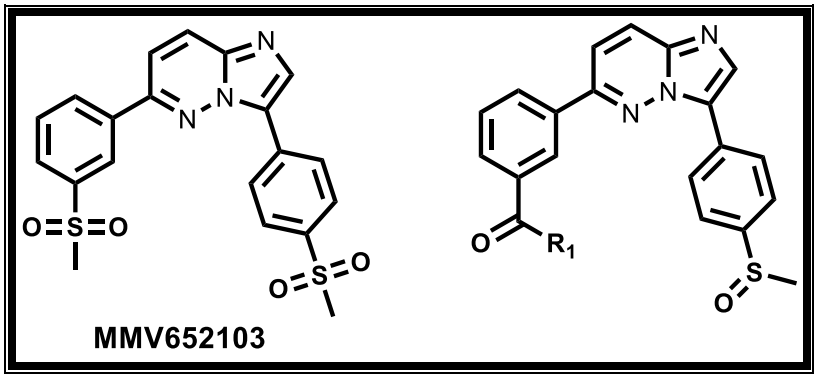

Compound code	R_1	Solubility (µM)	Melting point (°C)	cLogP	tPSA
MMV652103		(<5*)	134.0–136.0	2.50	98.47
77	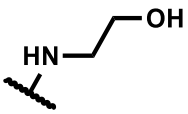	ND	ND	1.98	96.59
78	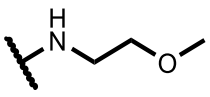	200	206.3-208.3	2.61	85.59
79	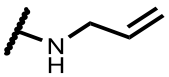	200	228.7-230.7	2.80	76.36
80	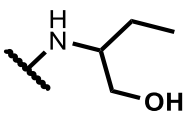	ND	ND	2.63	96.59

81	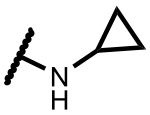	200	250.5–252.5	2.94	76.36
82		ND	ND	2.34	76.36
83		200	256.1–258.1	2.64	67.57
84	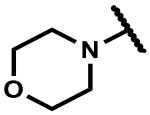	200	ND	3.83	67.57
85	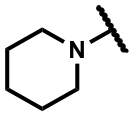	200	256.4–258.4	2.73	76.80
86	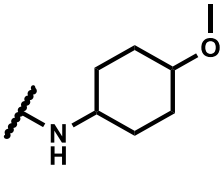	SM	308.4–310.4	3.91	85.59

ND = not determined; cLogP, calculated log P, determined using StarDrop version 6.4; tPSA, total polar surface area, determined using StarDrop version 6.4; SM, solid material not dissolved after vortexing (< 5 μM);* HPLC-based solubility.

4.3.2 Effects of changing physicochemical properties to improve solubility (Series 2)

Turbidimetric solubility**:** The changes in cLogP are shown in **Figure 40**. An excessively high cLogP value impacted the aqueous solubility, as observed in compound **86** (cLogP 3.91, <5 μM). Furthermore, **Figure 41** shows that cLogP is weakly correlated to solubility (R^2 = 0.3731), therefore, the observed changes on solubility was not be attributed to cLogP changes.

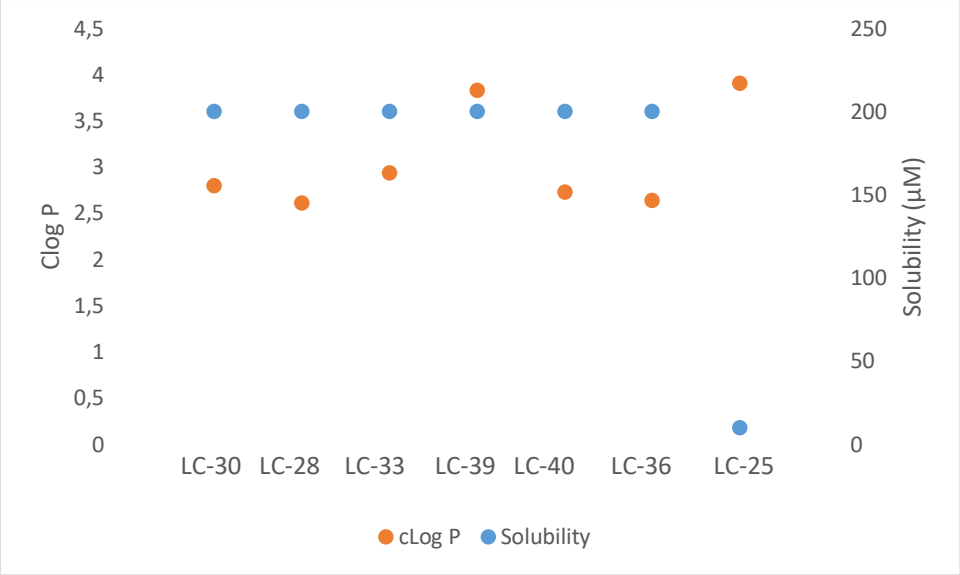

Figure 40: Solubility versus cLogP of Series 2 compounds.

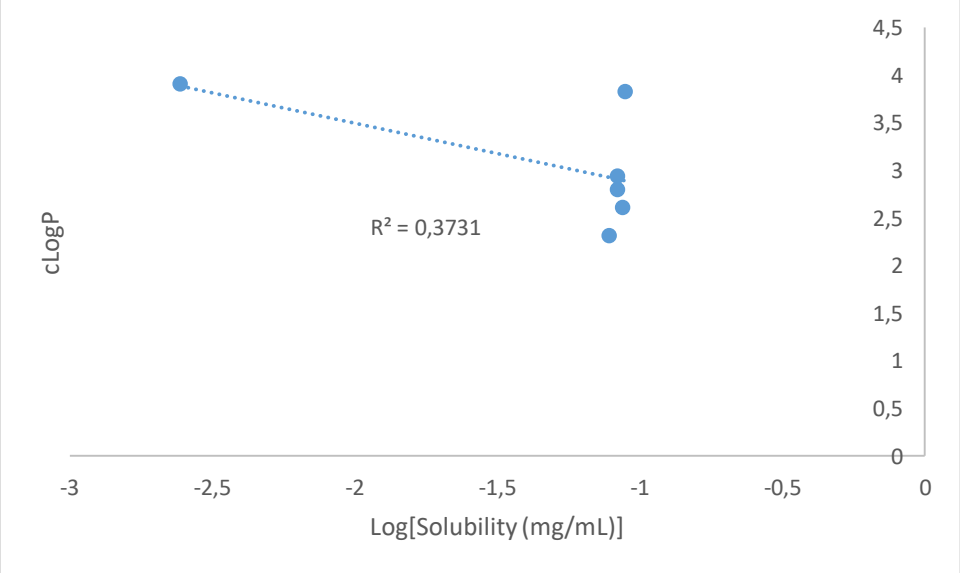

Figure 41: Series 2 log[Solubility (mg/mL)] versus cLogP.

The melting point and solubility are higher than the parent compound. As shown in **Figure 42**, melting point is strongly and negatively correlated, therefore, melting point was not causation for the observed changes on solubility.

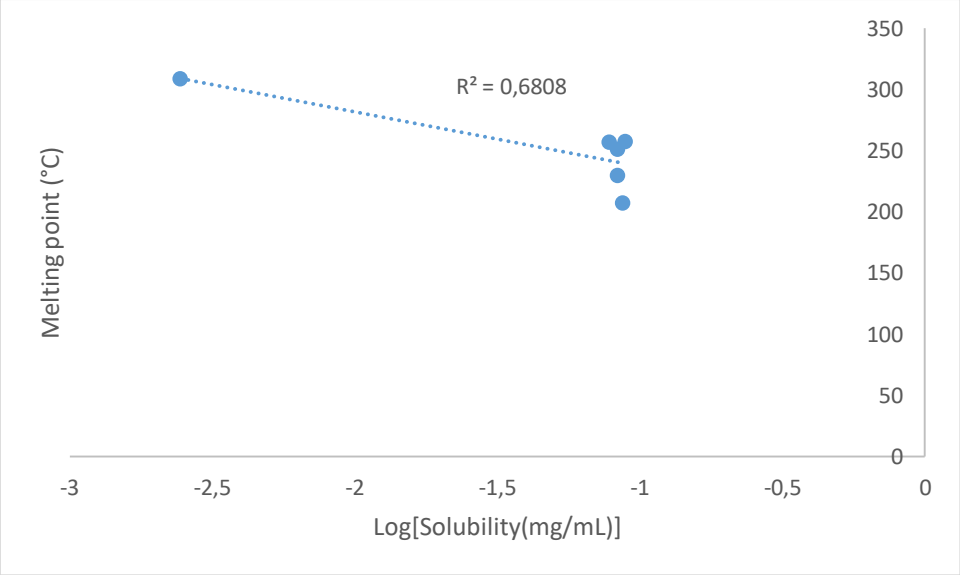

Figure 42: Series 2 log[Solubility (mg/mL)] versus melting point.

As shown in **Figure 43**, a plot of log(solubility) versus tPSA shows weakly correlated (R^2 = 0.2837), therefore, tPSA was not the causation for the changes observed on solubility.

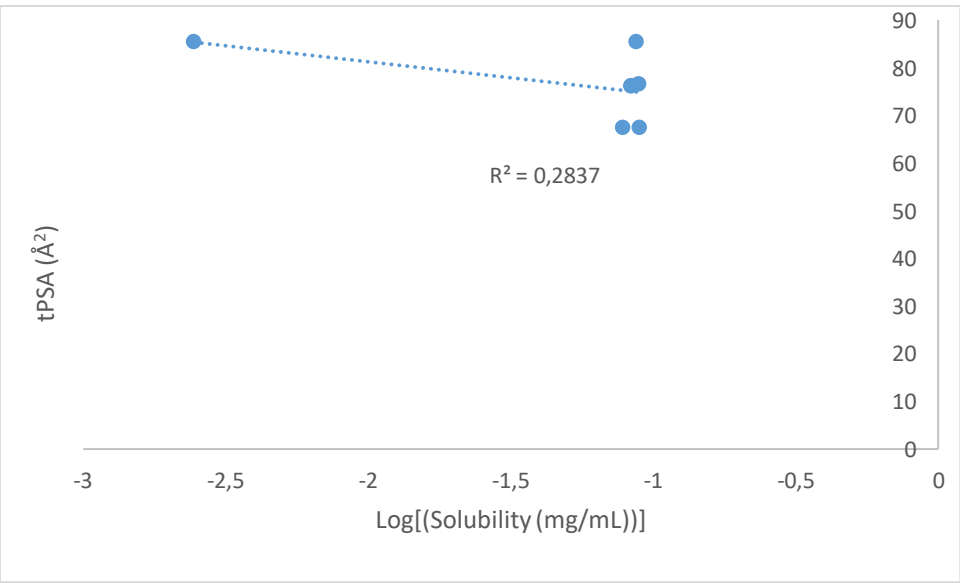

Figure 43: Series 2 log[Solubility (mg/mL)] versus tPSA.

4.5 Conclusions

Series 1 and Series 2 compounds were synthesized and their solubility was analysed using kinetic turbidimetric and HPLC-based methods. Physicochemical parameters affecting

solubility such as cLogP, tPSA and melting point were analysed to deduce which physicochemical factor affected solubility. The parent compound displayed poor solubility, which was improved by designing derivatives that incorporated hydrogen bonding donors and acceptors. The cLogP of both Series 1 and Series 2 compounds was negatively correlated, which implies that the observed improvements in aqueous solubility was not simply caused by increasing or decreasing cLogP. In Series 1 compounds melting point was negatively correlated with solubility but strongly negatively correlated in Series 2 compounds.

In Series 2 compounds, molecules returned highly soluble over the entire concentration range of 0–200 µM. In both series, tPSA was negatively correlated; hence it was not a key factor contributing to the observed improvement in solubility. In the Series 1 and Series 2, log(Solubility) was negatively correlated with melting point, cLogP, and tPSA. Therefore, incorporated hydrogen bonding donors and acceptors moieties were responsible for the improved aqueous solubility.

Chapter Five

Summary and conclusions

A series of amidated imidazopyridazine derivatives designed to improve solubility and address hERG potassium channel inhibition activity was synthesized and evaluated for *in vitro* antiplasmodium activity against asexual blood and sexual gametocyte stage parasites. All compounds were characterised by ^{1}H-NMR (1D and 2D), ^{13}C-NMR, LC-MS and melting point.

The solubility of the compounds was determined using kinetic solubility turbidimetric- and HPLC-based methods.

The following conclusions can be drawn from the *in vitro* antiplasmodium (asexual blood and sexual gametocyte stage parasites), hERG, cytotoxicity, and as solubility:

- In comparison to the lead compound **MMV652103**, structural modifications generally led to compounds with reduced potency albeit analogues showing potency in the low nanomolar range were identified.
- Switching moieties from the right-hand side to left-hand side did not necessarily preserve antiplasmodium activity.
- Compounds that displayed high antiplasmodium activity (IC_{50} < 100 nM) against asexual blood stage also displayed highest inhibition (> 70 %, 1 and 5 μM) against the sexual early and late-stage gametocytes.
- Relative to the parent compound, strategies to improve solubility generally resulted in solubility enhancement in the new amidated analogues.
- Several compounds were identified with encouraging cytotoxicity and hERG profiles.

5.1 Future work

Based on findings from Series 1 and Series 2 studies described in this dissertation, chemical features identified to be important for potency and solubility can be used to design the next generation of analogues proposed in **Figure 44**. Since the amide functionality is tolerated for both solubility and antiplasmodium activity, to further expand SAR, amide functionalities can be introduced on the right-hand and left-hand side portions of the molecule at the *para* and *meta* position. Furthermore, based on previous work done that delivered compounds active *in vivo*, SAR studies can be expanded to include a scaffold change from the imidazopyridazine scaffold to the pyrazolopyridine[68] scaffold as depicted in **Figure 44**.

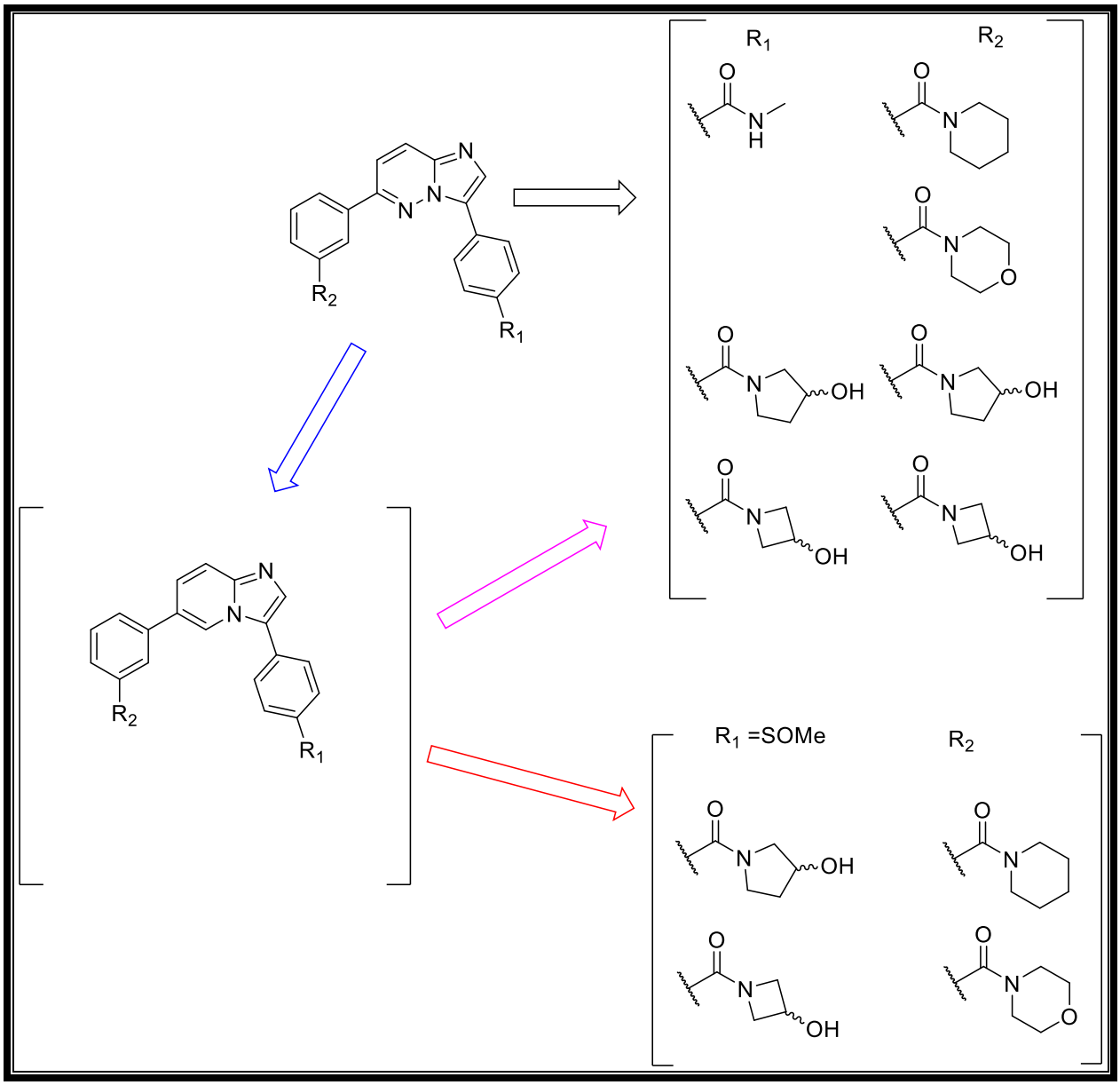

Figure 44: Future work molecules.

Chapter six

Experimental

6.1 Chemicals, solvents, and apparatus

Reagents and chemicals used during the experiments were purchased from Sigma-Aldrich and Combi-Blocks used without further purification. All solvents that were used during the experiments were anhydrous except ethanol which was analytical reagent (AR) grade and absolute (99.9 %). The progress of each reaction was monitored by a combination of thin layer chromatography (TLC) and liquid chromatography-mass spectrometry (LC-MS). The TLC plates employed were sourced from Merck (TLC Silica gel 60 F_{254} coated on aluminium sheets). All TLC plates were developed in a sealed container and the retardation factor (Rf) was used to determine a suitable mobile phase for purification in column chromatography. The TLC plates were visualized under ultraviolet light (UV 254 and 366 nm). An Agilent LC-MS instrument with the following components was used to monitor the progress of reactions including percent purity determinations: Agilent 1260® Infinity Binary Pump, Agilent 1260® Infinity Diode Array Detector, Agilent 1290® Infinity Column Compartment, Agilent 1260® Infinity Autosampler, Agilent 6120® Quadrupole LC/MS, and Peak Scientific® Genius 1050 Nitrogen Generator. An X-bridge® (C18, 2.5µm, 3.0 mm (ID) x 50 mm length) column maintained at 35 °C was used. The chromatographic mobile phase was composed of 10 mM aqueous ammonium acetate (NH_4Ac) spiked with 0.4 % acetic acid while the organic phase was composed of 10 mM NH_4Ac in methanol spiked with 0.4 % acetic acid. The mass spectra were acquired using electrospray ionisation (ESI) or atmospheric pressure chemical ionization (APCI) in the positive ionisation mode unless otherwise stated. The manual glass tube columns employed *Fluka* high purity grade silica gel (pore size 60 Å, 70–230 mesh, 63–200 µm). Additionally, Analtech Uniplate preparative TLC (prep-TLC) plates (20 × 20 cm, 2000 microns) were used for prep-TLC purifications.

The solvents used as mobile phases were AR grade and were used without further distillation. ^{1}H-NMR and ^{13}C-NMR spectra were acquired on either Bruker AV 400 (^{1}H 400.0, ^{13}C 100.6 MHz) or Varian Mercury 300 (^{1}H 300.1, ^{13}C 75.5 MHz) spectrometers housed in the Department of Chemistry at the University of Cape Town. All ^{1}H-NMR and ^{13}C-NMR spectra were acquired at 30 °C in deuterated solvents (DMSO-d_6 or CD_3OD). The one-dimensional ^{1}H-NMR and ^{13}C-NMR spectra were processed using MestReNova v10.0.2-15465. Multiplicity patterns are reported using the following abbreviations s = singlet, d = doublet, t = triplet, m = multiplet, dd = doublet of doublets, br = broad, br s = broad single, br m = broad multiplet, t = triplet, dt = doublet of triplets, td = triplets of doublets, q = quartet, qd = quadruplet of doublets, ddt = doublet of doublets of triplets. Coupling constants (*J* values) are reported in Hertz (Hz). Where assignment of ^{1}H-NMR and ^{13}C-NMR signals was ambiguous, two-dimensional NMR spectra from Correlation Spectroscopy (COSY), and Heteronuclear Single Quantum Coherence (HSQC) spectroscopy were acquired to facilitate accurate assignments. The Attached Proton Test (APT) was employed to identify negative and positive carbon. All final compounds were subjected to purity check experiments using LC-MS to ensure an acceptable level of purity (≥ 95 %).

6.2 Synthesis

6.2.1 Synthesis of 53.

A solution of 3-amino-6-chloropyridazine (1.0 equiv), deionized water (7.7 mmol/ 10 mL), ethanol (7.7 mmol/15 mL) and bromoacetaldeyde diethylacetal (2.0 equiv) and 48 % aqueous HBr (1.0 equiv) were added. The reaction mixture was refluxed at 103 °C over 16 h. After all starting material was consumed; the solvents were removed *in vacuo*. The crude material was dissolved in dichloromethane and washed with saturated solution of $NaHCO_3$, NaCl and dried over Na_2SO_4 anhydrous.

***6-Chloroimidazo [1, 2-b]pyridazine* 53.**[67]

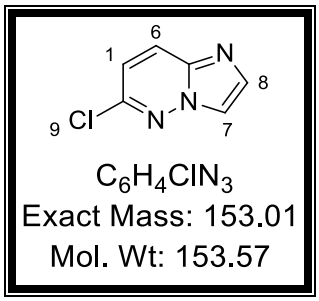

Beige solid (5.63 g, 79 %); m.p 117.9–119.9 °C; Rf = 0.23 (3 % MeOH/DCM); ^{1}H NMR (300 MHz, Methanol-d_4) δ 8.12–8.10 (br, 1H, H7), 8.02 (d, *J* = 9.5 Hz, 1H, H6), 7.78 (d, *J* = 1.3 Hz, 1H, H8), 7.28 (d, *J* = 9.5 Hz, 1H, H1); ^{13}C NMR (101 MHz, DMSO) δ 146.88, 137.63, 134.81, 128.00, 119.51, 117.94. LC-MS, ESI/APCI: *m/z* $[M + H]^+$ = 154.1, t_r = 0.339 min. Purity = 98 %.

6.2.2 General procedure for synthesis of 54 and 72.

The intermediate **53** (1.0 equiv) was dissolved in DMF (30 mmol / 30 mL), and the mixture was stirred and flushed with nitrogen for 30 mins. NIS (1.1 equiv) was added in one portion, stirred at 30 °C for 6 days. The DMF was removed *in vacuo*. The residue was dissolved in 80 mL DCM and was washed with saturated solution of $NaSO_2O_7$. The compound was dried over $MgSO_4$ and filtered and washed with DCM, DCM was removed *in vacuo*. The described method was also used to synthesize **72** and its starting material is compound **71**.

***6-Chloro-3-iodoimidazo[1,2-b]pyridazine* 54.**[67]

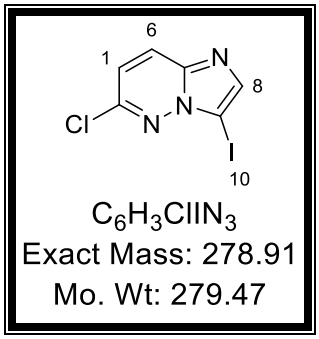

Yellow solid (8.56 g, 79 %); m.p 117.9–119.9 °C; Rf = 0.54 (2 %MeOH/DCM). ^{1}H NMR (300 MHz, Methanol-d_4) δ 8.02 (d, *J* = 9.5 Hz, 1H, H6), 7.87 (s, 1H, H8), 7.34 (d, *J* = 9.5 Hz, 1H, H1); ^{13}C NMR (101 MHz, $CDCl_3$) δ 148.52, 139.47, 126.23 (2C), 120.45, 77.42. LC-MS, ESI/APCI: *m/z* $[M + H]^+$ = 279.7, t_r = 2.52 min. Purity = 78 %.

***3-Iodo-6-(3-(methylsulfonyl)phenyl)imidazo[1,2-b]pyridazine* 72.**

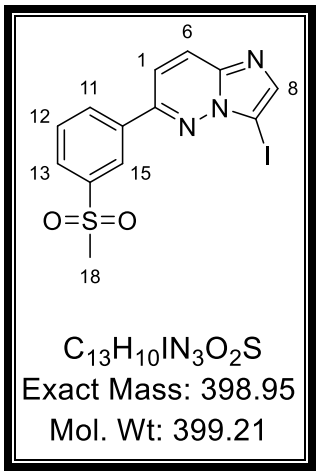

Yellow solid (0.855 g, 87 %). m.p 204.3–206.3 °C; Rf = 0.68 (4 % MeOH/DCM). ^{1}H NMR (400 MHz, DMSO-d_6) δ 8.65 (t, *J* = 1.9 Hz, 1H, H15), 8.48 (dt, *J* = 7.9, 1.83 Hz, 1H, H11), 8.29 (d, *J* = 9.5 Hz, 1H, H6), 8.13 (dt, *J* = 7.8, 1.9 Hz, 1H, H13), 8.03–7.97 (m, 2H, H1 & H8), 7.90 (t, *J* = 7.9 Hz, 1H, H12), 3.34 (s, 3H, H18); ^{13}C NMR (101 MHz, DMSO) δ 150.78, 142.41, 141.03, 140.76, 136.51, 132.34, 130.89, 128.96, 126.60, 125.75, 117.07, 72.70, 43.97. LC-MS, ESI/APCI: *m/z* $[M + H]^+$ = 399.6, t_r = 2.45 min. Purity = 100 %.

6.2.3 General procedure for Suzuki-Miyaura coupling at 80 °C and 100 °C of compounds 53, 54, 55 and 72.

The compound **54** (1.0 equiv), 4-boronobenzoic acid (1.1 equiv), $Pd(PPh_3)_2Cl_2$ (0.05 equiv) were dissolved in DMF (1.79 mmol / 5 mL). The resulting mixture was flushed in nitrogen for 30 mins, after which 1 M solution of K_2CO_3 (1.05 equiv) was added to the reaction mixture. The reaction mixture was heated to 80 °C and stirred for 12 h. DMF in the reaction

mixture was removed using toluene *in vacuo*. The intermediate was purified using flash column chromatography 1 % methanol / ethyl acetate and acidified with drops of glacial acetic acid. The same procedure was repeated at 100 °C for the following compounds as starting materials **55**, **72.**

***4-(6-Chloroimidazo [1,2-b]pyridazin-3-yl)benzoic acid* 55.**

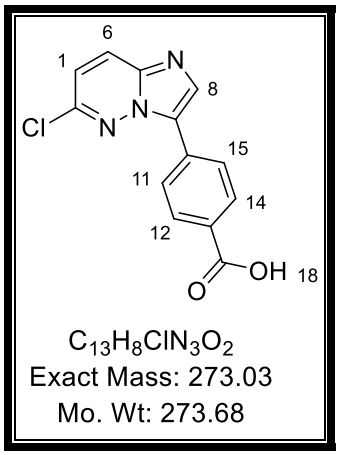

Yellow solid (4.42 g, 85 %); m.p not determined; Rf = 0.38 (4 % MeOH/ ethyl acetate); ^{1}H NMR (600 MHz, DMSO-d_6) δ 8.43 (s, 1H, H8), 8.32 (d, *J* = 9.4 Hz, 1H, H6), 8.23 (d, *J* = 8.8 Hz, 2H, H12 & H14), 8.08 (d, *J* = 8.8 Hz, 2H, H11 & H15), 7.46 (d, *J* = 9.5 Hz, 1H, H1); ^{13}C NMR (151 MHz, DMSO) δ 167.80, 147.02, 139.66, 135.22, 131.94, 131.28, 130.19 (2C), 128.71, 127.44, 126.33 (2C), 119.66. LC-MS, ESI/APCI: *m/z* $[M + H]^+$ = 273.87, t_r = 2.54 min. Purity = 93 %.

***4-(6-(3-(Methylsulfinyl)phenyl)imidazo[1,2-b]pyridazin-3-yl)benzoic acid* 56.**

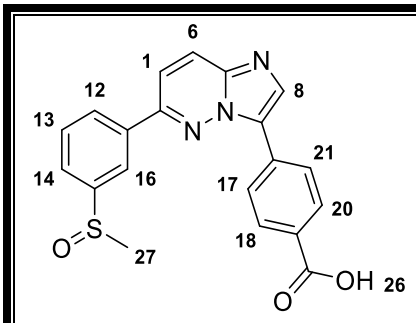

Chemical Formula: $C_{20}H_{15}N_3O_3S$
Exact Mass: 377,08
Molecular Weight: 377,42

Yellow solid (1.38 g, 59 %); m.p not determined; Rf = 0.36 (10 % MeOH / DCM). ^{1}H NMR (600 MHz, DMSO-d_6) δ 8.43 (t, *J* = 1.8 Hz, 1H, H16), 8.36–8.29 (m, 3H, H12 & H8 & H6), 8.18 (d, *J* = 8.4 Hz, 2H, H18 & H20), 8.05 (d, *J* = 8.3 Hz, 2H, H17 & H21), 7.96 (d, *J* = 9.5 Hz, 1H, H1), 7.87 (dt, *J* = 6.9, 1.2 Hz, 1H, H14), 7.81 (t, *J* = 7.7 Hz, 1H, H13), 2.86 (s, 3H, H27); ^{13}C NMR (151 MHz, DMSO) δ 169.65, 150.57, 148.14, 140.66, 139.63, 136.74, 134.20, 130.63, 129.86 (2C), 129.55 (2C), 128.79, 128.43, 126.95, 125.60 (2C), 122.52, 116.17, 43.73. LC-MS, ESI/APCI: *m/z* $[M + H]^+$ = 377.8, t_r = 2.52 min. Purity = 95 %.

***4-(6-(3-(Methylsulfonyl)phenyl)imidazo[1,2-b]pyridazin-3-yl)benzoic acid* 73.**

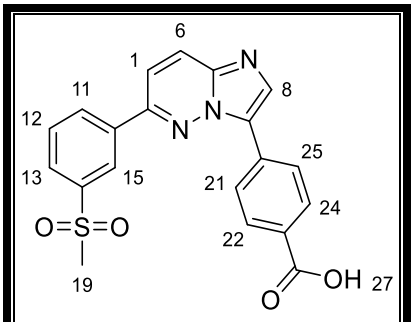

$C_{20}H_{15}N_3O_4S$
Exact Mass: 393,08
Mol. Wt: 393,42

Yellow solid (0.798 g, 41 %); Rf = 0.38 (4 % MeOH/DCM); ^{1}H NMR (400 MHz, DMSO-d_6) δ 8.67 (t, *J* = 1.8 Hz, 1H, H15), 8.52 (dt, *J* = 7.9, 1.9 Hz, 1H, H11), 8.43 (s, 1H, H8), 8.40 (d, *J* = 9.5 Hz, 1H, H6), 8.34 (d, *J* = 8.7 Hz, 2H, H22 & H24), 8.12 (dt, *J* = 7.8, 1.9 Hz, 1H, H13), 8.09 (d, *J* = 8.3 Hz, 2H, H21 & H25), 8.05 (d, *J* = 9.6 Hz, 1H, H1), 7.91 (t, *J* = 7.9 Hz, 1H, H12), 3.35 (s, 3H, H19); ^{13}C NMR (101 MHz, DMSO) δ 168.44, 150.23, 142.44, 140.08, 136.79, 135.04, 131.26, 132.36, 131.21, 130.96, 130.06 (2C), 128.82, 127.78, 127.17, 126.09 (2C), 125.87, 116.57, 43.96. LC-MS, ESI/APCI: *m/z* $[M + H]^+$ = 393.8, t_r = 3.56 min. Purity = 97 %.

***6-(3-(Methylsulfonyl)phenyl)imidazo[1,2-b]pyridazine* 71.**

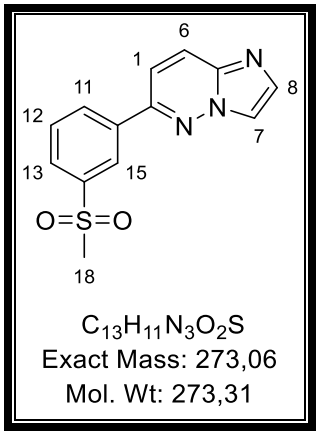

Yellow solid (0.650 g, 63 %); m.p 201.9–203.9 °C; Rf = 0.54 (4 % MeOH/DCM); ^{1}H NMR (400 MHz, DMSO-d_6) δ 8.54 (t, *J* = 1.9 Hz, 1H, H15), 8.41–8.35 (m, 2H, H8 & H 11), 8.23 (d, *J* = 9.5 Hz, 1H, H6), 8.07 (dt, *J* = 12.9, 1.2 Hz, 1H, H13), 7.88 (d, *J* = 9.8 Hz, 1H, H1), 7.85–7.81 (m, 2H, H12 & H7), 3.29 (s, 3H, H18); ^{13}C NMR (101 MHz, DMSO) δ 150.30, 142.14, 138.29, 136.60, 134.87, 132.39, 130.91, 128.73, 126.55, 125.53, 117.86, 116.81, 43.94. LC-MS, ESI/APCI: *m/z* $[M + H]^+$ = 273.9, t_r = 2.69 min. Purity = 98 %.

6.2.4 General procedure for amide coupling via propylphosphonic anhydride solution ≥ 50 wt. % in ethyl acetate to form 57-69.

An ice water cooled mixture containing a dissolved carboxylic acid intermediate **56** (1.0 equiv), DIPEA (7.0 equiv), appropriate amine (3.0 equiv) in DMF was stirred and propylphosphonic anhydride solution ≥ 50 wt. % in ethyl acetate (4.0 equiv) solution was added dropwise to afford a desired compounds.

***N-Allyl-4-(6-(3-(methylsulfinyl)phenyl)imidazo[1,2-b]pyridazin-3-yl)benzamide* 59.**

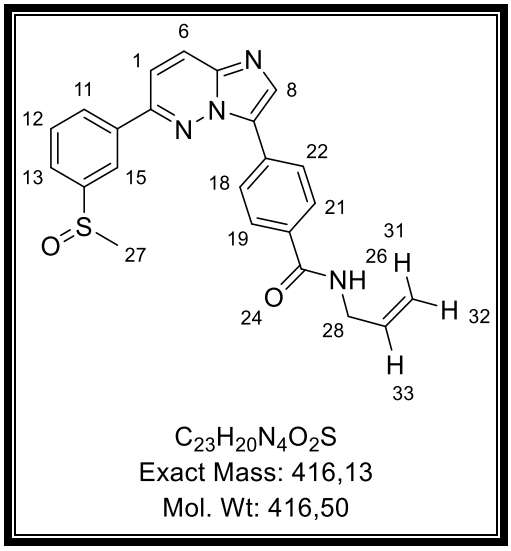

$C_{23}H_{20}N_4O_2S$
Exact Mass: 416,13
Mol. Wt: 416,50

Yellow solid (0.0232 g, 14 %); m.p 192.6–194.6 °C; Rf = 0.32 (2 % MeOH/DCM); ^{1}H NMR (600 MHz, Methanol-d_4) δ 8.41 (t, *J* = 1.8 Hz, 1H, H15), 8.26 (d, *J* = 8.6 Hz, 2H, H19 & H21), 8.23 (dt, *J* = 5.2, 1.26 Hz, 1H, H11), 8.18 (s, 1H, H8), 8.13 (d, *J* = 9.5 Hz, 1H, H6), 7.98 (d, *J* = 8.5 Hz, 2H, H18 & H22), 7.86–7.81 (m, 2H, H1 & H13), 7.75 (t, *J* = 7.9 Hz, 1H, H12), 6.00 (ddt, *J* = 17.1, 10.3, 5.5 Hz, 1H, H33), 5.30 (dq, *J* = 17.2, 1.7 Hz, 1H, H31), 5.18 (dq, *J* = 10.3, 1.5 Hz, 1H, H32), 4.06 (dt, *J* = 5.6, 1.7 Hz, 2H, H28), 2.89 (s, 3H, H27); ^{13}C NMR (151 MHz, MeOD) δ 167.97, 150.86, 146.36, 139.85, 136.81, 134.26, 133.54, 133.10, 131.25, 130.02, 129.53, 127.94, 127.34 (2C), 126.17 (2C), 125.64, 125.11, 121.99, 116.34, 114.98, 42.34, 41.98. LC-MS, ESI/APCI: *m/z* $[M + H]^+$ = 416.8, t_r = 2.66 min. Purity = 97 %.

***N-(2-Methoxyethyl)-4-(6-(3-(methylsulfinyl)phenyl)imidazo[1,2-b]pyridazin-3-yl)benzamide* 58.**

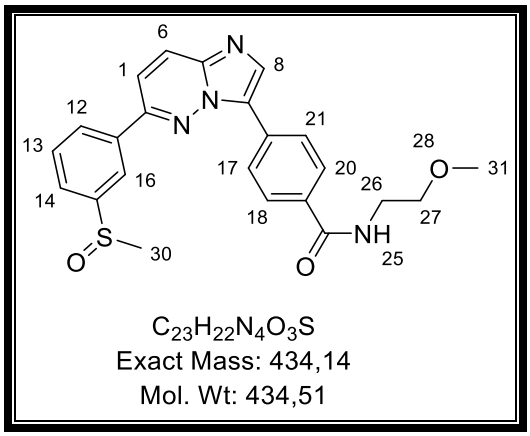

$C_{23}H_{22}N_4O_3S$
Exact Mass: 434,14
Mol. Wt: 434,51

Yellow solid (0.158 g, 69 %); m.p 315.7–317.5 °C; Rf = 0.40 (2 % MeOH/DCM); ^{1}H NMR (300 MHz, Methanol-d_4) δ 8.45 (t, *J* = 1.8 Hz, 1H, H16), 8.35–8.25 (m, 3H, (H18, H20 & H12)), 8.24 (s, 1H, H8), 8.18 (d, *J* = 9.6 Hz, 1H, H6), 7.99 (d, *J* = 8.3 Hz, 2H, H17 & H21), 7.94–7.81 (m, 2H, H14 & H1), 7.79 (t, *J* = 7.7 Hz, 1H, H13), 3.63 (s, 4H, H26 & H27), 3.43 (s, 3H, H31), 2.91 (s, 3H, H30); ^{13}C NMR (101 MHz, MeOD) δ 168.19, 157.97, 150.70, 146.16, 141.42, 136.61, 133.33, 133.06, 131.16, 130.04, 129.48, 127.33 (2C), 125.99 (2C), 125.57, 125.12, 121.91, 116.32, 70.66, 57.60, 42.30, 39.42. LC-MS, ESI/APCI: *m/z* $[M + H]^+$ = 434.8, t_r = 3.01 min. Purity = 98 %.

***N-Cyclopropyl-4-(6-(3-(methylsulfinyl)phenyl)imidazo[1,2-b]pyridazin-3-yl)benzamide* 61.**

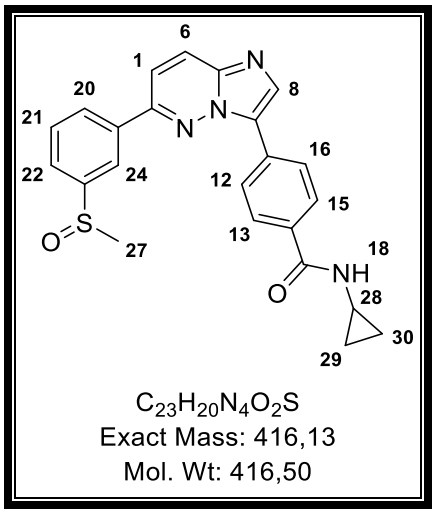

$C_{23}H_{20}N_4O_2S$
Exact Mass: 416,13
Mol. Wt: 416,50

Yellow solid (0.071 g, 43 %); m.p. 236.4–238.4 °C; Rf = 0.59 (10 % MeOH/DCM); ^{1}H NMR (300 MHz, DMSO-d_6) δ 8.53 (d, *J* = 4.2 Hz, 1H, H18), 8.46-8.43 (br , 1H, H24), 8.43–8.34 (m, 4H, (H8, H13, H15, & H20)), 8.31 (d, *J* = 7.5 Hz, 1H, H6), 8.05–7.96 (m, 3H, (H12, H16 & H22)), 7.89 (d, *J* = 7.7 Hz, 1H, H1), 7.82 (t, *J* = 7.7 Hz, 1H, H21), 2.87 (s, 3H, H27), 1.30–1.22 (m, 1H, H28), 0.77–0.68 (m, 2H, $H30_e$ & $H29_e$), 0.66–0.58 (m, 2H, $H30_a$ & $H29_a$); ^{13}C NMR (101 MHz, DMSO) δ 167.39, 150.93, 148.26, 140.14, 136.69, 135.04, 133.74, 131.35, 130.63, 129.62, 128.12, 127.42, 127.09 (2C), 126.12 (2C), 125.72, 122.67, 116.80, 43.77, 28.52, 23.58, 6.22. HPLC-MS, ESI/APCI: *m/z* $[M + H]^+$ = 417.0, t_r = 0.858 min. Purity = 97 %.

***N-(1-Hydroxybutan-2-yl)-4-(6-(3-(methylsulfinyl)phenyl)imidazo[1,2-b]pyridazin-3-yl)benzamide* 60.**

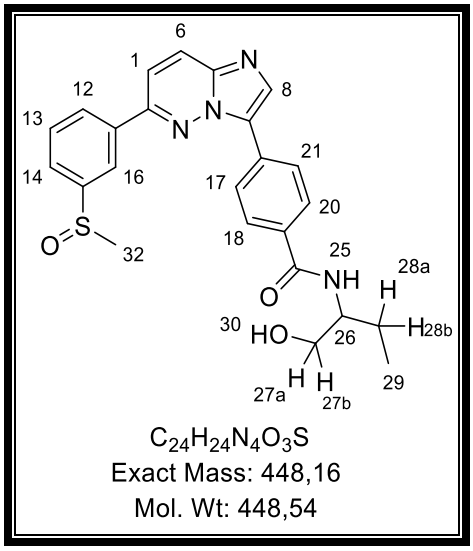

Yellow solid (0.0273 g, 38 %); m.p. 268.9–270.9 °C; Rf = 0.36 (8 % MeOH/DCM); ^{1}H NMR (400 MHz, DMSO-d_6) δ 8.44 (s ,1H, H8), 8.42 (t, *J* = 1.8 Hz, 1H, H16), 8.40–8.35 (m, 3H, (H6, H18 & H20)), 8.32 (dt, *J* = 7.7, 1.7 Hz, 1H, H12), 8.06 (d, *J* = 8.9 Hz, 2H, H17 & H21)), 8.01 (d, *J* = 9.5 Hz,1H, H1), 7.89 (dt, *J* = 8.1, 1.7 Hz, 1H, H14), 7.83 (t, *J* = 7.4 Hz, 1H, H13), 4.65 (t, *J* = 5.8 Hz, 1H, H30), 3.97–3.85 (m, 1H, H26), 3.55–3.48 (m, 1H, H27a), 3.48–3.41 (m, 1H, H27b), 2.87 (s, 3H, H32), 1.78–1.63 (m, 1H, H28a), 1.57–1.42 (m, 1H,

H28b), 0.92 (t, *J* = 7.4 Hz, 3H, H29); ^{13}C NMR (101 MHz, DMSO) δ 166.22, 150.96, 148.27, 140.14, 136.71, 135.03, 134.24, 131.26, 130.66, 129.62, 128.27, 127.48, 127.12 (2C), 126.12 (2C), 125.73, 122.70, 116.80, 63.60, 53.63, 43.76, 24.16, 11.15; HPLC-MS, ESI/APCI: *m/z* $[M + H]^+$ = 449.0, t_r = 0.834 min; Purity = 100 %.

***N-(2-Hydroxyethyl)-4-(6-(3-(methylsulfinyl)phenyl)imidazo[1,2-b]pyridazin-3-yl)benzamide* 57.**

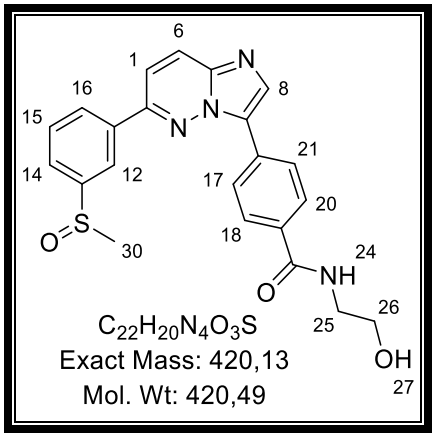

Yellow solid (0.0711 g, 10 %); m.p. 207.0–209.0 °C; Rf = 0.48 (10 % MeOH/DCM); ^{1}H NMR (300 MHz, Methanol-d_4) δ 8.64–8.58 (br, 1H, H12), 8.58–8.51 (m, 2H, H6 & H8), 8.44 (d, *J* = 9.6 Hz, 1H, H1), 8.37 (dt, *J* = 7.8, 1.40 Hz, 1H, H16), 8.31 (d, *J* = 8.5 Hz, 2H, H20 & H18), 8.10 (d, *J* = 8.6 Hz, 2H, H17 & H21), 7.94 (dt, *J* = 7.9, 1.5 Hz, 1H, H14), 7.86 (t, *J* = 7.8 Hz, 1H, H15), 3.78 (t, *J* = 5.8 Hz, 2H, H26), 3.58 (t, *J* = 5.8 Hz, 2H, H25), 2.92 (s, 3H, H30); ^{13}C NMR (151 MHz, DMSO) δ 166.26, 151.58, 148.21, 139.41, 136.33, 134.18, 132.77, 130.77, 130.72, 129.74, 128.18, 127.71 (2C), 126.51 (2C), 125.99 (2C), 122.73, 118.20, 60.23, 43.70, 42.70; LC-MS, ESI/APCI: *m/z* $[M + H]^+$ = 421.1, t_r = 2.08 min. Purity = 95 %.

***N*-(4-Methoxycyclohexyl)-4-(6-(3-(methylsulfinyl)phenyl)imidazo[1,2-b]pyridazin-3-yl)benzamide 62.**

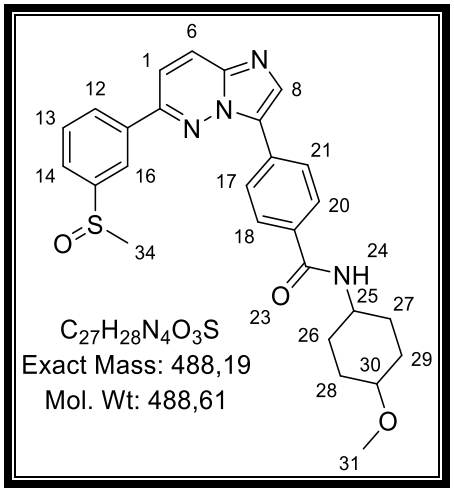

Yellow solid (0.0523 g, 40 %); m.p 264.0–266.0 °C; Rf = 0.66 (10 % MeOH/DCM); ^{1}H NMR (600 MHz, DMSO-d_6) δ 8.43 (s, 1H, H8), 8.40 (t, *J* = 1.9 Hz, 1H, H16), 8.38–8.34 (m, 3H, (H18, H20, H24)), 8.32–8.27 (m, 2H, H12 & H6), 8.02–7.97 (m, 3H, (H17, H21, & H1)), 7.88 (dt, *J* = 7.8, 1.7 Hz, 1H, H14), 7.81 (t, *J* = 7.7 Hz, 1H, H13), 3.83–3.74 (m, 1H, H25), 3.24 (s, 1H, H31), 3.15–3.08 (m,1H, H30), 2.85 (s, 3H, H34), 2.07–2.00 (m, 2H, H28e & H29e), 1.92–1.85 (m, 2H, H27e & H26e), 1.40 (qd, *J* = 12.9, 3.7 Hz, 2H, H26a & H27a), 1.21 (qd, *J* = 4.2, 3.4, 2.8 Hz, 2H, H28a & H29a); ^{13}C NMR (151 MHz, DMSO) δ 165.52, 150.92, 148.19, 140.13, 136.65, 135.03, 134.03, 131.27, 130.66, 129.62, 128.25, 127.40, 127.11 (2C), 126.08 (2C), 125.72, 122.67, 116.81, 78.307, 55.542, 48.439, 43.716, 42.87, 40.55, 30.77, 30.42. LC-MS, ESI/APCI: *m/z* $[M + H]^+$ = 489.1, t_r = 2.83 min. Purity = 96 %.

***N-Methyl-4-(6-(3-(methylsulfinyl)phenyl)imidazo[1,2-b]pyridazin-3-yl)*benzamide 64.**

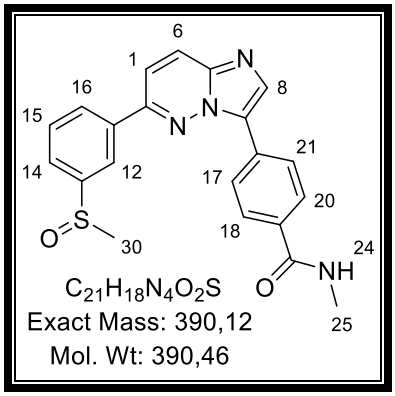

Yellow solid (0.0329 g, 28 %); m.p. 241.3–243.3 °C; Rf = 0.23 (4 % MeOH/DCM); ^{1}H NMR (300 MHz, DMSO-d_6) δ 8.53 (q, *J* = 4.6 Hz, 1H, H24), 8.48 (s, 1H, H8), 8.43 (t, *J* = 1.9 Hz, 1H, H12), 8.38 (d, *J* = 10.1 Hz, 2H, H18 & H20), 8.32 (dt, *J* = 7.6, 1.2 Hz, 1H, H16), 8.09–7.98 (m, 3H, (H1, H17 & H21)), 7.90 (dt, *J* = 7.8, 1.5 Hz, 1H, H14), 7.83 (t, *J* = 7.7 Hz, 1H, H15), 2.87 (s, 3H, H30), 2.83 (d, *J* = 4.5 Hz, 3H, H25). ^{13}C NMR (101 MHz, CDCl3) δ 167.48, 150.92, 147.61, 133.87, 130.11, 129.45, 127.33 (2C), 126.63 (2C), 126.41, 125.61 (2C), 125.05 (2C), 122.09, 115.69, 77.24, 76.93, 44.09, 26.77. LC-MS, ESI/APCI: *m/z* [M + H]$^{+}$ = 391.1, t_r = 3.50 min. Purity = 97 %.

***(3-Hydroxyazetidin-1-yl)(4-(6-(3-(methylsulfinyl)phenyl)imidazo[1,2-b]pyridazin-3-yl)phenyl)methanone* 67.**

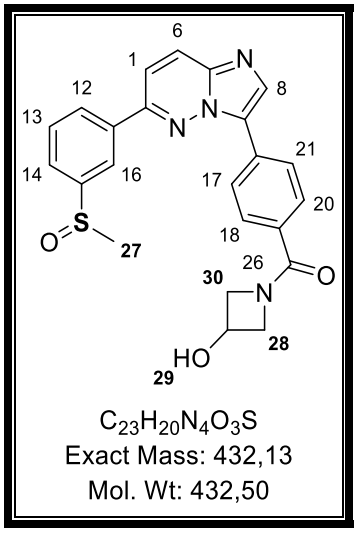

Yellow solid (0.0249 g, 13 %); m.p. 248–250 °C; Rf = 0.23 (4 % MeOH/DCM); ^{1}H NMR (400 MHz, $CDCl_3$) δ 8.32–8.30 (br s, 1H, H16), 8.20 (d, *J* = 8.5 Hz, 2H, H18 & H20) 8.17–8.11 (m, 3H, (H6, H12, & H8)), 7.79 (d, *J* = 8.5 Hz, 2H, H17 & H21), 7.75–7.69 (m, 2H, H13 & H14), 7.65 (d, *J* = 9.5 Hz, 2H, H1), 4.82–4.71 (m, 1H, H29), 4.64–4.47 (br s, 2H, $H28_b$ & $H30_b$), 4.23 (d, *J* = 57.9 Hz, 2H, $H28_a$ & $H30_a$), 2.83 (s, 3H, H27). ^{13}C NMR (101 MHz, $CDCl_3$) δ 169.79, 150.53, 147.08, 137.06, 134.19, 132.37, 131.09 (2C), 130.23, 129.61, 128.41 (2C), 126.49 (2C), 126.39, 125.07, 122.06 (3C), 115.70, 61.97, 44.05, 29.68. LC-MS, ESI/APCI: *m/z* $[M + H]^+$ = 433.1, t_r = 3.29 min. Purity = 96 %.

***N,N-Dimethyl-4-(6-(3-(methylsulfinyl)phenyl)imidazo[1,2-b]pyridazin-3-yl)benzamide* 63.**

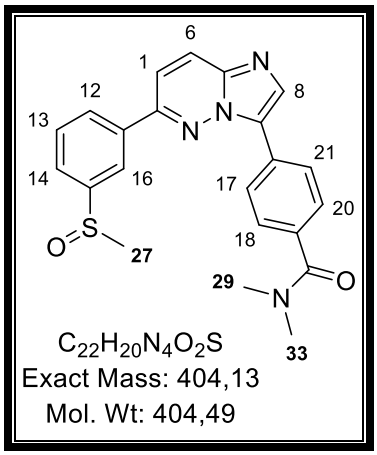

Yellow oil (0.0285 g, 24 %); m.p. ND; Rf = 0.69 (5 % MeOH/DCM); ^{1}H NMR (300 MHz, DMSO-d_6) δ 8.43–8.41 (m, 2H, H8 & H16), 8.38–8.30 (m, 4H, (H18, H20, H6 & H12), 8.00 (d, *J* = 9.5 Hz, 1H, H1), 7.89 (dt, *J* = 7.7, 2.35 Hz, 1H, H14), 7.82 (t, *J* = 7.7 Hz, 1H, H13), 7.60 (d, *J* = 8.2 Hz, 2H, H17 & H21), 3.06–2.97 (br s, 6H, H29 & H33), 2.86 (s, 3H, H27). ^{13}C NMR (101 MHz, $CDCl_3$) δ 171.17, 150.46, 147.25, 137.15, 135.79, 130.21, 129.62 (3C), 127.68 (3C), 126.64, 125.01 (2C), 122.05, 115.61, 44.15, 29.68 (2C). LC-MS, ESI/APCI: *m/z* $[M + H]^+$ = 405.1, t_r = 3.58 min. Purity = 98 %.

***(4-(6-(3-(Methylsulfinyl)phenyl)imidazo[1,2-b]pyridazin-3-yl)phenyl)(morpholino)methanone* 66.**

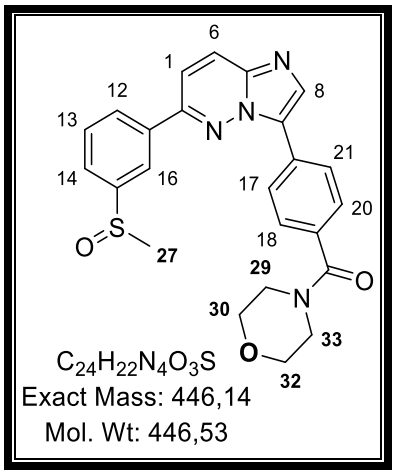

Yellow solid (0.0653 g, 47 %); m.p. 248.3–250.3 °C; Rf = 0.43 (5 % MeOH/DCM); ^{1}H NMR (400 MHz, $CDCl_3$) δ 8.48–8.33 (br, 1H, H16), 8.35 (s, 1H, H8), 8.23–8.17 (m, 4H, (H12, H6, H20 & H18)), 7.86–7.71 (m, 3H, (H1, H13 & H14))), 7.64 (d, *J* = 8.2 Hz, 2H, H21 & H17), 3.88–3.58 (br m, 8H,(H29, H30, H32 &H33)), 2.84 (s, 3H, H27). ^{13}C NMR (101 MHz, $CDCl_3$) δ 169.95, 150.87, 147.34, 136.99 (2C), 134.86, 130.23, 129.62, 127.79 (3C), 126.86 (2C), 126.74, 126.45, 125.15, 122.10 (2C), 116.10, 67.10 (2C), 66.93 (2C), 44.12. LC-MS, ESI/APCI: *m/z* $[M + H]^+$ = 447.1, t_r = 3.48 min. Purity = 100 %.

***(3-Hydroxypyrrolidin-1-yl)(4-(6-(3-(methylsulfinyl)phenyl)imidazo[1,2-b]pyridazin-3-yl)phenyl)methanone* 68.**

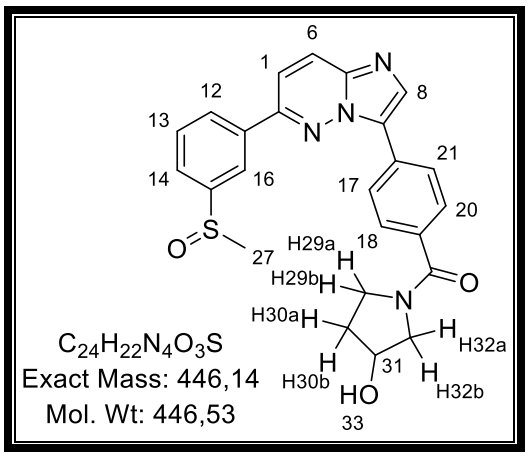

Yellow solid (0.0280 g, 20 %); m.p. ND; Rf = 0.55 (5 % MeOH/DCM); ^{1}H NMR (300 MHz, Methanol-d_4) δ 8.49 (t, *J* = 1.1 Hz, 1H, H16), 8.41–8.31 (m, 3H, (H18, H20, & H8)), 8.30–8.21 (m, 2H, H6 & H12), 7.96 (d, *J* = 9.4 Hz, 1H), 7.89 (dt, *J* = 7.5, 1.9 Hz, 1H, H14), 7.84 (t, *J* = 8.5 Hz, 1H, H13), 7.76 (d, *J* = 7.8 Hz, 2H, H21 & H17), 4.57–4.50 (m, 1H, H33), 4.46–4.39 (m, 1H, H31), 3.89–3.71 [m, 3H, (H29b, H30b, H32b)], 2.91 (s, 3H, H27), 2.23–1.87 (m, 3H, H29a, H30a, H32a). ^{13}C NMR (101 MHz, CDCl3) δ 169.57, 150.58, 150.39, 147.14, 137.05, 136.28, 133.85, 133.62, 130.16, 129.61, 129.50, 127.84, 127.74 (2C), 126.74 (2C), 126.46, 125.06, 122.04, 115.70, 53.40, 44.07, 29.68, 22.67. LC-MS, ESI/APCI: *m/z* [M + H]$^{+}$ = 447.1, t_r = 3.28 min. Purity = 100 %.

***(4-(6-(3-(Methylsulfinyl)phenyl)imidazo[1,2-b]pyridazin-3-yl)phenyl)(piperidin-1-yl)methanone* 65.**

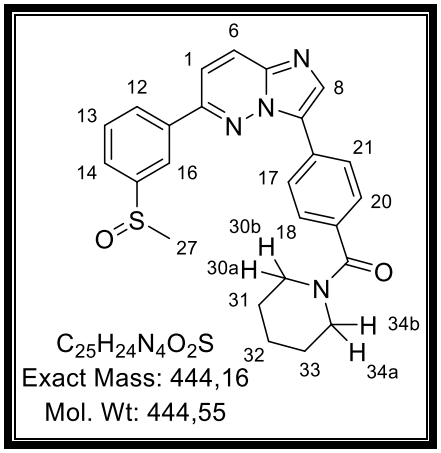

Yellow solid (0.0468 g, 27 %); m.p. 268.4–270.4 °C; Rf = 0.39 (5 % MeOH/DCM); ^{1}H NMR (600 MHz, Methanol-d_4) δ 8.42 (t, *J* = 1.8 Hz, 1H, H16), 8.29 (d, *J* = 8.4 Hz, 2H, H18 & H20), 8.26 (dt, *J* = 1.8, 1.53 Hz, 1H, H12), 8.20 (s, 1H, H8), 8.16 (d, *J* = 9.5 Hz, 1H, H6), 7.87 (d, *J* = 9.5 Hz, 1H, H1), 7.83 (dt, *J* = 7.9, 1.3 Hz, 1H, H14), 7.76 (t, *J* = 7.8 Hz, 1H, H13), 7.57 (d, *J* = 8.1 Hz, 2H, H17 & H21), 3.79–3.68 (m, 2H, H30a & H34a), 3.51–3.39 (m, 2H, H30b & H34b), 2.87 (s, 3H, H27), 1.77–1.52 [m, 6H, (H31, H32, H33)]. ^{13}C NMR (151 MHz, MeOD) δ 171.9, 152.3, 147.6, 141.1, 138.2, 136.8, 134.2, 131.5, 131.1, 131.0, 129.4,

128.4 (2C), 127.9 (2C), 127.0, 126.5, 123.4, 117.9, 50.2, 44.4, 43.7, 27.6, 26.8, 25.5. ESI/APCI: *m/z* $[M + H]^+$ = 444.7, t_r = 4.11 min. Purity = 97 %.

***(4-(6-(3-(Methylsulfinyl)phenyl)imidazo[1,2-b]pyridazin-3-yl)phenyl)(piperazin-1-yl)methanone* 70.**

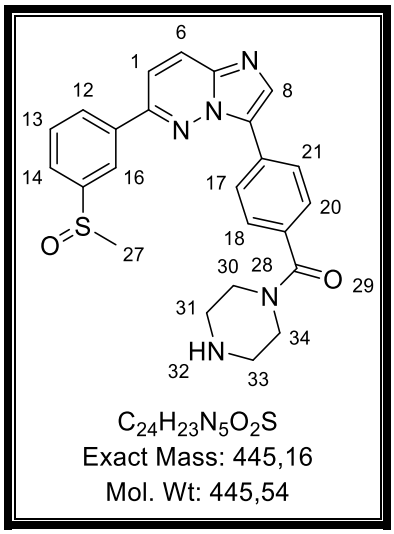

18.1 mg (0.033 mmol) of boc-protected precursor was dissolved in 2 ml of DCM (in an ice bath) and 0.2 ml (2.6 mmol) of trifluoroacetic acid (TFA) was added dropwise, in small portions, over 30 mins. The reaction was allowed to proceed until completion (LCMS, 90 mins) to remove boc. TFA was removed in vacuo, the residue was dissolved in 10 ml 10 % MeOH/DCM and neutralised using Amberlyst A21 for 90 mins. Compound was obtained after prep TLC in 10 % MeOH/DCM.

Yellow solid (0.0160 g, 5 %); m.p. ND; Rf = 0.14 (5 % MeOH/DCM); LC-MS, ESI/APCI: *m/z* $[M + H]^+$ = 446.1, t_r = 2.65 min. Purity = 96 %.

***(4-Hydroxypiperidin-1-yl)(4-(6-(3-(methylsulfinyl)phenyl)imidazo[1,2-b]pyridazin-3-yl)phenyl)methanone* 69.**

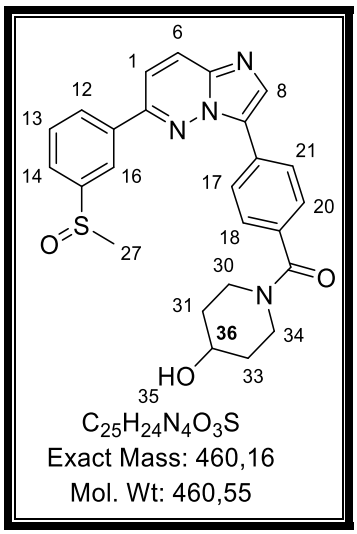

Yellow solid (0.0127g, 9 %); m.p. ND; Rf = 0.41 (5 % MeOH/DCM); LC-MS, ESI/APCI: *m/z* $[M + H]^+$ = 460.16, t_r = 3.36 min. Purity = 99 %.

6.2.5 General procedure for Suzuki-Miyaura coupling at 80 °C and 100 °C of compounds 75 and 76.

A similar method described in **6.2.3** was followed but with slight modification. First and second Suzuki-Miyaura coupling reactions were done in 1,4-dioxane instead of using DMF. A residue obtained after removing 1,4-dioxane *in vacuo* was washed with saturated NaCl and DCM. **75** was not purified and was used as is in second Suzuki-Miyaura reaction to obtain intermediate **76.**

***3-(3-(4-(Methylsulfinyl)phenyl)imidazo[1,2-b]pyridazin-6-yl)benzoic acid* 76.**

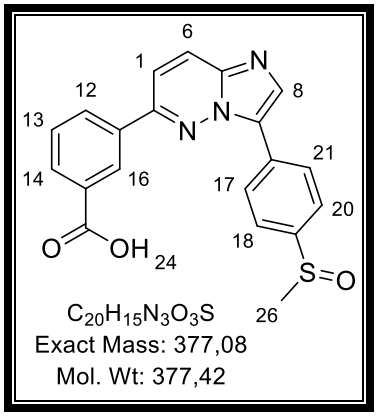

Column chromatography (10 % EtOH/DCM, 5 % MeOH/DCM); yellow solid (1.263 g, 68 %); m.p. not determined; Rf = 0.23 (10% MeOH/DCM). ^{1}H NMR (600 MHz, DMSO-d_6) δ 8.64-8.60 (br, 1H, H16), 8.46 (d, *J* = 8.8 Hz, 2H, H17 & H21), 8.40 (s, 1H, H8), 8.31 (d, *J* = 9.5 Hz, 1H, H6), 8.25 (dt, *J* = 7.8, 2.0 Hz, 1H, H12), 8.08 (dt, *J* = 7.7, 1.9 Hz, 1H, H14), 7.92 (d, *J* = 9.5 Hz, 1H, H1), 7.83 (d, *J* = 8.8 Hz, 2H, H18 & H20), 7.63 (t, *J* = 7.7 Hz, 1H, H13), 2.80 (s, 3H, H26); ^{13}C NMR (151 MHz, DMSO) δ 168.33, 151.63, 145.78, 140.13, 135.43, 134.91 (2C), 131.32, 131.19, 130.21, 129.52, 128.17, 127.94, 127.12, 127.04, 126.83, 124.59 (2C), 116.96, 43.62. LC-MS, ESI/APCI: *m/z* $[M + H]^+$ = 378.0, t_r = 2.74 min. Purity = 94 %.

6.2.6 General procedure for amide coupling via propylphosphonic anhydride solution ≥ 50 wt. % in ethyl acetate to form 77-86.

Similar approach described in **6.2.4** was followed with slight modification. Reaction was carried out in 1,4-dioxane instead of using DMF. Target compounds were purified with appropriate mobile phase (5 % EtOH/DCM, 5 % MeOH/DCM) using preparatory TLC plates. All compounds were triturated with hot hexane to obtain a solid material except for **84** which remained oily.

***N-Allyl-3-(3-(4-(methylsulfinyl)phenyl)imidazo[1,2-b]pyridazin-6-yl)benzamide* 79.**

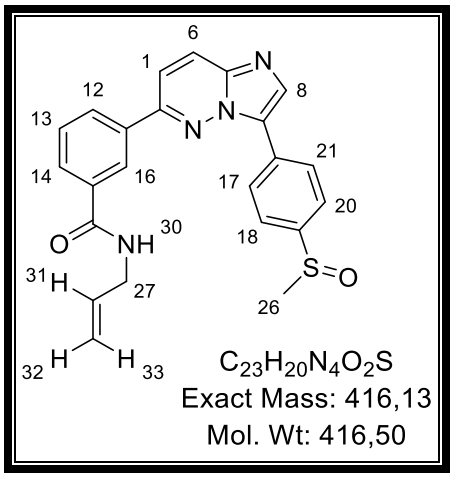

Yellow solid (0.0664 g, 60 %); m.p. 228.7–230.7 °C; Rf = 0.49 (10 % MeOH/DCM). ^{1}H NMR (300 MHz, DMSO-d_6) δ 8.88 (t, *J* = 5.7 Hz, 1H, H30), 8.60 (t, *J* = 1.5 Hz, 1H, H16), 8.50 (d, *J* = 8.5 Hz, 2H, H21 & H17), 8.44 (s, 1H, H8), 8.40 (d, *J* = 9.5 Hz, 1H, H6), 8.32 (dt, *J* = 7.9, 2.9 Hz, 1H, H12), 8.08–7.98 (m, 2H, H14 & H1), 7.87 (d, *J* = 8.4 Hz, 2H, H20 & H18), 7.72 (t, *J* = 7.8 Hz, 1H, H13), 6.06–5.86 (m, 1H, H31), 5.25 (dq, *J* = 17.2, 1.86 Hz, 1H, H33), 5.15 (dq, *J* = 10.2, 1.7 Hz, 1H, H32), 3.99 (t, *J* = 5.3 Hz, 2H, H27), 2.83 (s, 3H, H26); ^{13}C NMR (151 MHz, DMSO) δ 166.03, 151.35, 145.81, 140.14, 135.78, 135.64, 134.97 (2C), 131.13, 130.07, 129.84, 129.54, 127.19 (2C), 127.16, 127.07, 126.32, 124.63 (2C), 116.92, 115.80, 43.65, 42.06; LC-MS, ESI/APCI: *m/z* $[M + H]^+$ = 417.1, t_r = 2.57 min. Purity = 99 %.

N-(2-Methoxyethyl)-3-(3-(4-(methylsulfinyl)phenyl)imidazo[1,2-b]pyridazin-6yl)benzamide

78.

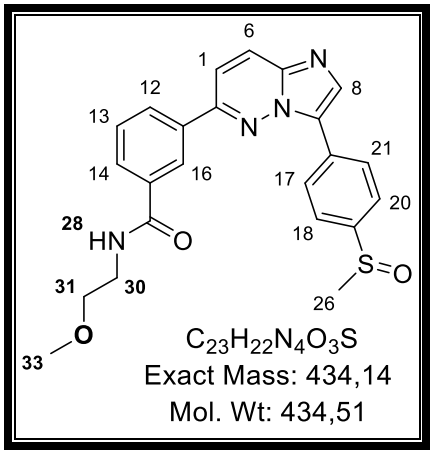

Yellow solid (0.0491 g, 43 %); m.p. 206.3–208.3 °C Rf = 0.49 (10 % MeOH/DCM). ^{1}H NMR (600 MHz, DMSO-d_6) δ 8.74 (t, *J* = 5.15 Hz, 1H, H28), 8.56 (t, *J* = 1.82 Hz, 1H, H16), 8.48 (d, *J* = 8.53 Hz, 2H, H17 & H21), 8.42 (s, 1H, H8), 8.38 (d, *J* = 9.51 Hz, 1H, H, H6), 8.30 (dt, *J* = 7.80, 1.90 Hz, 1H, H12), 8.02 (dt, *J* = 7.79, 1.34 Hz, 1H, H14), 7.99 (d, *J* = 9.57 Hz, 1H, H1), 7.86 (d, *J* = 8.50 Hz, 2H, H18 & H20), 7.69 (t, *J* = 7.75 Hz, 1H, H13), 3.52–3.46 (m, 4H, H30 & H31), 3.29 (s, 3H, H33), 2.81 (s, 3H, H26); ^{13}C NMR (151 MHz, DMSO) δ 166.25, 151.38, 145.82, 140.14, 135.75, 135.63, 134.98 (2C), 131.13, 130.06, 129.80, 129.53, 127.18 (2C), 127.15, 127.07, 126.33, 124.63 (2C), 116.93, 71.01, 58.45, 43.64.; LC-MS, ESI/APCI: *m/z* $[M + H]^+$ = 435.1, t_r = 2.93 min. Purity = 97 %.

***N-Cyclopropyl-3-(3-(4-(methylsulfinyl)phenyl)imidazo[1,2-b]pyridazin-6-yl)benzamide* 81.**

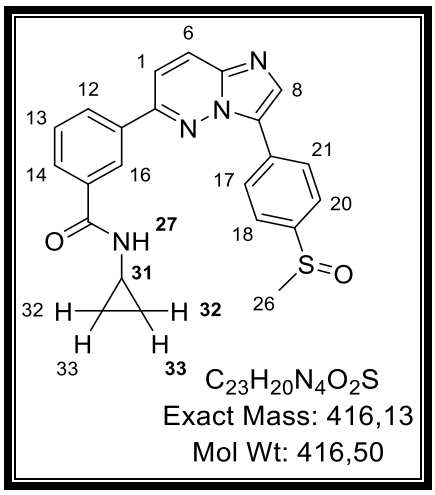

Yellow solid (0.0500 g, 45 %); m.p. 250.5–252.5 °C; Rf = 0.44 (10 % MeOH/DCM); ^{1}H NMR (600 MHz, DMSO-d_6) δ 8.62 (d, *J* = 4.2 Hz, 1H, H27), 8.49 (t, *J* = 1.8 Hz, 1H, H16), 8.46 (d, *J* = 8.5 Hz, 2H, H17 & H21), 8.41 (s, 1H, H8), 8.37 (d, *J* = 9.3 Hz, 1H, H6), 8.28 (dt, *J* = 7.8, 1.5 Hz, 1H, H12), 7.99–7.95 (m, 2H, H1 & H14), 7.84 (d, *J* = 8.6 Hz, 2H, H20 & H18), 7.66 (t, *J* = 7.8 Hz, 1H, H13), 2.92–2.86 (m, 1H, H31), 2.80 (s, 3H, H26), 0.75–0.70 (m, 2H, H33), 0.62–0.58 (m, 2H, H32); ^{13}C NMR (151 MHz, DMSO) δ 167.46, 151.34, 145.83, 140.13, 135.78, 135.56, 134.96 (2C), 131.13, 129.98, 129.74, 129.44, 127.20, 127.16 (2C), 127.06, 126.30, 124.62 (2C), 116.92, 43.64, 23.58, 6.28.; LC-MS, ESI/APCI: *m/z* [M + H]$^{+}$ = 417.1, t_r = 2.68 min. Purity = 99 %.

***N-(1-Hydroxybutan-2-yl)-3-(3-(4-(methylsulfinyl)phenyl)imidazo[1,2-b]pyridazin-6-yl)benzamide* 80.**

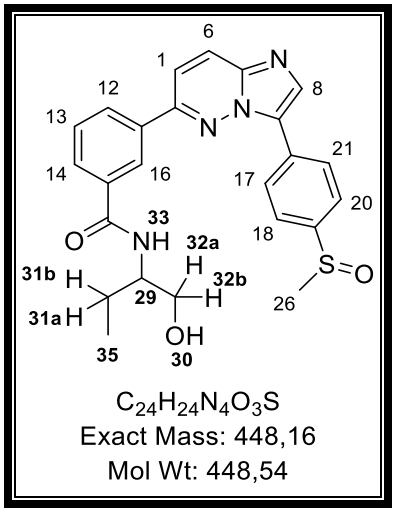

Yellow solid (0.0039 g, 13 %); m.p ND; Rf = 0.35 (10 % MeOH/DCM); ^{1}H NMR (300 MHz, DMSO-d_6) δ 8.59 (t, *J* = 1.1 Hz, 1H, H16), 8.50 (d, *J* = 8.4 Hz, 2H, H17 & H21), 8.44 (s, 1H, H8), 8.40 (d, *J* = 9.6 Hz, 1H, H6), 8.32 (dt, *J* = 7.9, 1.3 Hz, 1H, H12), 8.25 (d, *J* = 8.3 Hz, 1H, H133), 8.07–8.00 (m, 2H, H14 & H1), 7.87 (d, *J* = 8.4 Hz, 2H, H18 & H20), 7.70 (t, *J* = 7.8 Hz, 1H, H13), 4.70 (t, *J* = 5.7 Hz, 1H, H30), 4.01–3.87 (m, H32a), 3.58–3.40 (m, 1H, H32b), 2.82 (s, 3H, H26), 1.79–1.65 (m, 1H, H31a), 1.60–1.41 (m, 1H, H31b), 0.93 (t, *J* = 7.4 Hz, 3H, H35); ^{13}C NMR (151 MHz, DMSO) δ 166.30, 151.36, 145.83, 140.14, 136.32, 135.45, 134.98 (2C), 131.14, 129.87, 129.70, 127.21 (2C), 127.16, 127.06, 126.33, 124.62 (2C), 116.93, 63.56, 53.69, 43.65, 24.17, 11.15; LC-MS, ESI/APCI: *m/z* $[M + H]^+$ = 449.1, t_r = 3.45 min. Purity = 99 %.

***N-(2-Hydroxyethyl)-3-(3-(4-(methylsulfinyl)phenyl)imidazo[1,2-b]pyridazin-6-yl)benzamide* 77.**

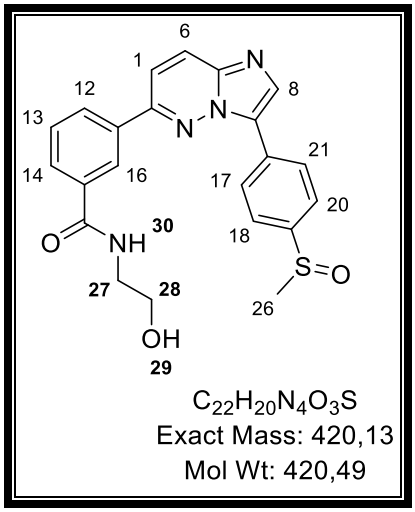

Yellow solid (0.00342 g, 4.0 %); m.p ND; Rf = 0.34 (10 % MeOH/DCM); ^{1}H NMR (300 MHz, DMSO-d_6) δ 8.67 (t, *J* = 5.5 Hz, 1H, H30), 8.59 (t, *J* = 1.8 Hz, 1H, H16), 8.50 (d, *J* = 8.4 Hz, 2H, H21 & H17), 8.44 (s, 1H, H8), 8.40 (d, *J* = 9.5 Hz, 1H, H6), 8.32 (dt, *J* = 7.8, 1.1 Hz, 1H, H12), 8.07–7.97 (m, 2H, H1 & H14), 7.88 (d, *J* = 8.4 Hz, 2H, H18 & H20), 7.71 (t, *J* = 7.8 Hz, 1H, H13), 4.76 (t, *J* = 5.6 Hz, 1H, H29), 3.58 (q, *J* = 5.9 Hz, 2H, H27), 3.41 (q, *J* = 5.8 Hz, 2H, H28), 2.83 (s, 3H, H26);^{13}C NMR (151 MHz, DMSO) δ 166.29, 151.39, 145.83, 140.14, 135.92, 135.59, 134.98 (2C), 131.13, 129.96, 129.77, 129.52, 127.19 (2C), 127.16, 127.08, 126.37, 124.64 (2C), 116.92, 60.243, 43.64, 42.78. LC-MS, ESI/APCI: *m/z* $[M + H]^+$ = 421.1, t_r = 3.36 min. Purity = 96 %.

***(3-(3-(4-(Methylsulfinyl)phenyl)imidazo[1,2-b]pyridazin-6-yl)phenyl)(morpholino)methanone* 84.**

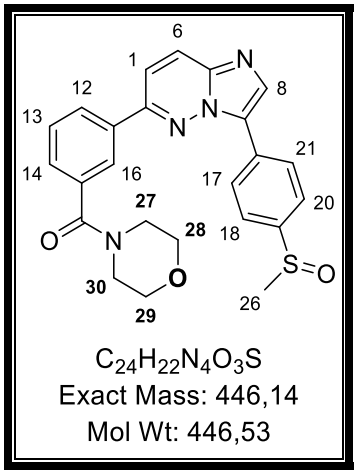

$C_{24}H_{22}N_4O_3S$
Exact Mass: 446,14
Mol Wt: 446,53

Yellow oil (0.0606 g, 51 %); Rf = 0.51 (10 % MeOH/DCM); ^{1}H NMR (300 MHz, Methanol-d_4) δ 8.48 (d, *J* = 8.7 Hz, 2H, H21 & H17), 8.29 (s, 1H, H8), 8.28–8.18 (m, 3H, (H6, H12, & H16)), 7.96–7.88 (m, 3H, (H1, H18, & H20)), 7.71 (t, *J* = 8.2 Hz, 1H, H13), 7.64 (dt, *J* = 7.7, 1.5 Hz, 1H, H14), 3.89–3.60 (br m, 8H, (H27, H28, H29, & H30)), 2.90 (s, 3H, H26); ^{13}C NMR (151 MHz, DMSO) δ 168.97, 151.26, 145.88, 140.13, 136.97, 135.77, 134.98 (2C), 131.14, 129.98, 129.29, 128.65, 127.19 (2C), 127.05, 126.04, 124.61 (2C), 117.02, 66.56 (2C), 43.66, 40.55 (2C). LC-MS, ESI/APCI: *m/z* $[M + H]^+$ = 447.1, t_r = 2.61 min. Purity = 97 %.

***(3-(3-(4-(Methylsulfinyl)phenyl)imidazo[1,2-b]pyridazin-6-yl)phenyl)(piperidin-1-yl)methanone* 85.**

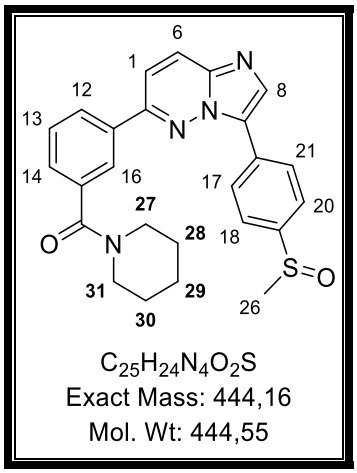

$C_{25}H_{24}N_4O_2S$
Exact Mass: 444,16
Mol. Wt: 444,55

Yellow solid (0.0422 g, 36 %); m.p. 256.4–258.4 °C; Rf = 0.53 (10 % MeOH/DCM); ^{1}H NMR (300 MHz, Methanol-d_4) δ 8.48 (d, *J* = 8.4 Hz, 2H, (H17 & H21)), 8.29 (s, 1H, H8), 8.26–8.13 (m, 3H, (H6, H16, & H12)), 7.97–7.85 (m, 3H, (H18, H20, & H1)), 7.70 (t, *J* = 7.7 Hz, 1H, H13), 7.60 (dt, *J* = 7.7, 1.00 Hz, 1H, H14), 3.86–3.70 (br m, 2H, H27e & H31e), 3.53–3.40 (br m, 2H, H27a & H31a), 2.90 (s, 3H, H26), 1.81–1.54 (br m, 6H, (H28, H29, & H30)); ^{13}C NMR (151 MHz, MeOD) δ 170.16, 151.63, 143.96, 139.97, 137.00, 135.77 (2C), 133.10, 131.51, 129.29, 128.20, 128.18, 127.57, 127.32, 125.64, 125.11, 123.99 (2C), 116.98, 48.74, 43.05, 42.15, 26.25, 25.36, 24.04. LC-MS, ESI/APCI: *m/z* $[M + H]^+$ = 445.1, t_r = 2.69 min. Purity = 98 %.

***N*-Methyl-3-(3-(4-(methylsulfinyl)phenyl)imidazo[1,2-b]pyridazin-6-yl)benzamide 83.**

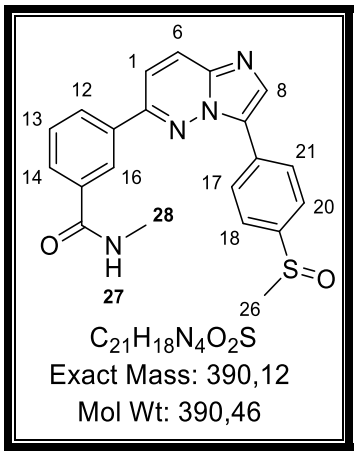

$C_{21}H_{18}N_4O_2S$
Exact Mass: 390,12
Mol Wt: 390,46

Yellow solid (0.0196 g, 18 %); m.p. 256.1–258.1°C; Rf = 0.40 (10 % MeOH/DCM); ^{1}H NMR (300 MHz, DMSO-d_6) δ 8.64 (q, *J* = 5.1 Hz, 1H, H27), 8.54 (t, *J* = 2.0 Hz, 1H, H16), 8.48 (d, *J* = 8.6 Hz, 2H, H17 & H21), 8.44 (s, 1H, H8), 8.39 (d, *J* = 9.5 Hz, 1H, H6), 8.31 (dt, *J* = 7.8, 1.6 Hz, 1H, H12), 8.05–7.94 (m, 2H, H1 & H14), 7.87 (d, *J* = 8.4 Hz, 2H, H18 & H20), 7.70 (t, *J* = 7.8 Hz, 1H, H13), 2.86 (d, *J* = 4.5 Hz, 3H, H28), 2.83 (s, 3H, H6); ^{13}C NMR (151 MHz, DMSO) δ 166.58, 151.44, 145.82, 140.13, 135.85, 135.70, 134.98 (2C), 131.13, 129.97, 129.82, 129.29, 127.18 (2C), 127.09, 126.27, 124.64 (2C), 116.94, 43.63, 26.79. LC-MS, ESI/APCI: *m/z* $[M + H]^+$ = 391.1, t_r = 2.46 min. Purity = 96 %.

***N,N-Dimethyl-3-(3-(4-(methylsulfinyl)phenyl)imidazo[1,2-b]pyridazin-6-yl)benzamide* 82.**

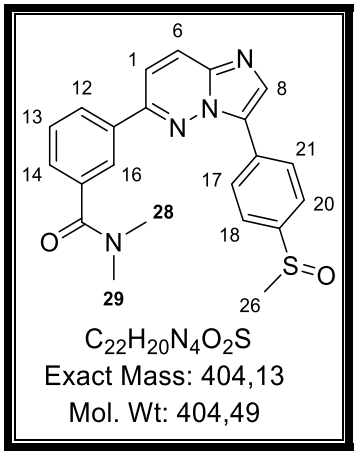

Yellow solid (0.0112 g, 10 %); m.p ND; Rf = 0.48 (10 % MeOH/DCM); ^{1}H NMR (300 MHz, DMSO-d_6) δ 8.52–8.38 (m, 3H, (H16, H21, & H17)), 8.33 (d, *J* = 9.4 Hz, 1H, H6), 8.21 (dt, *J* = 7.4, 3.2 Hz, 1H, H12), 8.13 (s, 1H, H8), 7.95 (d, *J* = 9.5 Hz, 1H, H1), 7.86 (d, *J* = 8.0 Hz, 2H, H20 & H18), 7.74–7.53 (m, 2H, H13 & H14), 3.14–2.92 (br s, 6H, H28 & H29), 2.83 (s, 3H, H26); ^{13}C NMR (151 MHz, DMSO) δ 169.96, 151.35, 145.81, 140.11, 137.81, 135.63, 134.94 (2C), 131.13, 129.76, 129.20, 128.42, 127.16, 127.13, 127.01, 126.05, 124.59 (2C), 117.00, 43.633, 35.33 (2C); LC-MS, ESI/APCI: *m/z* $[M + H]^+$ = 405.1, t_r = 2.49 min. Purity = 97 %.

***N-(4-Methoxycyclohexyl)-3-(3-(4-(methylsulfinyl)phenyl)imidazo[1,2-b]pyridazin-6-yl)benzamide* 86.**

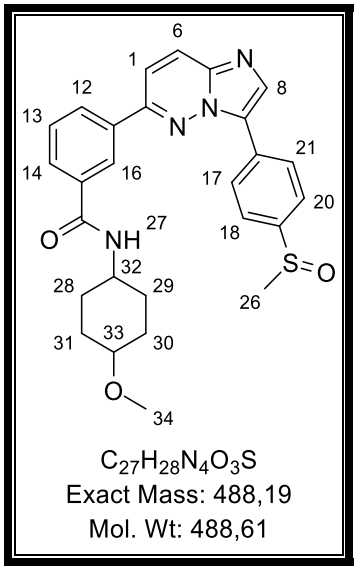

Yellow solid (0.0589 g, 45 %); m.p 308.4–310.4 °C; Rf = 0.65 (10 % MeOH/DCM); ^{1}H NMR (300 MHz, DMSO-d_6) δ 8.55 (t, *J* = 1.8 Hz, 1H, H16), 8.49 (d, *J* = 8.2 Hz, 2H, H17 & H21), 8.44 (s, 1H, H8), 8.39 (d, *J* = 9.6 Hz, 1H, H6), 8.32 (dt, *J* = 8.3, 0.83 Hz, 1H, H12), 8.05–7.96 (m, 2H, H1 & H14), 7.87 (d, *J* = 8.1 Hz, 2H, H18 & H20), 7.69 (t, *J* = 7.8 Hz, 1H, H13), 3.93–3.74 (m, 1H, H32), 3.27 (s, 3H, H34), 3.23–3.08 (m, 1H, H33), 2.83 (s, 3H, H26), 2.14–2.00 (m, 2H, H31e & H30e), 2.01–1.85 (m, 2H, H28e & H39e), 1.51–1.33 (m, 2H, H31a & H30a), 1.33–1.14 (m, 2H, H28a & H29a). ^{13}C NMR (151 MHz, DMSO) δ 165.76, 151.36, 146.05, 140.16, 136.40, 135.53, 134.92 (2C), 131.20, 129.80, 129.62, 129.55, 127.28 (2C), 127.00, 126.35, 124.59 (2C), 116.83, 78.29 (2C), 55.51, 48.57, 43.75, 30.68 (2C), 30.42. LC-MS, ESI/APCI: *m/z* $[M + H]^+$ = 489.2, t_r = 2.35 min. Purity = 95 %.

6.3 Pharmacological assays

6.3.1 *In vitro P. falciparum* asexual blood parasite stage assay

The antiplasmodium activities of the test compounds were assessed against the CQ-sensitive *P. falciparum* strain NF54, in duplicate. Continuous *in vitro* cultures of *P. falciparum* parasites at the asexual erythrocyte stages were maintained following a modified version of

the method developed by Trager and Jensen.[88] Quantitative assessment of the compounds' *in vitro* antiplasmodium activities was conducted via a parasite lactate dehydrogenase assay using the modified method described by Makler *et al*. with slight modifications.[89]

The test compounds were suspended in 100 % DMSO to obtain stock solutions of 20 mg/mL, which were sonicated to enhance solubility and stored at -20 ℃. The stock solutions were further diluted on the day of the experiment. The activities of the test compounds were compared to those of CQ and artesunate which were used as reference compounds. A full dose-response analysis was performed for all compounds to determine the concentration at which 50 % of parasite growth was inhibited. Ten stock solutions were prepared via 2-fold serial dilution to obtain a 10-point dose-response curve for each compound, at concentrations ranging from 0.02 to 10 µg/mL.

The starting concentration of the compounds was 1 µg/mL, with the highest concentration of solvent used to dissolve the compounds not affecting parasite viability. Samples were incubated with parasites at 37 ℃ for 72 h, after which cells were re-suspended. A 15 µL aliquot was removed and transferred to another plate containing 100 µL Malstat reagent and 25 µL nitroblue tetrazolium and phenozine ethosulphate (Makler). The plates were incubated in the dark until completion of the reaction. Absorbance was then measured at 620 nm on a spectrophotometer. From these data, IC_{50} values were calculated via non-linear dose-response curve fitting analysis using GraphPad Prism v.4.0 software (GraphPad, San Diego, CA, USA).

6.3.2 Gametocidal activity assay

The luciferase reporter assay was established to enable accurate, reliable and quantifiable investigations of the stage-specific action of gametocytocidal compounds for the early and late

gametocyte marker cell line NF54-*Pf*S16-GFP-Luc.[90] Drug assays were set up on day 5 and 10

(Representing > 90 % of either early stage II/III or mature stage IV/V gametocytes, respectively). In each instance, assays were set up using a 2-3 % gametocytaemia, 1.5 % haematocrit culture and 48 h drug pressure in a gas chamber (90 % N_2, 5 % O2, and 5 % CO_2) at 37 ^{o}C.[90] Luciferase activity was determined in 30 µL parasite lysates by adding 30 µL luciferin substrate (Promega Luciferase Assay System) at room temperature and detection of resultant bioluminescence at an integration constant of 10 s with the GloMax® Explorer Detection System with Instinct® Software. Methylene blue (5 µM) and internal project specific controls (**MMV390048**, 5 µM) are routinely included as controls.

6.3.3 *In vitro* cytotoxicity assay

Cytotocxicity was measured using the method described by Mosmann *et al*, this procedure uses MTT (3-(4,5-Dimethylthiazol-2-yl)-2,5-Diphenyltetrazolium Bromide)-assay (MTT-assay) to measure cellular growth and survival calorimetrically.[91] All growth and chemosensitivity was measured by the formation of tetrazolium salt. The test samples were evaluated in triplicate. The test samples were dissolved in DMSO to prepare a stock solution of 2 mg/mL and insoluble samples were tested as suspensions. The prepared stock solution were stored at -20 °C until required. Emetine drug was used for calibration in all experiments. 10-fold serial dilutions in complete medium to give 6 concentrations were made from an initial concentration of 100 µg/mL with the lowest concentration being 0.001 µg/mL. Though cells were exposed to high solvent concentration remained capable of surviving. The IC_{50} values were determined from full dose-response curves plotted using a non-linear dose-response curve fitting analysis using GraphPad Prism v.4.0 software (GraphPad, San Diego, CA, USA).

6.4 Solubility assays

6.4.1 Preparation of of 0.01M pH 7.4 phosphate buffered saline (PBS)

One intact PBS buffer tablet was dissolved in deionized water to make 1000 mL solution that is consist of 0.14M NaCl, 0.003M KCl and 0.01M phosphate buffer. The solution was passed through a 0.22 µM nylon filter to remove any particulate contaminants and ascertain the pH using a pH meter.[92]

6.4.2 Turbidimetric solubility procedure

Each compound (2–3 mg) was dissolved in DMSO to prepare 10 mM stock solutions.[93] Heterogeneous solutions were mixed by vortexing until all material was dissolved. Serial dilutions of 1, 2, 3, and 4, ranging from 10 mM to 0 mM were prepared in a 96 well plate (**Figure 45**) in triplicate, a blank well was included as a reference.

Conc (µM)		Compound 1			Compound 2			Compound 3			Compound 4		
0,00	A	0,00	0,00	0,00	0,00	0,00	0,00	0,00	0,00	0,00	0,00	0,00	0,00
0,25	B	0,25	0,25	0,25	0,25	0,25	0,25	0,25	0,25	0,25	0,25	0,25	0,25
0,50	C	0,50	0,50	0,50	0,50	0,50	0,50	0,50	0,50	0,50	0,50	0,50	0,50
1,00	D	1,00	1,00	1,00	1,00	1,00	1,00	1,00	1,00	1,00	1,00	1,00	1,00
2,00	E	2,00	2,00	2,00	2,00	2,00	2,00	2,00	2,00	2,00	2,00	2,00	2,00
4,00	F	4,00	4,00	4,00	4,00	4,00	4,00	4,00	4,00	4,00	4,00	4,00	4,00
8,00	G	8,00	8,00	8,00	8,00	8,00	8,00	8,00	8,00	8,00	8,00	8,00	8,00
10,00	H	10,00	10,00	10,00	10,00	10,00	10,00	10,00	10,00	10,00	10,00	10,00	10,00

Figure 45: Pre-dilution plate layout.
Rows B to H contain stock solutions with increasing concentrations.

The layout of the secondary dilution plate containing compound solutions prepared in DMSO and 0.01 M pH 7.4 PBS, is shown in **Figure 46**. Columns 1 to 6 contain compound solutions prepared in DMSO, while columns 7 to 12 contain compound solutions in PBS.[93] The final volume in each well is 200 µL (4 µL solvent from the pre-dilution plate and 196 µL DMSO or PBS). The assay plate was incubated for 2 h at 26 °C, after which the absorbance of the assay plate contents was measured at 620 nm.

		DMSO						0,01 M pH 7,4 PBS					
		Compound 1(Triplicate)			Compound 2 (Triplicate)			Compound 1 (Triplicate)			Compound 2 (Triplicate)		
Conc (µM)		1	2	3	4	5	6	7	8	9	10	11	12
0	A	4 µL (Pipette from pre-dilution)+196 µL DMSO						4 µL (Pipette from pre-dilution)+196 µL 0,01 M pH 7,4 PBS					
5	B												
10	C												
20	D												
40	E												
80	F												
160	G												
200	H												

Figure 46: Turbidimetric assay plate lay-out.

The raw absorbance data were corrected by subtracting the absorbance of the blank samples (DMSO and 2 % DMSO in PBS) from the absorbance of the test samples. The solubility of the compounds was determined by plotting a graph of the corrected absorbance versus concentration. The solubility curves of hydrocortisone and reserpine (reference compounds) are shown in **Figure 47** and **Figure 48** respectively. The assay was considered valid if the DMSO graph did not deviate from the x-axis. The compound solubility threshold is determined as the concentration the PBS graph deviates from the DMSO graph. In the given examples, hydrocortisone is soluble over the entire concentration range, whereas the solubility threshold of reserpine is approximately 10 µM.

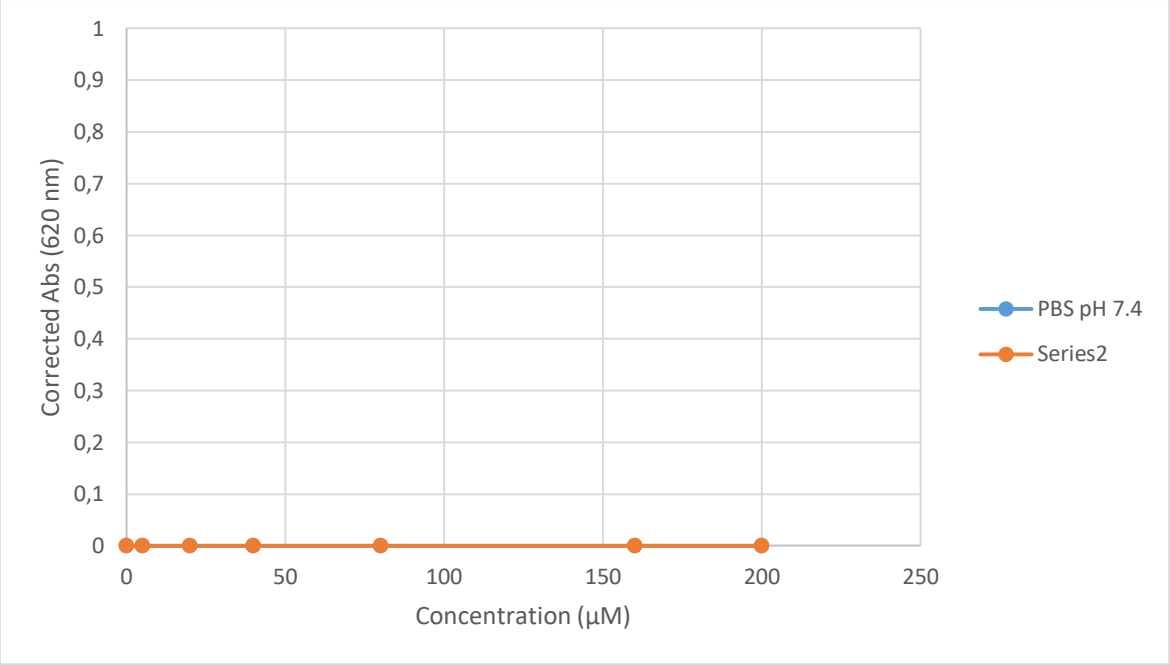

Figure 47: Solubility of hydrocortisone.

DMSO, dimethylsulfoxide; PBS, phosphate buffered saline.

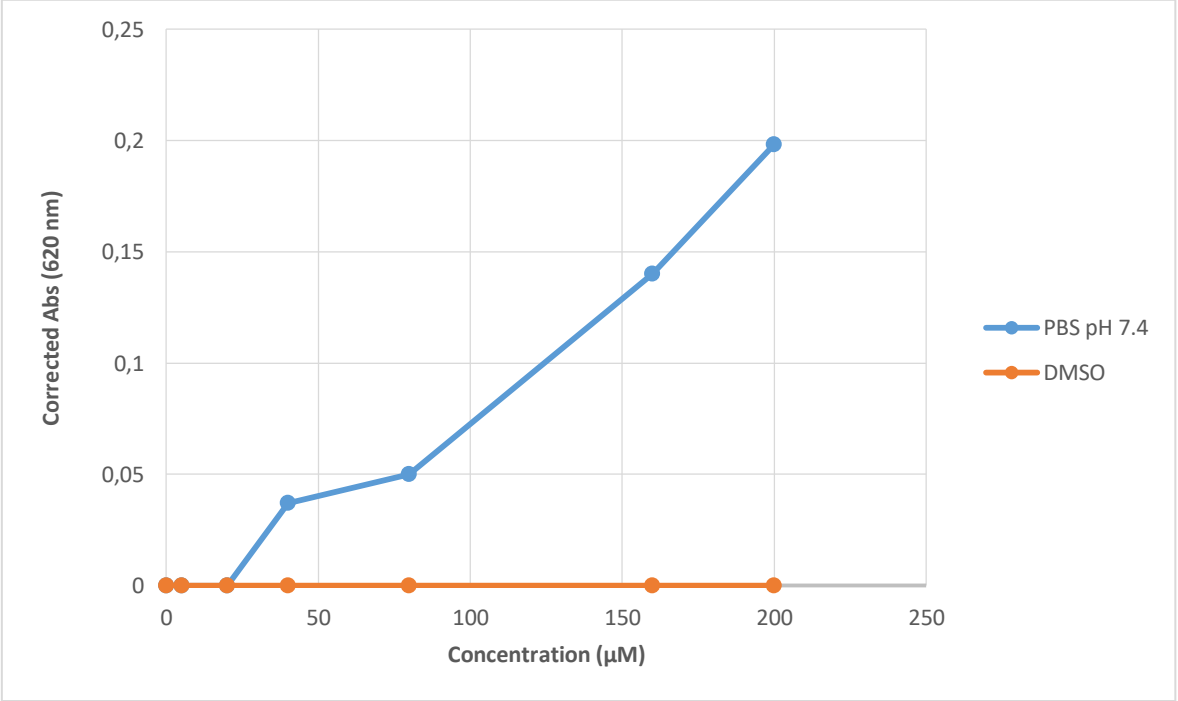

Figure 48: Solubility of reserpine.

DMSO, dimethylsulfoxide; PBS, phosphate buffered saline.

Turbidimetric solubility results were used to rank the compounds as poorly, moderately, or highly soluble, following the classification listed in **Table 14**.[43,84]

Table 14: Turbidimetric solubility rankings

Classification	Turbidimertic solubility (µM)
Poorly soluble	< 1
Moderately soluble	1 - 100
Highly soluble	> 100

6.4.3 HPLC-based kinetic solubility assay

The method named HPLC-based solubility in this dissertation is a miniaturized shake flask method. The compounds were dissolved in DMSO to prepare 10 mM solutions, and spiked (1:50) into PBS at pH 7.4, in duplicate. The DMSO suspension were shook for 18 h at 25 °C, the solution were centrifuged, filtered and analysed using HPLC-DAD (Agilent 1200 Rapid Resolution HPLC with a diode array detector). Aqueous compounds' solubility was determined through best fit calibration curves which were constructed using calibration standard.[49]

Chapter seven

References

(1) The History of Malaria, an Ancient Disease https://www.cdc.gov/malaria/about/history/index.html (accessed Nov 26, 2018).

(2) Cox, F. E. History of the Discovery of the Malaria Parasites and Their Vectors. *Parasit. Vectors* **2010**, *3* (1), 5-13.

(3) Crawley, J.; Nahlen, B. Prevention and Treatment of Malaria in Young African Children. *Semin. Pediatr. Infect. Dis.* **2004**, *15* (3), 169–180.

(4) Gallup, J. L.; Sachs, J. D. The Economic Burden of Malaria. *Am. J. Trop. Med. Hyg.* **2001**, *64* (1-2 Suppl), 85–96.

(5) Sachs, J.; Malaney, P. The Economic and Social Burden of Malaria. *Nature* **2002**, *415* (6872), 680–685.

(6) WHO. *World Malaria Report 2017*; WHO.

(7) Njoroge, M.; Njuguna, N. M.; Mutai, P.; Ongarora, D. S. B.; Smith, P. W.; Chibale, K. Recent Approaches to Chemical Discovery and Development Against Malaria and the Neglected Tropical Diseases Human African Trypanosomiasis and Schistosomiasis. *Chem. Rev.* **2014**, *114* (22), 11138–11163.

(8) Prudêncio, M.; Rodriguez, A.; Mota, M. M. The Silent Path to Thousands of Merozoites: The Plasmodium Liver Stage. *Nat. Rev. Microbiol.* **2006**, *4* (11), 849–856.

(9) Swann, J.; Corey, V.; Scherer, C. A.; Kato, N.; Comer, E.; Maetani, M.; Antonova-Koch, Y.; Reimer, C.; Gagaring, K.; Ibanez, M.; et al. High-Throughput Luciferase-Based Assay for the Discovery of Therapeutics That Prevent Malaria. *ACS Infect. Dis.* **2016**, *2* (4), 281–293.

(10) Wells, T. N. C.; Burrows, J. N.; Baird, J. K. Targeting the Hypnozoite Reservoir of Plasmodium Vivax: The Hidden Obstacle to Malaria Elimination. *Trends Parasitol.* **2010**, *26* (3), 145–151.

(11) Bannister, L.; Mitchell, G. The Ins, Outs and Roundabouts of Malaria. *Trends Parasitol.* **2003**, *19* (5), 209–213.

(12) Eisele, T. P.; Larsen, D.; Steketee, R. W. Protective Efficacy of Interventions for Preventing Malaria Mortality in Children in *Plasmodium Falciparum* Endemic Areas. *Int. J. Epidemiol.* **2010**, *39* (suppl_1), i88–i101.

(13) Lengeler, C. Insecticide-Treated Bed Nets and Curtains for Preventing Malaria. *Cochrane Database Syst. Rev.* **2004**.

(14) Indoor Residual Spraying https://www.cdc.gov/malaria/malaria_worldwide/reduction/irs.html (accessed Jul 30, 2018).

(15) Mosquito Control https://www.malariasite.com/mosquito-control/ (accessed Oct 8, 2018).

(16) Mueller, A. K.; Labaied, M.; Kappe, S.; Matuschewski, K. Erratum: Genetically Modified Plasmodium Parasites as a Protective Experimental Malaria Vaccine. *Nature* **2007**, *446* (7131), 102–102.

(17) Desai, M.; ter Kuile, F. O.; Nosten, F.; McGready, R.; Asamoa, K.; Brabin, B.; Newman, R. D. Epidemiology and Burden of Malaria in Pregnancy. *Lancet Infect. Dis.* **2007**, *7* (2), 93–104..

(18) No Title https://www.malariasite.com/prophylaxis/ (accessed Oct 8, 2018).

(19) Radeva-Petrova, D.; Kayentao, K.; ter Kuile, F. O.; Sinclair, D.; Garner, P. Drugs for

Preventing Malaria in Pregnant Women in Endemic Areas: Any Drug Regimen versus Placebo or No Treatment. *Cochrane Database Syst. Rev.* **2014**.

(20) Kayentao, K.; Garner, P.; Maria van Eijk, A.; Naidoo, I.; Roper, C.; Mulokozi, A.; MacArthur, J. R.; Luntamo, M.; Ashorn, P.; Doumbo, O. K.; ter Kuile, F. Intermittent Preventive Therapy for Malaria During Pregnancy Using 2 vs 3 or More Doses of Sulfadoxine-Pyrimethamine and Risk of Low Birth Weight in Africa. *JAMA* **2013**, *309* (6), 594-604.

(21) Anthony, M. P.; Burrows, J. N.; Duparc, S.; JMoehrle, J.; Wells, T. N. The Global Pipeline of New Medicines for the Control and Elimination of Malaria. *Malar. J.* **2012**, *11* (1), 316-340.

(22) US FDA approves Krintafel (tafenoquine) for the radical cure of *P. vivax* malaria https://www.mmv.org/newsroom/press-releases/us-fda-approves-krintafel-tafenoquine-radical-cure-p-vivax-malaria (accessed Jul 31, 2018).

(23) Single-dose tafenoquine for radical cure of *P. vivax* malaria submitted for regulatory approval in Brazil https://www.mmv.org/newsroom/news/single-dose-tafenoquine-radical-cure-p-vivax-malaria-submitted-regulatory-approval (accessed Oct 8, 2018).

(24) Rajapakse, S.; Rodrigo, C.; Fernando, S. D. Tafenoquine for Preventing Relapse in People with *Plasmodium Vivax* Malaria. *Cochrane Database Syst. Rev.* **2015**, 1-55.

(25) Immunization, Vaccines and Biologicals http://www.who.int/immunization/research/development/malaria/en/ (accessed Oct 8, 2018).

(26) (MVIP), Q. on the malaria vaccine implementation programme. Q&A on the malaria vaccine implementation programme http://www.who.int/malaria/media/malaria-

vaccine-implementation-qa/en/#What is RTS,S/AS01? (accessed Jul 30, 2018).

(27) RTS,S https://www.malariavaccine.org/malaria-and-vaccines/first-generation-vaccine/rtss (accessed Oct 8, **2018**).

(28) Flannery, E. L.; Chatterjee, A. K.; Winzeler, E. A. Antimalarial Drug Discovery — Approaches and Progress towards New Medicines. *Nat. Rev. Microbiol.* **2013**, *11* (12), 849–862.

(29) Lin, J. T.; Juliano, J. J.; Wongsrichanalai, C. Drug-Resistant Malaria: The Era of ACT. *Curr. Infect. Dis. Rep.* **2010**, *12* (3), 165–173.

(30) *Guidelines for the Treatment of Malaria*, second, WHO, World Health Oragnisation; **2010**.

(31) Ashley, E. A.; Dhorda, M.; Fairhurst, R. M.; Amaratunga, C.; Lim, P.; Suon, S.; Sreng, S.; Anderson, J. M.; Mao, S.; Sam, B.; et al. Spread of Artemisinin Resistance in Plasmodium Falciparum Malaria. *N. Engl. J. Med.* **2014**, *371* (5), 411–423.

(32) Dondorp, A. M.; Nosten, F.; Yi, P.; Das, D.; Phyo, A. P.; Tarning, J.; Lwin, K. M.; Ariey, F.; Hanpithakpong, W.; Lee, S. J.; Ringwald, P.; Silamut, K.; Imwong, M.; Chotivanich, K.; Lim, P.; Herdman, T.; Shunmay Yeung, S.S.; Singhasivanon, P.; Day, N.P.J.; Lindegardh, N.; Socheat,D.; White, F.R.S.;. Artemisinin Resistance in *Plasmodium Falciparum* Malaria. *N. Engl. J. Med.* **2009**, *361* (5), 455–467.

(33) Delves, M.; Plouffe, D.; Scheurer, C.; Meister, S.; Wittlin, S.; Winzeler, E. A.; Sinden, R. E.; Leroy, D. The Activities of Current Antimalarial Drugs on the Life Cycle Stages of Plasmodium: A Comparative Study with Human and Rodent Parasites. *PLoS Med.* **2012**, *9* (2), e1001169.

(34) MMV annual report; Medicines for Malaria Ventures, 2017.

(35) Paquet, T.; Gordon, R.; Waterson, D.; Witty, M. J.; Chibale, K. Antimalarial Aminothiazoles and Aminopyridines from Phenotypic Whole-Cell Screening of a SoftFocus ® Library. *Future Med. Chem.* **2012**, *4* (18), 2265–2277.

(36) MMV390048 https://www.mmv.org/newsroom/film/mmv390048 (accessed Nov 28, 2018).

(37) Lachman, L.; Lieberman, H.; Kanig, J. *The Theory and Practice of Industrial Pharmacy*, 3rd edition.; Philadelphia : Lea & Febiger, **1986**.

(38) Lemke, T.; Williams, D.; Williams, L. *Foye's Principles of Medicinal Chemistry*, 2nd edition.; Lippincott & Wilkins, 2008, 31-32.

(39) Savjani, K. T.; Gajjar, A. K.; Savjani, J. K. Drug Solubility: Importance and Enhancement Techniques. *ISRN Pharm.* **2012**, *2012*, 1–10.

(40) Alelyunas, Y. W.; Empfield, J. R.; McCarthy, D.; Spreen, R. C.; Bui, K.; Pelosi-Kilby, L.; Shen, C. Experimental Solubility Profiling of Marketed CNS Drugs, Exploring Solubility Limit of CNS Discovery Candidate. *Bioorg. Med. Chem. Lett.* **2010**, *20* (24), 7312–7316.

(41) Morissette, S. L.; Soukasene, S.; Levinson, D.; Cima, M. J.; Almarsson, O. Elucidation of Crystal Form Diversity of the HIV Protease Inhibitor Ritonavir by High-Throughput Crystallization. *Proc. Natl. Acad. Sci.* **2003**, *100* (5), 2180–2184.

(42) Jain, N.; Yalkowsky, S. H. Estimation of the Aqueous Solubility I: Application to Organic Nonelectrolytes. *J. Pharm. Sci.* **2001**, *90* (2), 234–252.

(43) Lipinski, C. A.; Lombardo, F.; Dominy, B. W.; Feeney, P. J. Experimental and Computational Approaches to Estimate Solubility and Permeability in Drug Discovery and Development Settings1PII of Original Article: S0169-409X(96)00423-1. *Adv.*

Drug Deliv. Rev. **2001**, *46* (1–3), 3–26.

(44) Saal, C.; Petereit, A. C. Optimizing Solubility: Kinetic versus Thermodynamic Solubility Temptations and Risks. *Eur. J. Pharm. Sci.* **2012**, *47* (3), 589–595.

(45) Kerns, Edward H. Di, L. *Drug-like Properties: Concepts, Structure Design and Methods*, 1st ed.; 2008.

(46) Le Manach, C.; Paquet, T.; Gonzàlez Cabrera, D.; Younis, Y.; Taylor, D.; Wiesner, L.; Lawrence, N.; Schwager, S.; Waterson, D.; Witty, M. J.; et al. Medicinal Chemistry Optimization of Antiplasmodial Imidazopyridazine Hits from High Throughput Screening of a SoftFocus Kinase Library: Part 2. *J. Med. Chem.* **2014**, *57* (21), 8839–8848.

(47) Ishikawa, M.; Hashimoto, Y. Improvement in Aqueous Solubility in Small Molecule Drug Discovery Programs by Disruption of Molecular Planarity and Symmetry. *J. Med. Chem.* **2011**, *54* (6), 1539–1554.

(48) Ritchie, T. J.; Macdonald, S. J. F. The Impact of Aromatic Ring Count on Compound Developability – Are Too Many Aromatic Rings a Liability in Drug Design? *Drug Discov. Today* **2009**, *14* (21–22), 1011–1020.

(49) Hill, A. P.; Young, R. J. Getting Physical in Drug Discovery: A Contemporary Perspective on Solubility and Hydrophobicity. *Drug Discov. Today* **2010**, *15* (15–16), 648–655.

(50) Fauber, B. P.; René, O.; de Leon Boenig, G.; Burton, B.; Deng, Y.; Eidenschenk, C.; Everett, C.; Gobbi, A.; Hymowitz, S. G.; Johnson, A. R.; La H.; Liimatta M.; Lockey P.; Norman M.; Ouyang W.; Wang W.; Wong H.;. Reduction in Lipophilicity Improved the Solubility, Plasma–Protein Binding, and Permeability of

Tertiary Sulfonamide RORc Inverse Agonists. *Bioorg. Med. Chem. Lett.* **2014**, *24* (16), 3891–3897.

(51) Savjani, K. T.; Gajjar, A. K.; Savjani, J. K. Drug Solubility: Importance and Enhancement Techniques. *ISRN Pharm.* **2012**, *2012*, 1–10.

(52) Jamieson, C.; Moir, E. M.; Rankovic, Z.; Wishart, G. Medicinal Chemistry of HERG Optimizations: Highlights and Hang-Ups. *J. Med. Chem.* **2006**, *49* (17), 5029–5046.

(53) Cavalli, A.; Buonfiglio, R.; Ianni, C.; Masetti, M.; Ceccarini, L.; Caves, R.; Chang, M. W. Y.; Mitcheson, J. S.; Roberti, M.; Recanatini, M. Computational Design and Discovery of "Minimally Structured" HERG Blockers. *J. Med. Chem.* **2012**, *55* (8), 4010–4014.

(54) Aronov, A. M. Common Pharmacophores for Uncharged Human Ether-a-Go-Go-Related Gene (HERG) Blockers. *J. Med. Chem.* **2006**, No. 23, 6917–6921.

(55) Louvel, J.; Carvalho, J. F. S.; Yu, Z.; Soethoudt, M.; Lenselink, E. B.; Klaasse, E.; Brussee, J.; IJzerman, A. P. Removal of Human *Ether-à-Go-G*o Related Gene (HERG) K + Channel Affinity through Rigidity: A Case of Clofilium Analogues. *J. Med. Chem.* **2013**, *56* (23), 9427–9440.

(56) Sanguinetti, M. C.; Jiang, C.; Curran, M. E.; Keating, M. T. A Mechanistic Link between an Inherited and an Acquired Cardiac Arrhythmia: HERG Encodes the IKr Potassium Channel. *Cell* **1995**, *81* (2), 299–307.

(57) Moss, A. J.; Zareba, W.; Kaufman, E. S.; Gartman, E.; Peterson, D. R.; Benhorin, J.; Towbin, J. A.; Keating, M. T.; Priori, S. G.; Schwartz, P. J.; et al. Increased Risk of Arrhythmic Events in Long-QT Syndrome with Mutations in the Pore Region of the Human *Ether-a-Go-Go*-Related Gene Potassium Channel. *Circulation* **2002**, *105* (7),

794–799.

(58) Pearlstein, R. A.; Vaz, R. J.; Kang, J.; Chen, X.-L.; Preobrazhenskaya, M.; Shchekotikhin, A. E.; Korolev, A. M.; Lysenkova, L. N.; Miroshnikova, O. V; Hendrix, J.; et al. Characterization of HERG Potassium Channel Inhibition Using CoMSiA 3D QSAR and Homology Modeling Approaches. *Bioorg. Med. Chem. Lett.* **2003**, *13* (10), 1829–1835.

(59) Sacchi, A.; Laneri, S.; Arena, F.; Abignente, E.; Gallitelli, M.; D'amico, M.; Filippelli, W.; Rossi, F. Research on Heterocyclic Compounds, XLI. 2-Phenylimidazo[1,2-b]Pyridazine-3-Acetic Derivatives: Synthesis and Anti-Inflammatory Activity. *Eur. J. Med. Chem.* **1999**, *34* (11), 1003–1008.

(60) Choi, H.-S.; Rucker, P. V.; Wang, Z.; Fan, Y.; Albaugh, P.; Chopiuk, G.; Gessier, F.; Sun, F.; Adrian, F.; Liu, G.; et al. (R)-2-Phenylpyrrolidine Substituted Imidazopyridazines: A New Class of Potent and Selective Pan-TRK Inhibitors. *ACS Med. Chem. Lett.* **2015**, *6* (5), 562–567.

(61) Peterson, E. A.; Boezio, A. A.; Andrews, P. S.; Boezio, C. M.; Bush, T. L.; Cheng, A. C.; Choquette, D.; Coats, J. R.; Colletti, A. E.; Copeland, K. W.; et al. Discovery and Optimization of Potent and Selective Imidazopyridine and Imidazopyridazine MTOR Inhibitors. *Bioorg. Med. Chem. Lett.* **2012**, *22* (15), 4967–4974.

(62) Nawijn, M. C.; Alendar, A.; Berns, A. For Better or for Worse: The Role of Pim Oncogenes in Tumorigenesis. *Nat. Rev. Cancer* **2011**, *11* (1), 23–34.

(63) Santio, N. M.; Vahakoski, R. L.; Rainio, E.-M.; Sandholm, J. A.; Virtanen, S. S.; Prudhomme, M.; Anizon, F.; Moreau, P.; Koskinen, P. J. Pim-Selective Inhibitor DHPCC-9 Reveals Pim Kinases as Potent Stimulators of Cancer Cell Migration and Invasion. *Mol. Cancer* **2010**, *9* (1), 279-291.

(64) Magnuson, N. S.; Wang, Z.; Ding, G.; Reeves, R. Why Target PIM1 for Cancer Diagnosis and Treatment? *Futur. Oncol.* **2010**, *6* (9), 1461–1478.

(65) Wurz, R. P.; Sastri, C.; D'Amico, D. C.; Herberich, B.; Jackson, C. L. M.; Pettus, L. H.; Tasker, A. S.; Wu, B.; Guerrero, N.; Lipford, J. R.; Winston J.T.; Yang Y.; Wang P.; Nguyen Y.; Andrews K.L.; Huang X.; Lee M.R.; Mohr C.; Zhang J.D.; Reid D.L.; Xu Y.; Zhou Y.; Wang H.L.;. Discovery of Imidazopyridazines as Potent Pim-1/2 Kinase Inhibitors. *Bioorg. Med. Chem. Lett.* **2016**, *26* (22), 5580–5590.

(66) Hamdouchi, C.; Sanchez-Martinez, C.; Gruber, J.; del Prado, M.; Lopez, J.; Rubio, A.; Heinz, B. A. Imidazo[1,2- b]Pyridazines, Novel Nucleus with Potent and Broad Spectrum Activity against Human Picornaviruses: Design, Synthesis, and Biological Evaluation. *J. Med. Chem.* **2003**, *46* (20), 4333–4341.

(67) Le Manach, C.; Gonzàlez Cabrera, D.; Douelle, F.; Nchinda, A. T.; Younis, Y.; aylor, D.; Wiesner, L.; White, K. L.; Ryan, E.; March, C.; Duffy S.; Avery V.M.; Waterson D.; Witty M.J.; Wittlin S.; Charman S.A.; Street L.J.; Chibale K.;. Medicinal Chemistry Optimization of Antiplasmodial Imidazopyridazine Hits from High Throughput Screening of a SoftFocus Kinase Library: Part 1. *J. Med. Chem.* **2014**, *57* (6), 2789–2798.

(68) McNamara, C. W.; Lee, M. C. S.; Lim, C. S.; Lim, S. H.; Roland, J.; Nagle, A.; Simon, O.; Yeung, B. K. S.; Chatterjee, A. K.; McCormack, S. L.; et al. Targeting Plasmodium PI(4)K to Eliminate Malaria. *Nature* **2013**, *504* (7479), 248–253.

(69) Bendjeddou, L. Z.; Loaëc, N.; Villiers, B.; Prina, E.; Späth, G. F.; Galons, H.; Meijer, L.; Oumata, N. Exploration of the Imidazo[1,2-b]Pyridazine Scaffold as a Protein

Kinase Inhibitor. *Eur. J. Med. Chem.* **2017**, *125*, 696–709.

(70) Green, J. L.; Moon, R. W.; Whalley, D.; Bowyer, P. W.; Wallace, C.; Rochani, A.; Nageshan, R. K.; Howell, S. A.; Grainger, M.; Jones, H. M.; Ansell K.H.; Chapman T.M.; Taylor D.L.; Osborne S.A.; Baker D.A.; Tatu U. Holder A.A.;. Imidazopyridazine Inhibitors of *Plasmodium Falciparum* Calcium-Dependent Protein Kinase 1 Also Target Cyclic GMP-Dependent Protein Kinase and Heat Shock Protein 90 To Kill the Parasite at Different Stages of Intracellular Development. *Antimicrob. Agents Chemother.* **2016**, *60* (3), 1464–1475.

(71) Green, J. L.; Rees-Channer, R. R.; Howell, S. A.; Martin, S. R.; Knuepfer, E.; Taylor, H. M.; Grainger, M.; Holder, A. A. The Motor Complex of *Plasmodium Falciparum*: Phosphorylation By A Calcium-Dependent Protein Kinase. *J. Biol. Chem.* **2008**, *283* (45), 30980–30989.

(72) Azevedo, M. F.; Sanders, P. R.; Krejany, E.; Nie, C. Q.; Fu, P.; Bach, L. A.; Wunderlich, G.; Crabb, B. S.; Gilson, P. R. Inhibition of *Plasmodium Falciparum* CDPK1 by Conditional Expression of Its J-Domain Demonstrates a Key Role in Schizont Development. *Biochem. J.* **2013**, *452* (3), 433–441.

(73) Chapman, T. M.; Osborne, S. A.; Bouloc, N.; Large, J. M.; Wallace, C.; Birchall, K.; Ansell, K. H.; Jones, H. M.; Taylor, D.; Clough, B.; Large, J. M.; Wallace, C.; Birchall, K.; Ansell, K. H.; Jones, H. M.; Taylor, D.; Clough, B.; Green, J.L.; Holder, A.A.;. Substituted Imidazopyridazines Are Potent and Selective Inhibitors of Plasmodium Falciparum Calcium-Dependent Protein Kinase 1 (PfCDPK1). *Bioorg. Med. Chem. Lett.* **2013**, *23* (10), 3064–3069.

(74) Nair, S.; Nash, D.; Sudimack, D.; Jaidee, A.; Barends, M.; Uhlemann, A.-C.; Krishna, S.; Nosten, F.; Anderson, T. J. C. Recurrent Gene Amplification and Soft Selective

Sweeps during Evolution of Multidrug Resistance in Malaria Parasites. *Mol. Biol. Evol.* **2006**, *24* (2), 562–573.

(75) Imwong, M.; Hien, T. T.; Thuy-Nhien, N. T.; Dondorp, A. M.; White, N. J. Spread of a Single Multidrug Resistant Malaria Parasite Lineage (*Pf*Pailin) to Vietnam. *Lancet Infect. Dis.* **2017**, *17* (10), 1022–1023.

(76) Yeung, S.; Socheat, D.; Moorthy, V. S.; Mills, A. J. Artemisinin Resistance on the Thai–Cambodian Border. *Lancet* **2009**, *374* (9699), 1418–1419.

(77) Beshir, K.; Sutherland, C. J.; Merinopoulos, I.; Durrani, N.; Leslie, T.; Rowland, M.; Hallett, R. L. Amodiaquine Resistance in *Plasmodium Falciparum* Malaria in Afghanistan Is Associated with the *Pf*crt SVMNT Allele at Codons 72 to 76. *Antimicrob. Agents Chemother.* **2010**, *54* (9), 3714–3716.

(78) Clayden, Jonathan; Greeves, Nick; Warren, S. *Organic Chemistry*, 1st edition; Oxford University Press Inc., New York, **2001**, 342-346.

(79) Carreño, M. C.; García Ruano, J.; Sanz, G.; Toledo, M. A.; Urbano, A. Mild and Regiospecific Nuclear Iodination of Methoxybenzenes and Naphthalenes with N-Iodosuccinimide in Acetonitrile. *Tetrahedron Lett.* **1996**, *37* (23), 4081–4084.

(80) Sicre, C.; Alonso-Gómez, J.-L.; Cid, M. M. Regioselectivity in Alkenyl(Aryl)-Heteroaryl Suzuki Cross-Coupling Reactions of 2,4-Dibromopyridine. A Synthetic and Mechanistic Study. *Tetrahedron* **2006**, *62* (48), 11063–11072.

(81) Ion channel Discovery Services https://www.essenbioscience.com/media/uploads/files/hERG_10xcpd_Exemplar_Report.pdf (accessed Nov 25, 2018).

(82) Harmer, A. R.; Abi-Gerges, N.; Easter, A.; Woods, A.; Lawrence, C. L.; Small, B. G.;

Valentin, J.-P.; Pollard, C. E. Optimisation and Validation of a Medium-Throughput Electrophysiology-Based HNav1.5 Assay Using IonWorks™. *J. Pharmacol. Toxicol. Methods* **2008**, *57* (1), 30–41.

(83) Whitebread, S.; Hamon, J.; Bojanic, D.; Urban, L. Keynote Review: In Vitro Safety Pharmacology Profiling: An Essential Tool for Successful Drug Development. *Drug Discov. Today* **2005**, *10* (21), 1421–1433.

(84) Moos, W. H.; Green, G. D.; Pavia, M. R. Chapter 33. Recent Advances in the Generation of Molecular Diversity; **1993**; 315–324.

(85) Evans, J. D. *Straightforward Statistics for the Behavioral Science*; Brooks/Cole, **1995**.

(86) Lanier, M. C.; Moorjani, M.; Luo, Z.; Chen, Y.; Lin, E.; Tellew, J. E.; Zhang, X.; Williams, J. P.; Gross, R. S.; Lechner, S. M.; Markison S.; Joswig T.; Kargo W.; Piercey J.; Santos M.; Malany S.; Zhao M.; Petroski R.; Crespo M.I.; Díaz J.L.; Saunders J.; Wen J.; O'Brien Z.; Jalali K.; Madan A.; Slee D.H.;. N -[6-Amino-2-(Heteroaryl)Pyrimidin-4-Yl]Acetamides as A 2A Receptor Antagonists with Improved Drug Like Properties and i*n Vivo* Efficacy. *J. Med. Chem.* **2009**, *52* (3), 709–717.

(87) Huang, S.-X.; Li, H.-Y.; Liu, J.-Y.; Morisseau, C.; Hammock, B. D.; Long, Y.-Q. Incorporation of Piperazino Functionality into 1,3-Disubstituted Urea as the Tertiary Pharmacophore Affording Potent Inhibitors of Soluble Epoxide Hydrolase with Improved Pharmacokinetic Properties. *J. Med. Chem.* **2010**, *53* (23), 8376–8386.

(88) Trager, W.; Jensen, J. Human Malaria Parasites in Continuous Culture. *Science (80-.).* **1976**, *193* (4254), 673–675.

(89) Hinrichs, D. J.; Makler, M. T. Measurement of the Lactate Dehydrogenase Activity of *Plasmodium Falciparum* as an Assessment of Parasitemia. *Am. J. Trop. Med. Hyg.*

1993, *48* (2), 205–210.

(90) Reader, J.; Botha, M.; Theron, A.; Lauterbach, S. B.; Rossouw, C.; Engelbrecht, D.; Wepener, M.; Smit, A.; Leroy, D.; Mancama, D.; Coetzer, T.L ; Birkholtz, L.M.;. Nowhere to Hide: Interrogating Different Metabolic Parameters of *Plasmodium Falciparum* Gametocytes in a Transmission Blocking Drug Discovery Pipeline towards Malaria Elimination. *Malar. J.* **2015**, *14* (1), 213-229.

(91) Mosmann, T. Rapid Colorimetric Assay for Cellular Growth and Survival: Application to Proliferation and Cytotoxicity Assays. *J. Immunol. Methods* **1983**, *65* (1–2), 55–63.

(92) Bevan, C. D.; Lloyd, R. S. A High-Throughput Screening Method for the Determination of Aqueous Drug Solubility Using Laser Nephelometry in Microtiter Plates. *Anal. Chem.* **2000**, *72* (8), 1781–1787.

(93) Alsenz, J.; Kansy, M. High Throughput Solubility Measurement in Drug Discovery and Development. *Adv. Drug Deliv. Rev.* **2007**, *59* (7), 546–567.